AD NUMBER
AD331749
CLASSIFICATION CHANGES
TO: **unclassified**
FROM: **secret**
LIMITATION CHANGES
TO: **Approved for public release; distribution is unlimited.**
FROM: **Controlling Organization: British Embassy, 3100 Massachusetts Avenue, NW, Washington, DC 20008.**
AUTHORITY
DSTL, DSIR 23/30207, 11 Dec 2008; DSTL, DSIR 23/30207, 11 Dec 2008

TECH. NOTE
WE. 5

ROYAL AIRCRAFT ESTABLISHMENT

(FARNBOROUGH)

TECHNICAL NOTE No. WE. 5

THE EFFECT OF AERODYNAMIC NON-LINEARITIES AND CROSS-COUPLINGS ON THE PERFORMANCE OF A CRUCIFORM MISSILE

by

W. S. Brown, W. E. Dean, P. Hampton, H. Lewis and D. I. Paddison

MAY, 1962

MINISTRY OF AVIATION

U.D.C. No.533.6.013.418 : 629.192 : 518.5 : 53.082.5

Technical Note No. WE.5

May, 1962

ROYAL AIRCRAFT ESTABLISHMENT

(FARNBOROUGH)

THE EFFECT OF AERODYNAMIC NON-LINEARITIES AND CROSS-COUPLINGS ON THE PERFORMANCE OF A CRUCIFORM MISSILE

by

W.S. Brown, W.E. Dean, P. Hampton,
H. Lewis and D.I. Paddison

SUMMARY

This Note describes an investigation, made with the aid of TRIDAC and MERCURY computers, into the effect of aerodynamic non-linearities and cross-couplings on the performance of a cruciform guided missile, including the effects of such aerodynamic characteristics on stability and homing. Aerodynamic data, obtained from wind tunnel tests of the English Electric D.4 configuration used to develop THUNDERBIRD, and of W.2 (V.R.725) together with control and guidance system data, were employed to construct the mathematical model.

The main conclusions reached were that, in spite of some of the awkward aerodynamic characteristics assumed, a cruciform missile provided with a suitable feedback control system can function satisfactorily up to large body incidences (30°) and need not become unstable. The main difficulty posed by the aerodynamic characteristics is with respect to rolling behaviour, in that they cause the missile to have preferred planes of incidence. With roll rate stabilisation, this may result in considerable rolling during homing, with some increase in miss distance. A slow rate of roll, demanded continuously to smooth out the effects of fortuitous bias, also tended to increase miss distance when applied to a missile without bias. There was some indication that roll position stabilisation leads to mainly smaller miss distances than does roll rate stabilisation in homing on targets turning off course at a steady rate. The importance of accurately representing the aerodynamics of the missile is emphasised.

Although TRIDAC proved to be capable of generating the response and stability characteristics of the missile accurately, it was not able to generate miss distances with the precision required to assess non-linear effects accurately, although trends and orders of magnitude were correctly indicated. Shortcomings of the equipment were responsible for small errors present in the axis transformations to which the values of miss distance were sensitive. Consequently, most of the results on homing were obtained digitally on MERCURY.

LIST OF CONTENTS

LIST OF CONTENTS (Cont'd)

LIST OF APPENDICES

LIST OF TABLES

LIST OF ILLUSTRATIONS

LIST OF PRINCIPAL SYMBOLS

(See also Appendix 1 and Fig.2.)

b,c	Components of lateral acceleration of missile in its principal axes
c	reference length (see Table 1)
c_ℓ	rolling moment coefficient
c'_m, c'_n	pitching and yawing moment coefficients in rotated axes
c'_y, c'_z	lateral force coefficients in rotated axes (see Section 3.2.1)
D	subscript denoting "demanded value"
d	subscript denoting "in demand axes"
D_ℓ, D_m, D_n	control surface deflection coefficients (see Table 2)
F-functions	see Section 3.2.2
H	altitude
i	subscript denoting "indicated value"
L_ϕ, L_ξ	rolling moment derivatives
ℓ_ϕ, ℓ_ξ	derivatives of rolling moment coefficients
$\ell(\bar{\theta},\phi)=\ell_\phi\phi$	(Fig.11)
M	Mach number
p	ambient static pressure (in other contexts, missile angular velocity in roll)
p_{ref}	ambient static pressure at reference altitude
S	reference area (see Table 1)
T	subscript denoting "target"
u_{TEE}, v_{TEE}, w_{TEE}	components of target velocity relative to earth in earth axes
u_{TMM}, v_{TMM}, w_{TMM}	components of target velocity relative to missile in missile axes
X_G, Y_G, Z_G	gimbal angles of earth to missile axis transformation
X_{Go}	initial value of X_G = missile roll angle (see Fig.28)

LIST OF PRINCIPAL SYMBOLS (Cont'd)

α,β	partial incidences (see Fig.2)
$\bar{\alpha},\bar{\beta}$	sines of partial incidences
γ	ratio of specific heats of air
ε	error angle
ξ,η,ζ	equivalent control surface angles (see Fig.2)
θ	total incidence
$\bar{\theta}$	sine of total incidence
$\sigma_1,\sigma_2,\sigma_3,\sigma_4$	control surface deflections (see Fig.2)
ϕ	angle defining plane of wind vector (see Fig.2)
θ_D,ψ_D	dish gimbal angles

1 INTRODUCTION

The work described in this Note grew out of a suggestion that Cartesian missiles, required to operate at high altitudes, might be in trouble because of non-linearities and cross-couplings in their aerodynamics. This impression had gained currency following a report[1] that some American missiles of cruciform design had performed erratically during their early flight trials, having shown a tendency to roll instability at large incidences, a feature which was later ascribed to aerodynamic characteristics of the type mentioned above. It was suggested that the non-linearities and cross-couplings, which had occurred in fixed wing missiles with rearward control surfaces, affected the pitching and yawing moments and could result in loss of stability in pitch or yaw, while the cross-coupling also produced a rolling moment which, under conditions of combined pitch and yaw, increased with incidence. The worst effects, however, were stated to be confined to incidences exceeding 15° and were, therefore, unlikely to affect performance at low altitudes.

The non-linearities were attributed in the main to partial shielding of the control surfaces by the body, while the cross-coupling was thought to be due, in part, to vortices shed from the nose and forward part of the body of the missile. Whatever the cause, it seemed more than likely that British missiles of this type would show similar characteristics and that THUNDERBIRD, in particular, would be affected, since it had been designed with high-altitude capabilities in mind.

It was agreed, therefore, that there should be a general investigation of the effect of aerodynamic non-linearities and cross-couplings on cruciform missile performance, and that a mathematical model of a cruciform missile should be constructed on TRIDAC. Depending on the outcome of the work, a programme of flight tests was also envisaged.

A prime requirement for the simulator work was obviously the provision of detailed information on the aerodynamic characteristics of some missile. In the event, the only suitable data related to the D.4 test vehicle used to develop THUNDERBIRD, a 1/15th scale model of which had been tested at R.A.E. This was not inappropriate however, for reasons given above.

The wind tunnel tests[2] had been made at Mach numbers of 1·58 and 2·02, up to a total incidence of 22° at the lower Mach number, and 25° at the higher. The control surfaces had been deflected singly and in combination, during the tests, and the model had been rolled by stages through 360°. A fair amount of information on cross-couplings was, therefore, available.

This information formed the basis of a three-dimensional mathematical model of the D.4 test vehicle which was constructed on TRIDAC. To this model there was added, first, the control system of W.1 (THUNDERBIRD) and, later, that of W.2 (V.R.725). These hybrid models were used to study the effects of the aerodynamic characteristics on stability and, in parallel with this work, a mathematical analysis[4] was made of the static stability characteristics by perturbation methods. Later, it was deemed essential to obtain more extensive aerodynamic data. The development of THUNDERBIRD into W.2 (V.R.725) was in hand, and as this involved certain changes in the aerodynamic configuration of the missile, it was clearly desirable to have up to date data for the mathematical model. A series of wind tunnel tests was therefore arranged in the A.R.A. supersonic tunnel at Bedford. These covered a much wider range of incidence and Mach number than the D.4 tests and included a more detailed investigation of the control surface characteristics. The data so obtained were used to construct on TRIDAC a three-dimensional model of V.R.725, complete with its control system, as a replacement of the earlier model.

After the response and stability of this model, which included a representation of the missile's autopilot, had been investigated, the simulation was extended to include the guidance and homing system of V.R.725, and this final model, which required some 500 amplifiers and used most of the available capacity of TRIDAC, was employed to find the effect of aerodynamic characteristics on homing performance. The work on V.R.725 forms the main topic of this Note.

2 MODEL OF D.4 TEST VEHICLE

2.1 Aerodynamic characteristics

A half-sectional outline of the D.4 test vehicle is shown in Fig.1, and its principal dimensions and parameters are listed in Table 1. As mentioned in the introduction, information on its aerodynamic characteristics was obtained from Ref.2. These characteristics had been put in mathematical form in Ref.3, the basis of the formulation being the use of power series in the sines of the partial incidences α and β, defined in Fig.2, and the standard ξ,η,ζ representing the aileron, elevator and rudder angles. This scheme had been selected because TRIDAC had been provided with equipment designed to suit it, namely, high-grade hydraulic servo-multipliers with accurate multiple potentiometers. The proposal as envisaged, however, proved far too complicated, and was impracticable because the polynomials representing the pitching and yawing moments contained product terms of orders up to the seventh: these introduced awkward problems of scaling which resulted in loss of accuracy. A revised scheme, starting from the assumption that the missile was flying at constant height and Mach number was therefore prepared, in which no polynomial was of higher degree than the third. The revised expression for the pitching moment is quoted on Fig.3, where a comparison is made with the fit provided by the seventh order polynomial. It will be seen that the revised fit is certainly no worse than the original one, and in some respects better.

The objection to both fits is that they were based on data limited to incidences less than 22°, yet were employed to generate aerodynamic characteristics at all incidences up to 30°. Later work showed the extrapolation to have been greatly in error, and some of the conclusions reached in the earlier work to be invalid for this particular configuration.

2.2 Co-ordinate reference system

Fig.2 indicates the system of reference axes and notation employed throughout the work as the basis of the equations describing the mathematical model. G,XYZ are principal axes through the mass centre G of the missile, which define its longitudinal axis and the planes through the two pairs of wings. θ is the angle between the velocity vector GV and the longitudinal axis and, therefore, represents the total incidence. ϕ is the angle between the XZ plane and the plane containing the longitudinal axis and the velocity vector. Hence, $\tan\phi = v/w$, where v and w are the sideslip velocities in the directions GY and GZ. The partial incidences α and β are used to define the quantities $\bar{\alpha} = \sin\alpha = w/V$ and $\bar{\beta} = \sin\beta = v/V$, where V is the speed of the missile, and the quantity $\bar{\theta} = \sin\theta$ is also introduced, so that $\bar{\alpha} = \bar{\theta}\cos\phi$, $\bar{\beta} = \bar{\theta}\sin\phi$, and $\bar{\theta}^2 = \bar{\alpha}^2 + \bar{\beta}^2$.

2.3 Equations of motion

The standard equations applicable to the motion of a rigid body in space, where the motion is referred to a set of moving axes which are principal axes of inertia in the body, were used. The equations are listed in Appendix 1. Since the moments of inertia about the Y and Z axes (viz. B and C) were assumed to be equal, the equations of angular acceleration were simplified; moreover, the equation of linear momentum in the

direction of the X axis was replaced by a programmed variation of the total velocity V, or by V = constant. What this implies is indicated in Appendix 1.

The quantities Y,Z,L,M,N, in the equations of motion are functions of pressure, Mach number and Reynolds number, as well as $\bar{\alpha}$, $\bar{\beta}$, etc. Besides this, they depend to some extent on p, q, r, and, except in steady conditions, on the time derivatives of these. It was assumed however, that such time-wise variations could be neglected, indeed, in practically all the work, the aerodynamic characteristics were assumed to be independent of p, q, and r. The wind tunnel tests had given no information on rotary dorivatives, but the damping due to them was unlikely to be important compared with the artificial damping provided by the autopilot. Reynolds number effects, likewise, were unknown and had to be neglected, though evidence of their presence appeared later during flight trials. Gravity forces were neglected, since their inclusion in the earlier stages of the work would have meant adding an earth-to-missile axis transformation to the simulation. After such a transformation had been added for other reasons at a later stage, the gravity terms in the equations were still omitted, since their effect seemed likely to be secondary and in the nature of a bias which might obscure the main issue. The effect of gravity was included, however, in digital studies undertaken to compare the performance of the model with that of flight rounds. Since the non-linearities and couplings were greater at Mach number 1·58, this value was selected and adhered to in most of the work on D.4. An altitude of 40,000 ft was chosen as suitable, and this fixed the missile speed at 1528 ft/sec.

2.4 Control system

D.4, like its successors W.1, and W.2 (V.R.725), was fitted with an autopilot based on rate feedback and designed to give rapid initial response to demands for rate of turn. Suitable shaping networks were employed to modify the outputs of pitch and yaw angular-rate gyros so that the resulting lag in the feedback path was approximately equal to the incidence lag of the missile. Since the latter varied with altitude, however, provision was made to vary the lag and loop gain by switching at predetermined altitudes. The shaped feedback signals were subtracted from the demanded rates of turn in missile axes to provide inputs to the control surface actuators, which were driven by hydraulic servo-motors having a natural frequency of about 20 c.p.s. A closed loop system also provided control of roll rate. The W.1 and W.2 (V.R.725) autopilots are illustrated in Fig.4.

2.5 Simulator model

Fig.5 is a block diagram of the D.4 simulation. The main variables, $\bar{\alpha}$ and $\bar{\beta}$, which describe the aerodynamic characteristics, were applied as inputs to hydraulic servo-multipliers which formed the polynomial terms. There were insufficient servos of this type, however, to generate the control surface contributions and, in consequence, these had to be formed on electric servo-multipliers of greatly inferior performance. For these servos to operate satisfactorily, it was necessary to abandon real-time working and substitute a 5:1 time scale. Although this retarded progress, it was advantageous from the point of view of accuracy in recording the results, since the full traverse of the plotting tables could be used. Digital check solutions were provided and the simulator results showed good agreement with these.

2.6 Tests of D.4

As mentioned previously, the extrapolation of the aerodynamic data on D.4 to incidences exceeding 22° was incorrect; hence the conclusions drawn from the high-incidence tests were invalid for this configuration. For this reason, no records of the work on D.4 are included in this Note other than the following general statement.

The response of the model to demands for lateral acceleration was determined both in single plane, with roll prevented, and in three-dimensions, in the presence of roll. Demands were applied in missile axes and also in axes which were fixed as regards rotation in roll but which coincided initially with the principal axes of the missile. These were termed "roll-position-stabilised axes". Since the roll equilibrium was unstable when the incidence was in either wing plane, but stable in the median planes (ϕ = 45° or 135°), demands in roll-position-stabilised axes usually caused roll until the wind vector lay in one of the median planes. As the incidence increased, instability developed, leading to divergence in pitch, or yaw, in a principal plane at incidences exceeding 26° when roll was prevented, or in combined pitch and yaw in a median plane, at incidences exceeding 22°. This was attributable to the markedly unstable pitching, or yawing, moment which resulted from the faulty extrapolation of the data, a fact which was confirmed by a mathematical analysis based on perturbation methods. When the aerodynamic characteristics were artificially linearised, the instability disappeared. In order to prevent the instability from affecting the rolling motion, and possibly obscuring a genuine effect, linear characteristics in pitch and yaw were substituted while the non-linear rolling moment characteristic was retained. There was no evidence of roll oscillation under such conditions once the missile had settled down with the incidence in a median plane, and roll instability could be induced only by inserting lags in the roll control loop. These might be thought of as delays in the generation of the aerodynamic moment resisting roll - and small delays do occur owing to the time taken for a disturbance of the flow to propagate - but the lags which had to be introduced were greater than could be accounted for in this way. An approximate analysis of the roll loop was made, based on the assumption that, since the moment of inertia of the missile in roll was much less than in pitch or yaw, any significant oscillation in roll must be relatively fast and, therefore, likely to have little effect on pitch or yaw. The work on TRIDAC had confirmed this theory, for the total incidence, θ, had remained steady during the roll oscillations. Since an oscillation purely in roll implies $p = \dot{\phi}$, the conditions for oscillation were determined by analysing the roll loop on this assumption. The results obtained completely confirmed those obtained from the simulator.

3 MODEL OF V.R.725

The earlier work on the hybrid model based on D.4 had shown that more extensive wind tunnel tests, covering a greater range of incidence, were essential if the results were to have any validity. In the meantime, the D.4, W.1 and early W.2 designs had given way to V.R.725 and, in the process, the aerodynamic configuration, as well as the autopilot, had been modified. A completely new set of wind tunnel tests was therefore arranged, and these were conducted in the supersonic wind tunnel at A.R.A., Bedford.

The V.R.725 missile is a fixed-wing cruciform design with four moving control surfaces at the rear. A half-section on the centre line is shown in Fig.1, and the principal dimensions and parameters of the missile are listed in Table 1.

3.1 Wind tunnel tests

The ranges of incidence and Mach number covered in the A.R.A. tests were much wider than those of the early R.A.E. tests on D.4; for example, at Mach numbers of 1·2, 1·4, 1·6, 1·8, 2·0, 2·5 and 3·0, the maximum incidences reached in the tunnel were 25°, 25°, 35°, 40°, 40°, 43° and 43° respectively. The tests were in two parts, the first consisting of runs with the control surfaces undeflected, the second including tests with one control panel deflected. Tests were also made to determine the interaction between adjacent control surface panels but, except at the smaller Mach numbers, the interaction between panels was very slight. Refs.5 to 8

discuss the organisation of these wind tunnel tests and also give the results in some detail. Figs.6 to 10 summarise the aerodynamics of V.R.725 in the form used in the simulation.

After the measured forces and moments had been reduced to non-dimensional coefficients by division by a suitable factor, e.g. $\frac{1}{2}\gamma pSM^2$ or $\frac{1}{2}\gamma pScM^2$, the quotients were functions of Reynolds number, Mach number, two components of incidence defining the position of the wind vector, and three angles representing the control surface deflections. As in the case of D.4, the effect of Reynolds number was neglected. It was then necessary to devise a scheme whereby these quantities might be generated on the simulator.

3.2 Representation of aerodynamics

3.2.1 Tail-fixed aerodynamics

Two methods were considered. The first involved the expansion of the force and moment coefficients as polynomials in $\bar{\alpha}$ and β, the method which had been used previously on D.4. TRIDAC is well suited to this method when the functions to be generated are reasonably linear. When marked non-linearities are present, however, it is much less satisfactory. More terms in the expansions are then necessary and, almost invariably, both positive and negative signs occur. The associated constant multipliers usually vary greatly in magnitude and present a formidable problem of scaling, with a resulting loss of accuracy.

The second method, which was the one actually employed, involves the use of the polar co-ordinates $\bar{\theta}$ and ϕ which have already been defined. If G,XY'Z' is an auxiliary set of axes having the X axis coincident with that of the missile but the Y and Z axes rotated through the angle ϕ, so that the wind vector lies in the XZ' plane, it follows from the symmetry of the missile with its control surfaces undeflected that the forces and moments expressed in these axes are periodic in 4ϕ. The coefficients may therefore be expressed as Fourier sine or cosine series in 4ϕ, the coefficients being functions of $\bar{\theta}$. The general form adopted to express the force and moment coefficients in the G,XY'Z' system, with the control surfaces undeflected, was therefore

$$F(\bar{\theta},\phi) = \sum_{n} \left[G_n(\bar{\theta}) \sin 4n\phi + H_n(\bar{\theta}) \cos 4n\phi \right]$$

TRIDAC is well equipped to generate such expressions, since it has several highly accurate multiple sine and cosine resolvers driven by hydraulic servo motors. The general term in sin $4n\phi$ or cos $4n\phi$ is easily obtained as a sum of products of powers of sin 4ϕ and cos 4ϕ. The corresponding coefficients in body axes were obtained from the others by resolution through the angles ϕ and $90^\circ - \phi$. The whole process of generation and resolution was accomplished on one servo by having two resolver units coupled by a gear box of 4:1 ratio. The ϕ servo is described in Appendix 2.

3.2.2 Evaluation of G_n and H_n functions

The wind tunnel data were first reduced to arrays of values of the force and moment coefficients, corresponding to a matrix of simultaneous values of θ and ϕ, itself the product of serial values of θ and ϕ, θ ranging in steps of 5° from zero to the maximum incidence attainable at each Mach number, and ϕ from zero to 45° in steps of $7\frac{1}{2}^\circ$. A greater range of ϕ was unnecessary by reason of the symmetry, although spot checks at other angles of roll were made.

Satisfactory fits in functional form were obtained in all cases with not more than two terms in each Fourier series. The co-ordinates of the G_n and H_n functions at each experimental value of θ were determined by applying the method of Least Squares to the appropriate section of the data at that incidence. In their final form, the aerodynamic coefficients were as follows:

$$C_\ell = F_4(\bar{\theta}) \sin 4\phi \ (1 + b_4 \cos 4\phi)$$

$$C'_m = F_1(\bar{\theta}) + F_2(\bar{\theta}) \cos 4\phi$$

$$C'_n = F_3(\bar{\theta}) \sin 4\phi \ (1 + b_3 \cos 4\phi)$$

$$C'_z = F_5(\bar{\theta}) + F_6(\bar{\theta}) \cos 4\phi$$

$$C'_y = F_7(\bar{\theta}) \sin 4\phi \ (1 + b_7 \cos 4\phi) \ ,$$

where the functions $F_n(\bar{\theta})$ and the coefficients b_n are introduced in place of G_n and H_n for simplicity. In these expressions b_4, b_3, and b_7 vary little with $\bar{\theta}$ and little error is introduced if they are assumed constant.

The variation of the F functions with incidence and Mach number is shown in Figs.6 to 9. The curves defining the moments are particularly non-linear in $\bar{\theta}$, and their variation with Mach number is far from regular. In fact, no wholly satisfactory method of reducing some of these functions to products of functions of a single variable was found. On the simulator, variation of Mach number was achieved by resort to linear interpolation between the values of the coefficients at fixed Mach numbers. Nevertheless, the accuracy of representation of the aerodynamics by the method outlined was estimated to be as good as that of the wind tunnel data from which it was derived. Nowhere did errors exceeding 2 per cent of the maximum value occur except where a datum point was completely out of the pattern, suggesting that the measurement itself was wrong.

3.2.3 Function generators

The F functions were simulated by diode-type function generators working in conjunction with standard amplifiers. These are fully described in Ref.9, and little further comment is called for. Each generator was initially set up with a maximum error not exceeding 1 per cent of full scale. Occasional checks were made subsequently, followed by adjustments, but the maximum error did not exceed 2 per cent of full scale over periods of some months. Seven function generators were installed for the tail-fixed aerodynamic coefficients at each Mach number and provision was made for simulation at three Mach numbers.

3.2.4 Control surface aerodynamics

As might be expected, the contribution of the tail surfaces when deflected consisted of a major term, which was a linear function of the deflection of the control surface, and a secondary part which was a complicated function of all the variables involved. Although the missile has four separate control panels, they are coupled together by the autopilot so as to provide only three independent variables, ξ, η and ζ. The transformation between the two sets of co-ordinates is simple.

Fig.10 shows the increment D on the moment coefficients caused by deflecting the control panel σ_1 (see Fig.2). The lateral aerodynamic forces due to the control panels were assumed to be equal to the moment divided by a moment arm which was taken as the distance from the control hinge line to the centre of gravity of the missile. The figure shows the data points, and the full lines represent the least-squares fit to these points by a polynomial in $\bar{\alpha}$, $\bar{\beta}$ and σ_1. The effect of negative values of σ_1, and of the deflection of other control panels may be obtained from these curves by consideration of symmetry, using the relationships of Table 2. Table 2 also gives the relations between the σ's and ξ, η and ζ, as defined in Fig.2. The poor control effectiveness when ϕ is near zero is due to the combination of body incidence and control panel incidence which effectively gives the control panel a large incidence. This condition rarely arises in practice. It will be noted that it is accompanied by a relatively large and undesirable moment in the other plane, giving rise to appreciable coupling between the planes. A more detailed account of the fitting process, with further results, may be found in Ref.10.

The polynomials referred to above were generated with the aid of electric servo-multipliers; not those referred to in the discussion of D.4, which had been discarded, but an improved pattern, described in Ref.11. The effect of the cross-product terms arising from the control panel deflections was found to be slight; hence, in most of the work they were omitted.

3.2.5 Damping derivatives

The wind tunnel tests provided only the static aerodynamic characteristics of the missile. Theoretical estimates of the derivatives ℓ_p, m_q, and n_r were provided by Aerodynamics Department, R.A.E., and these were included in the model. The effect of the latter two, in particular, was found to be very small in comparison with the damping provided by the autopilot; thus, for the most part, they were omitted from the simulation. The effect of ℓ_p, as determined by TRIDAC, is discussed in Section 6.4.

3.3 Gravity forces

As in the case of D.4, and for reasons given earlier in this Note, gravity forces were not included in the simulation, except in a few special tests.

3.4 Variation of centre of gravity

Provision was made in the digital programme for variation of the position of the centre of gravity of the missile resulting from the burning of the sustainer. This causes a change in the leverage of the forces which produce the moments about the centre of gravity. The variation was assumed to be linear in time. Variation of the missile mass was also included but the changes in the moments of inertia were neglected.

3.5 Variation of altitude and Mach number

To obtain the aerodynamic forces and moments from their respective coefficients, it is necessary to multiply the latter by $\frac{1}{2}\gamma SpM^2$ or $\frac{1}{2}\gamma ScpM^2$. Provision was made to vary both Mach number and altitude, although most of the work was done at Mach number 1·6 and a simulated height of 40,000 ft. Better scaling was obtained by absorbing one M into the F functions and converting to forces and moments by multiplying by KM_p/p_{ref}, with $K = \frac{1}{2}\gamma Sp_{ref}$, or $\frac{1}{2}\gamma Scp_{ref}$. As interest centred on large incidences, only

altitudes exceeding that of the tropopause were simulated. The speed of sound was, therefore, assumed constant and Mach number taken to be proportional to the speed of the missile.

3.6 Simulator model

A block diagram of the arrangement employed on the simulator to represent V.R.725 and its control system is shown in Fig.11.

3.7 Digital computation

The primary purpose of the digital computation was to provide a separate solution against which the analogue simulation could be checked. It was, however, eventually used to make comparisons between the mathematical model of the missile and flights of the actual missile. In the later stages of the programme, when it was appreciated that TRIDAC was not able to produce miss distance values sufficiently accurately for comparisons to be made between a missile with linear aerodynamics and one with non-linear aerodynamics, the digital simulation was used to produce the curves of miss distance presented in this Note.

Because the programme was originally intended to be used for checking purposes only, for which only a few typical runs would be required, some computing speed was sacrificed to achieve speed and flexibility of programming and operation. Mercury Autocode was used almost entirely, and all the work was done on the Ferranti Mercury computer at R.A.E. The well tried procedure of reducing the differential equations to a series of first order equations and integrating them by a Runge-Kutta sub-routine was employed.

The model used was the same as that used on TRIDAC, although the TRIDAC simulation never included all the detail of the Mercury simulation. A series of Mercury programmes was written, but they were all based on the first one which was designed to check the simulation of the missile alone. They included the provision of variable Mach number and altitude, a centre of gravity position moving linearly with time, and linearly decaying mass and inertias. Slight modifications were made to this programme to make it suitable for simulation of the flight rounds. The only major modification necessary was when homing was added to the model. The provisions for varying Mach number, altitude, etc, continuously were removed but transformations between earth, missile and dish axis systems were added. Radome aberation and angular noise were also included.

The F functions were evaluated by a four point interpolation on a table of values of each function at equally spaced intervals in $\bar{\theta}$. The tables were extended at each end of the range of $\bar{\theta}$ so as to avoid the time-consuming operation of making allowance for the effect of being at the end of the range.

The transfer functions of the actuators were left out in most of the work. The small time constants would have necessitated a very short integration step; as it was, the integration step was 0·02 sec for the missile alone and 0·01 sec when the homing head was added. With the programme for the homing missile on which much of the production work was done, 8 seconds of flight took a little under 30 minutes to compute - a ratio of about 210:1. This compares with a time scale of 5:1 on TRIDAC. On the analogue machine however, the time taken to vary parameters and re-set initial conditions is quite large compared with the time of computation, whereas the opposite is true of the digital machine. Hence, a more realistic figure for the TRIDAC computing ratio would be 10:1. The time spent on programming and eradicating faults must also be reckoned. This amounted to three or four weeks in the digital case, whereas the similar operation on TRIDAC ran into months.

4 RESPONSE OF V.R.725 MODEL

4.1 General

Many responses were recorded as checks of the accuracy and symmetry of the model and the repeatability of the simulator under a wide variety of conditions. Most parameters of the system were investigated, but Figs.12 to 16 refer only to those of most interest and indicate the responses to demands for angular rates of the missile. Although the actual demand in each case was a step change, this was shaped into the form indicated by a simple lag before reaching the autopilot, since the latter is designed to accept rate demands produced by tho homing system. The effect of artificially linearising the aerodynamics is also shown. For the wing-body contributions, this involved replacing the true aerodynamic characteristics by straight lines having the same avorage slope over a range of incidence from zero to 20° approximately. In the case of the tail contributions, the major term only of the complete expression was retained in each case. All responses quoted are at Mach number 1·6 and height 40,000 ft, with a fixed c.g. position corresponding to two-thirds of the sustainer burnt.

4.2 Responses in single plane

When the motion was restricted to one principal plane, as with perfect roll position stabilisation, the responses were as shown in Fig.12 for the pitch plane. The non-linearity of the pitching, or yawing, moment caused the double humped response in q, or r, in contrast to the single peak of the response in the case of linear aerodynamics. The system was completely stable in both instances. The large difference between the control surface angles in the two cases is attributable to the choice of slope for the linear pitching moment characteristic. The similarity between the plots of incidence, θ, and latoral acceleration, c, is marked, and indicates that the contribution of the control surfaces to the acceleration is small.

4.3 Responses in 45° plano

Under equal demands for rate of pitch and yaw, the missile remains in the stable 45° plane and corresponding parameters in the two planes are equal. The resultant total incidence and angular rate are in the 45° plane and, in the case of linear aerodynamics, are the same as those achieved in a roll-stabilised principal plane if the demand in the latter case is $\sqrt{2}$ times that in both pitch and yaw in the former. For this reason, responses in the 45° plane are not illustrated in tho case of linear aerodynamics; but Fig.13 shows results obtained with non-linear wing-body contributions which markedly affect the operation of the control system. In the figure which indicates $r, \zeta, \bar{\beta}$, and $\bar{\theta}$, (the corresponding curves in the pitch plane being identical) equal demands r_D and q_D have been selected to produce approximately the same steady state value of $\bar{\theta}$ as in Fig.12 for fully non-linear aerodynamics. The demands are equivalent to a total demand for 0·2 rads/sec, in tho 45° plane, but result in much the same steady-state incidence as a single plane demand for 0·3 rads/sec. All tho response curves are different, however, and, in particular, it will be observed that the control surface angle in Fig.13, passes through zero and has a steady state value opposite in sign to that in Fig.12. The explanation of this can be seen in the functions illustrated in Fig.11, which shows the type of non-linearity occurring in the wing-body aerodynamics. In the single plane case, the angle 4ϕ is always zero and the functions F_1 and F_2 of Para.3.2.2 add to give the total moment. In the 45° planes, however, 4ϕ is always 180° and the F_2 term suffers a sign change. At large incidences, this term can be numerically larger than F_1, with the result that the total moment becomes small and of the opposite sign. The necessary reversal of the control surface deflections is accomplished by the

autopilot, the missile rates of turn in the steady state being slightly greater than the demanded rates. In the single plane case, the reverse is true, the missile rate being slightly less than that demanded.

4.4 Response in three-dimensions

The effect of applying demands in roll-position-stabilised axes but simultaneously allowing the missile to roll is shown in Figs.14 to 16. These figures illustrate the various responses obtained by simulating combinations of linear and non-linear wing-body and tail aerodynamics with the same three demands in each case. Here, the demand, denoted by q_{Dd}, where D indicates "demanded" and d "in demand axes", is in the ZX plane of a set of demand axes having the same origin and X axis as those of the missile but not rolling with the latter. The initial angle X_{Go} between the two ZX planes was 5° in order that the missile should roll positively towards the stable 45° plane and not be subject to the uncertainty existing at $X_{Go} = 0$. The missile's angular rates and lateral accelerations in its own axes were resolved into the demand axes, giving the quantities q_d, r_d, c_d, and b_d, p being unaffected since no change of roll axis occurs.

The figures illustrate the motion which develops as the missile rolls towards the 45° plane, which it eventually reaches. The angular velocity r_d and the lateral acceleration b_d eventually decay to zero, whilst q_d and c_d reach non-zero steady state values, that of q_d being close to q_{Dd}, the demanded rate. The manoeuvre is completely stable and the double-humped feature of the rate response under large demands is again evident in Figs.15 and 16. The effect on the response of substituting linear aerodynamics, wholly or in part, for non-linear is shown in Figs.14 and 15 and may be compared with the result in single plane (Fig.12). Where only the wing-body aerodynamic characteristics are non-linear, Fig.15 reveals that the second hump of the q_d and r_d responses is somewhat reduced, as compared with that in Fig.16, and there is a similar effect on the response in roll.

5 SIMULATION OF FLIGHT CONTROL-ROUNDS

5.1 General

As mentioned in the Introduction, a programme of flight trials had been envisaged as a possible addition to the work on the simulator. For various reasons which need not be elaborated, a proposal to purchase English Electric control-rounds for flight trials was abandoned but, during the course of the simulator exercise, data became available on the performance of similar rounds fired as part of the development of V.R.725. Some of these rounds showed peculiarities in flight which merited further investigation. The next sections of this Note deals with this subject.

5.2 Flight rounds

In all, five of the missiles flown manoeuvred satisfactorily at altitudes and speeds relevant to the investigation. Demands for rate of turn were in the form of a step through a simple lag. Various lags up to 2·0 sec were used, but the significant factor was the nature of the demand itself, that is, whether it was a single demand for acceleration in one wing plane or equal demands in two wing planes for manoeuvre in a median plane. The following table summarises the rounds which were of interest.

Round 033. Demand 10°/sec thro' 1·5 sec in pitch and yaw.

Round 034. Demand 15°/sec thro' 2·0 sec in pitch.

Round 035. Demand 10°/sec thro' 1·5 sec in pitch and yaw.

Round 036. Demand 15°/sec thro' 1·5 sec in pitch

Round 036. Demand 15°/sec thro' 0·15 sec in pitch

Round 040. Demand 13°/sec thro' 0·28 sec in pitch and yaw.

5.3 Comparison with model results

The mathematical model was able to reproduce most of the features of these rounds with a reasonable degree of accuracy. Fig.17 shows a comparison of the model results with some of the curves recorded by the telemetry. The time interval shown covers the build up of incidence in response to the demand quoted above. Small adjustments to some of the parameters in the system were needed for the agreement to be as good as that shown. The major modification required resulted from the fact that the rounds were more stable than the wind tunnel tests suggested. A centre of pressure shift of two inches was required to compensate for this.

The major disparities between model and missile occurred in the roll response. Because there is no position feedback in the roll autopilot, the roll attitude depends intimately on the rolling moment induced by combined pitch and yaw, and the latter would have to be reproduced accurately if the roll response, as determined by the simulation, were to agree with that of the rounds. The general character of the roll response in the simulation agreed well with that observed in the rounds except for two details which may well be related, but for which no explanation has been found. Fig.18 shows extracts from the records of roll rate gyro output of four of the rounds, and also gives some indication of the range of speed and altitude covered. In the rounds where the demand was for rate of turn in one wing plane only, the induced rolling moment made the missile roll in an attempt to reach the stable state of equal incidences in two planes. In the transient so formed there were small peaks in the records from the rounds, which were not reproduced by the simulation. This is shown for Round 034 in Fig.18. The other three rounds, records of which are shown in this figure, are those in which the stable state with equal incidences in two wing planes should have been attained without any disturbances in roll; but, as can be seen, each one developed an oscillation. A considerable amount of time was spent in trying to make the model oscillate in a similar manner, so that the cause of this oscillation might be understood, but no real success was achieved. The telemetry records of Round 035 were particularly good, showing the oscillation to be of about 3 c/s frequency with a modulating frequency of about 0·3 c/s. A detailed analysis of the records at various points in the roll loop was made by the manufacturers. Sections of the model were checked independently and all but the aerodynamic rolling moment appeared correct. The work on TRIDAC is described in the next section.

6 INVESTIGATION OF ROLL STABILITY

6.1 General

With the aerodynamic and control system data appropriate to M = 1·6, H = 40,000 ft, which were adopted as representative values, there was no evidence on the simulator of roll oscillation at any incidence up to 30°. Attempts were made to induce oscillations by various methods, viz: (1) introduction of a small lag in the forward path of the roll loop, i.e., in L/A, (2) introduction of a small lag in the feedback path of the roll loop, i.e., in $L_\xi \xi$, together with a small lag in the demand for roll, i.e., in $L_\phi \phi$, (3) introduction of backlash and dead-space in the control surface displacements,

(4) changes in gains and time constants in the autopilot loops of up to ±10 per cent, (5) simulation of non-linear control surface aerodynamics. The results of these experiments are described below.

6.2 Investigation of roll loop

Since the circular frequency of the roll oscillation observed in flight had been recorded as 20 rads per second, approximately, the outer loop, through the couplings with pitch and yaw, was broken at the demand for roll, i.e. at the $L_\phi\phi$ input, and amplitude and phase measurements were made at this frequency. The values obtained were 0·59 and -305·5° respectively. In order to produce instability in roll due to the outer loop, therefore, it would be necessary to introduce a gain of about 1·7 and a phase lag of 54·5° into the outer loop. Assuming that the value of L_ϕ was correct, it would be possible, on a linear basis, to do this by the introduction of a second order lag having a damping ratio of 0·3 and a time constant of 41 m.s., or by a phase delay, $1-sT/1+sT$, with a time constant T of 26 m.s., together with a gain of 1·7. For a simple lag of 70 m.s., the gain required would be about 2·9. With a symmetrical missile, none of these possibilities seemed feasible. It was assumed, therefore, that, apart from a possible variation in the magnitude of L_ϕ, any lag occurring in the system must be in the roll loop itself.

6.3 Effect of lag in L/A

In order to investigate the effect of lags within the inner roll loop, equal demands for q and r were provided in roll position stabilised axes so that the missile took up a position in the 45° plane. The demands were such that the steady state value of $\bar{\theta}$ was 0·462, corresponding to an incidence of 27·5°. A lag of 36 m.s. in L/A then produced a continuous oscillation in p, and increasing the time constant of the lag caused instability in roll. The frequency of the oscillation was 3·4 c.p.s., which was of the right order. The effect of changing the value of L_ϕ is shown in Fig.19. Similar results were obtained at altitudes of 25,000 ft and 53,500 ft, the lag required being reduced at the lower altitude. Further results were obtained for Mach numbers of 1·4 and 2·0, and these showed that the lag required was slightly less at the higher Mach number. At the normal value of L_ϕ, the smallest lag required to cause oscillation was 25 m.s., at Mach number 2·0, and altitude 25,000 ft. The frequency of oscillation was 5·5 c.p.s. With a gain of 2·0 on L_ϕ, this lag was reduced to 12 m.s. On the assumption that the value of L_ϕ used on the simulator was correct, the lag required to produce roll oscillation was considered to be more than was likely to arise in the roll autopilot loop.

The results obtained in this section of the work were checked by perturbation theory, good agreement being obtained. The digital check solutions gave similar results.

6.4 Effect of roll damping derivative ℓ_p

As was expected, the introduction of a value of ℓ_p (which had been estimated to be -6·3) had a stabilising effect. With a positive ℓ_p of the same magnitude, the stability was reduced, but as much as 16 m.s. lag was still required to produce continuous oscillation at M = 1·6 and H = 40,000 ft.

6.5 Effect of lag in $L_\xi\xi$

It is unlikely that any lag in $L_\phi\phi$ could occur unless it had an aerodynamic origin, but lags in $L_\xi\xi$ are possible if imperfections exist in the control system components and in the roll-rate gyro. It was not possible, however, to start an oscillation in roll by means of such lags alone. With a lag of 50 m.s. in $L_\xi\xi$, for example, a lag of 10 m.s. in $L_\phi\phi$ was necessary to start oscillation at an incidence of 30°. Various combinations of lags in $L_\xi\xi$ and $L_\phi\phi$ were explored, the results being shown in Fig.20.

6.6 Theoretical estimate of aerodynamic lags

It had been suggested that lags in the control system might occur owing to the finite time required for aerodynamic loads to reach steady values after a disturbance. Tobak[12], who used indicial functions to study unsteady airflow, concluded that the time, t, required for loads on lifting surfaces to attain steady values after a sudden change of flow is equal to the chord of the lifting surface divided by the velocity at which the disturbance passes downstream, i.e.,

$$t = \frac{L}{u-a}$$

where t = time in seconds

L = streamwise chord of lifting surface (i.e. wing chord) or, alternatively, distance from wing leading edge to tail leading edge

u = free stream velocity

a = speed of sound in free stream

In the case of Round 035, the Mach number and altitude when the roll oscillations commenced indicated a lag of about 17 m.s. for the wing-tail combination, and a lag of 8·5 m.s. for the wing alone. These times are too short to account for the oscillation, as the work described above shows.

6.7 Effect of control equipment non-linearities

To determine the contribution, if any, of possible non-linearities in the control gear to roll instability, dead-space and backlash were simulated, the former to represent overlap in the hydraulic control valves and the latter to represent mechanical imperfections in the control surface drives.

Dead-space

It was found necessary to simulate control valves in which the overlap was 25 per cent of the total travel before an oscillation in roll of the right amplitude was produced. In practice, such overlaps are nominally zero and, in any case, would be very small; hence dead-space was ruled out as a possible cause of instability.

Backlash

A realistic amount of backlash, viz: 0·1° in a total travel of 30° was simulated but did not cause any noticeable decrease in roll stability. An increase of backlash beyond this amount could not be justified; hence, it was concluded that a non-linearity of this type could be discounted.

6.8 Effect of loop gains and time constants

For variations in the gains and time constants in the autopilot loops between ±10 per cent, no noticeable effect on roll stability was observed.

6.9 Effect of control surface aerodynamic non-linearities

The non-linearities in the control surface aerodynamic characteristics, when simulated, had a stabilising effect on the roll loop for incidences up to 30°.

6.10 Effect of missile asymmetries

All the tests mentioned so far were made on the assumption that the missile was completely symmetrical in both the pitch and yaw planes. To disturb the symmetry, various biases were added to the force and moment equations but, for what were considered to be reasonable values, no noticeable effect on roll stability was produced.

Also, to upset the symmetry of the system, gravity components were included. Although these appoared to decrease the stability, and an oscillation for a limited time was observed, its amplitude was very small compared with that of the flight rounds.

6.11 Conclusions on roll instability

With the V.R.725 missile and control system simulated as described, no significant roll oscillation could be produced by the introduction of what were considered to be reasonable lags and changes in gains, time constants and other parameters. It was concluded, therefore, that, if the oscillations in roll observed in flight represented a genuine instability, its cause must be aerodynamic - probably a transient, or unsteady, phenomenon which had not been observed in the wind tunnel and which, therefore, had not been simulated.

7 INVESTIGATION OF HOMING PERFORMANCE

7.1 System adopted for study

The ultimate criterion of performance in a missile aimed at a target is lethality. If fuse and warhead performances are not to be considered, miss distance is generally accepted as the criterion of performance. It was a natural extension of the work, therefore, to seek to determine the effects of the aerodynamic non-linearities and cross-couplings on the miss distance achieved by the missile. The simulation was extended, therefore, to include the V.R.725 homing head with its servo dish and feedback loops.

7.2 Details of extension to simulation

Two axis transformations had to be constructed. The first of these was a three-dimensional, three gimbal system to transform the assumed target velocities from earth to missile axes. The second was a two gimbal system to transform the relative velocities of missile and target, and the missile rates of turn, from missile to dish axes. These transformations were accomplished with the aid of five hydraulic servo-resolvers which are part of the equipment of TRIDAC provided specially for such purposes. The servos may be used either as velocity servos with tachometer feedback, or as position servos with position potentiometer feedback. At the start of the work, the former arrangement was employed, but it was abandoned later in favour of the latter, on account of the errors caused by a small amount of drift in the servos. In the early stages also, the relative velocities of missile and target were integrated in missile axes before transformation into dish axes. This resulted in the appearance of considerable noise superposed on the

components of relative position in dish axes, owing to the limited resolution of the potentiometers. The trouble was overcome by integrating the relative velocities in dish axes after their transformation from missile axes.

Integration in dish axes brought the further advantage that the scaling could be improved. Usually, in a homing manoeuvre, the dish points very nearly at the target throughout, so that the lateral components of target position in dish axes are always small. Only the axial component varies greatly in magnitude. Measured in missile or earth axes, however, all three components of relative position are, in general, large when the missile and target are far apart, and small when they are near. Consequently, the voltages representing the lateral components of miss distance in missile or earth axes are small in relation to their maximum values when the missile and target are near, whereas this is not true of the components in dish axes.

In order to form error signals representing the radar output, the two lateral components of target position in dish axes were divided by the third component measured along the dish axis which is virtually the range. The division process was accomplished with the aid of an electric servo-multiplier. The V.R.725 homing system uses two such error signals as inputs to the dish servo drives, and also as the demands for missile rate of turn to the pitch and yaw autopilots. The simulator model, when extended to include the homing system and target motion as indicated above, is shown diagrammatically in Fig.21, with the detailed representation of the homing head in Fig.22.

7.2.1 Measurement of miss distance

As was stated earlier, the assumed criterion of homing performance was the miss distance. Various methods of measuring miss distance were considered and tried. The objection to forming the sum of the squares of the displacements and extracting the square root, i.e., the range, is that the magnitude of the latter varies so much that good scaling is impossible. As an alternative, one may form the predicted miss distance, i.e., the miss that would result if, subsequent to the instant of prediction, the relative motion were linear at constant velocity. This quantity has the advantage that it varies more slowly than the range but, in three dimensions, its formation is somewhat complicated and the process is liable to error unless highly accurate equipment is available. In the end, it was found best, when studying approaching targets and also for comparative purposes, to form the resultant of the two lateral components of range in missile axes and record it over the last few seconds at the end of the engagement in order to determine the minimum. A further convenient assumption made when miss distances were being recorded for comparative purposes was that the minimum range occurred when its component along the missile longitudinal axis, was zero. This is not strictly accurate, but it is a good approximation when dealing with nearly head-on targets. The miss distance was then recorded by feeding the voltage representing the root-mean-square of the two lateral components of range in missile axes to the initial-condition input of an integrator, the signal input to the integrator being grounded. When the longitudinal component of range went through zero, the integrator was started automatically, so that its output was held at the miss distance as defined above. This output was then displayed on a digital voltmeter. Besides miss distance, the other variables of chief interest were recorded continuously on a conventional servo-driven plotting table, and on a 12-channel ultra-violet recorder. The latter had the advantage of good response, whereas the former could be used for comparing the results of two engagements by direct superposition of records. The target was always assumed to be travelling at 1000 ft/sec and the missile at a Mach number of 1·6 at 40,000 ft altitude.

At a range of 300 ft, the homing system was assumed to be saturated by the signal, and a diode switch was included to stop the range servo when

the longitudinal component of range, measured in dish axes, reached this value. As an alternative, the switch was arranged to earth the inputs to the dish actuators and autopilot, thus reducing the demand to zero. The difference in recorded miss distance was usually negligible, so the precise assumption made did not appear to matter. Miss distance was also found to be insensitive to a variation in the cut-off point between 300 and 500 ft.

7.2.2 Acceleration limiter

Although interest in the work was primarily in the effects of high incidence, the aerodynamic data did not extend beyond 35°. A lateral acceleration limiter was installed to contain the incidence within any desired range. It took the form of a diode switch which, when the acceleration reached the limit, operated to reduce the inputs to the pitch and yaw autopilots to one hundredth of their normal values. This limit was normally set to operate when the incidence reached about 30°. Whenever possible, homing runs in which this limit was not reached were favoured, as the effect of the limiter confused the results.

It should be mentioned that, throughout the simulation, for reasons already given, the time scale employed was five times real time.

7.3 Targets investigated

Homing was studied against fixed targets, straight-flying targets, and targets making manoeuvres such as weaves and steady turns. In performance studies, the weaving target is often considered to be the most difficult one to intercept. Large miss distances are obtained because the navigation system is not well suited to the requirements in this case. Weaving target manoeuvre was not considered very appropriate in the present investigation however, because, although it was tried, and resulted in large miss distances on occasion, the missile usually did not attain large incidences during its homing run. Since interest centred on effects occurring mainly at large incidences, a steadily turning target was more suitable.

It is only in the final stage of an engagement that incidences are large, so this was the only part of the homing attack considered. The standard engagement was one in which the missile and target were assumed to be approaching at constant speed at an altitude of 40,000 ft until they were within 20,000 ft. The target was then assumed to begin a steady 2g turn. this was the starting point of the simulation. Target motions were produced by resolving the total velocity, V_T, of the target, assumed to be a point, into components u_{TEE} and v_{TEE}, or u_{TEE} and w_{TEE}, in fixed earth axes.

8 EFFECT OF AERODYNAMICS ON MISS DISTANCE

8.1 General

In the earlier part of the programme, the method of assessing the effect of aerodynamic non-linearities and cross-couplings had been to compare the performance of the missile with that of a hypothetical missile identical with it except for the absence of non-linearities and cross-couplings from its aerodynamics. In fact, however, when it came to comparing miss distances, it was found that TRIDAC did not generate the latter accurately enough for the comparison to be meaningful. To obtain the required accuracy, it was necessary to resort to digital simulation, using the MERCURY autocode programme, which had been written primarily to check TRIDAC. As each run took about half an hour on MERCURY, the range of conditions investigated had to be curtailed and, thus, a number of parameters which might have been varied had to be fixed.

The digital results, presented in Figs.23 to 27, are designed to show the effects of the various forms of non-linearity and cross-coupling, as well as the interactions between them. Non-linear characteristics were replaced by straight lines to show the effect of the non-linearities, and the rolling moment due to combined pitch and yaw was suppressed to indicate its effect.

8.2 Homing in single plane

The initial range, i.e., the range at which the target started its manoeuvre, was varied and miss distance was measured whilst the missile was constrained to fly with incidence in one wing plane only. The effect of non-linearities in pitch (or yaw) is shown in Fig.23. It will be noted that the miss distance is always greater when non-linearities are present. As the initial range is decreased, the missile is forced to manoeuvre at progressively higher incidences to achieve the necessarily higher accelerations (Fig.24). The disparity between the linear and non-linear results increases to the point where the acceleration limiter operates. At still shorter initial ranges the missile has little time in which to manoeuvre, so that the miss distance is largely determined by the lateral displacement of the target during the engagement. The change of sign of miss distance indicates that beyond a certain range the missile over-anticipates the target's motion and passes the target on the opposite side.

8.3 Homing in three dimensions

The effects of the in-plane non-linearities may now be compared with those arising from non-linearities and cross-couplings in three dimensions. Fig.25 compares results at two ranges, viz, 14,000 ft and 20,000 ft, where the peak incidence reached during the engagement ranges from 21° to 25° and from 17° to 18°, respectively. A new parameter introduced by the third dimension is the roll attitude of the missile relative to the plane in which the target is manoeuvring. Since the roll autopilot serves only to damp the rolling motion, the missile is free to assume any roll position during a run. Hence, the parameter chosen to represent this new degree of freedom was the initial roll angle X_{Go}, the definition of which can most easily be understood by reference to Fig.28. It will be recalled that the rolling moment due to combined pitch and yaw, which alone causes the rolling, is zero for ϕ = 0, 45, 90, 135, etc, degrees, these angles representing, alternately, unstable and stable roll positions. During the early part of the engagement, before the missile has rolled, the angles X_G and ϕ will be nearly equal, (not quite equal, because the responses in the two planes differ slightly since the dish is mounted on two gimbals, one of which is inside the other); but, as its incidence increases, the missile will tend to roll so as to make ϕ approach one of its stable values. Up to a point, the nearer the initial position to one of unstable equilibrium in roll, (ϕ = 0, 90, 180, ... degrees), the more violent is the rolling motion and, as will be seen from Fig.25, there is a corresponding increase in miss distance. Fig.25 also indicates that the non-linearities of the pitch and yaw aerodynamics have their effect; for the increase in miss distance does not occur if either the rolling is suppressed or the pitch and yaw aerodynamic characteristics are linearised. The asymmetry in the curves is due to the asymmetry in the dish gimbal system.

Although to suppress rolling entirely is somewhat artificial, it may be regarded as changing the control system to one of perfect roll position stabilisation. The results suggest, therefore, that roll position stabilisation is preferable to stabilisation of roll rate, at any rate for the type of homing manoeuvre investigated.

9 OTHER EFFECTS

9.1 General

It is important to know whether the large peaks in miss distance referred to in the previous sections are reduced by some of the phenomena present in the missile system, which have, so far, not been mentioned. The effects of noise and of a steady non-zero rate demand were investigated.

9.2 Effect of angular noise

In order to assess the effect noise would have on the curve of miss distance variation with initial roll angle, several runs were made with angular noise included. Noise which was white within the bandwidth of the homing head and of spectral density 10^{-7} rad^2/rad/sec was added to the error inputs to the dish system. The two sources of noise were uncorrelated. Fig.27 shows the miss distances obtained with an initial range of 14,000 ft, and compares them with the noise-free results. It can be seen from the Fig. that the effect is not one of smoothing out the curve but of increasing the miss distance overall.

9.3 Effect of steady roll

Fig.26 compares the miss distances obtained under a steady roll-rate demand of 0·25 rad/sec with those for zero roll rate demand already shown in Fig.25. The initial range in this case was 20,000 ft. Again, the effect is not to smooth out the curve but rather to cause a general increase in miss distance. It is understood that V.R.725 has a steady demanded rate of roll of this order to reduce the effects of possible biases.

10 SIMULATOR ACCURACY

10.1 General

The simulation entailed a great deal of duplication in that identical pitch and yaw planes were represented, gravity being omitted. Hence, a valuable check on correct operation could be made by comparing responses in separate planes to equivalent demands; further, for either plane, checks of symmetry of response for symmetry of demand were possible on all parameters. Thus, if four responses of identical shape could be achieved, together with good repeatability, confidence that the simulator was functioning correctly would be increased. If these responses then matched those obtained digitally to a satisfactory degree, confidence that the system simulated was correct would follow. Similar comparisons could also be made in the 45° planes to provide additional checks.

10.2 Missile without homing system

Excellent repeatability of all parameters associated with response to missile rate demands was obtained, together with good symmetry. As shown by Fig.29, however, agreement with the digital check solution was less satisfactory in some places, the greatest error recorded being about 3 per cent of the full scale value. As far as the investigation of stability was concerned, these errors could be ignored, although considerable effort was made to reduce them, without success. Their presence was a reminder that TRIDAC was not built for absolute measurements on complex systems, and presaged an increasing divergence from the digital solutions as complexity grew.

10.3 Homing missile

The homing system was simulated in considerable detail, and a great increase in the amount and complexity of the equipment resulted. Where

possible, individual components of the homing simulation were checked with the aid of calculated responses, and tests for symmetry were made similar to those applied to the missile. An acceptable standard was obtained in all cases, after which the system was coupled up.

A deterioration in the accuracy of the simulator was immediately apparent in homing manoeuvres. After a fairly lengthy process of elimination of unreliable components, short term repeatability of responses was achieved, longer-term random variations remaining. These, however, were less than the general asymmetry of the responses to symmetrical inputs (applied in single planes or with $X_G = 45°$). It was significant that the accuracy with which the various response curves matched the digital solutions had decreased.

Methods used to try to improve the accuracy of the system and to pin-point the chief factors leading to an accumulation of errors are described in Appendix 3. Ultimately, the errors in response were accepted and emphasis was placed on miss distance measurement. As expected, long term repeatability and symmetry in the measurements were poor, but it was found that the average of four values of miss distance, obtained under symmetrical conditions of target manoeuvre, often agreed well with the digital figure, see Figs.30 and 31. It was considered, therefore, that useful information could be obtained from the simulator on the general effect of system changes on miss distance.

11 CONCLUSIONS

Marked non-linearities and cross-couplings occur in the aerodynamic characteristics of cruciform missiles of conventional design - of which V.R.725 may be regarded as typical.

The most important characteristic is a rolling moment which increases with incidence and which, if the missile is not roll-position stabilised, causes rolling until the demanded manoeuvre (e.g. curvature of the flight path in one plane) is in a plane inclined at 45° to the wing planes.

If there is marked rolling of the missile during homing, miss distances may be appreciably increased. Tests indicated roll-position stabilisation to be preferable to stabilisation of roll rate in such cases.

Aerodynamic non-linearities and cross-couplings appear to have little adverse effect on stability, provided that the missile has a suitable auto-pilot. Cruciform missiles so provided should be capable of manoeuvre at incidences up to 30° at least.

The autopilot of V.R.725 appeared to be satisfactory from this point of view, despite some evidence from flight trials that, at least, transitory instability in roll may occur when the missile incidence exceeds 15° in a median plane. The cause of such behaviour was not discovered, but may have been unsteady air flows which were not observed or simulated.

In the configuration studied, the non-linearities in pitch and yaw occurred mainly in the aerodynamic moments, and affected response, particularly at incidences exceeding 15°. When the relative wind was not parallel to a wing plane, the response was further modified by aerodynamic cross-coupling between the pitch and yaw planes, and by the non-linear rolling moment referred to above.

A constant demand for a slow rate of roll - to even out the effects of fortuitous bias - appeared to be detrimental to the performance of a missile free from bias, miss distances being increased in general.

A limited investigation of the effects of noise, in the presence of aerodynamic characteristics of the type mentioned, indicated that angular noise

tended to increase miss distance without obscuring the effects of rolling which have been mentioned above.

A comparison of digital and analogue solutions showed that TRIDAC reproduced the response and stability characteristics of the mathematical model with generally high, and always adequate, precision, but did not generate miss distances sufficiently accurately for the effects of aerodynamic non-linearities on homing performance to be established precisely. The effeot on miss distance being generally small, resort to digital computation was necessary to obtain the differentials with sufficient accuracy for definite conolusions to be drawn.

12 ACKNOWLEDGEMENTS

The authors wish to acknowledge the advice and assistance of members of the staff of English Electric Aviation, Limited, on a number of matters.

LIST OF REFERENCES

Ref.No.	Author	Title, etc.
1	Walker, N.K.	Aerodynamic cross coupling of tail control missiles, with particular reference to advanced TERRIER and TARTAR. B.J.S.M./G.W. Liaison Note No.57/1, January, 1957.
2	Watts, P.E. Southgate, A.C. Anderson, J.R.	Overall force and moment measurements on the English Electric D.4 test vehicle. R.A.E. Report No. Aero 2572, June, 1956.
3	Howie, R.C. Garrett, R.E.J.	A proposed three dimensional study on TRIDAC of a high incidence cruciform missile with non-linear aerodynamics. R.A.E. Technical Memo. No. G.W.340, September 1958.
4	Brown, W.S. Garrett, R.E.J.	The stability of a cruciform missile investigated by perturbation methods. R.A.E. Technical Note (In preparation).
5	Stevens, A.E.	Five-component force and moment wind tunnel tests of M = 1·58 and 2·02 on a 1/16 scale model of W.1/W.2. English Electric Co. Report No.LA.t.083, December, 1959.
6	Ryan, P.D.	Overall force and moment measurements at M = 1·6, 2·0, 2·5, and 3·0 on a 1/16 scale model of W.2. English Electric Co. Report No.5HD/LA.5004, December, 1959.
		Ditto. - Addendum, with results at M = 1·4, May, 1960.

LIST OF REFERENCES (Cont'd)

Ref.No.	Author	Title, etc.
7	Humphreys, G.D.O.	Wind tunnel measurements of overall force and moment at high incidence at Mach numbers from 1·6 to 3·0 on 1/16 scale models of W.1 and W.2 with zero control setting. English Electric Co. Report No.5HD/LA.5011, March, 1960.
8	Males, M.F.	Overall force and moment measurements at M = 1·2 on a 1/16 scale model of W.2. English Electric Report No.5HD/LA.5019, June, 1961.
9	Laws, A.	An arbitrary function generator employing silicon diodes and an A.C. shaping signal. R.A.E. Technical Note No. G.W.559, September, 1960.
10	Richardson, D.J.	An analytic formulation of experimental force and moment measurements on a 1/16 scale model of W.1 and W.2. English Electric Co. Report No.5HD/LA.5010, May, 1960.
11	Laws, A. Blake, J.R.	The TRIDAC high-speed electric servomultipliers. R.A.E. Technical Memo. No. G.W.385, December, 1960.
12	Tobak, M.	On the use of the indicial function concept in the analysis of unsteady motions of wings and wing-tail combinations. N.A.C.A. Report No.1188, (1954).
13	Dean, W.E.	The TRIDAC hydraulically powered computing servos. Part I - Velocity servos. R.A.E. Technical Note No. G.W.487, March, 1958.
14	Garner, K.C. Spearman, F.R.J.	Design of TRIDAC - Part III. Kinematics and axis transformation. R.A.E. Tochnical Note No. G.W.265, July, 1953.

Technical Note No. WE.5

ATTACHED:-

Appendices 1 to 3
Tables 1 to 5
Figs.1-32 (GW/P/9966, 9974, 9978, 9981
WE.R.1578 to 1601 and 1603)
Detachable Abstract Cards

ADVANCE DISTRIBUTION LIST:-

M.O.A.

Chief Scientist
CGWL
DGW
DGBM
GW(G & C)5 - 11 copies
TIL -180 copies
Director,RRE - 5 copies
Mr. Twinn, RRE - 2 copies

R.A.E.

Director
DDRAE(A)
DDRAE(E)
Pats 1
Library
Head of Aero Dept
" " IAP "
" " Space " - 3 copies
" " Weapons "
" " Maths Services Dept
O/C Aberporth
Bedford Library

External to M.O.A. (through TIL)

Air Ministry - ADI Tech
" " - Science 1 Library - 2 copies
War Office - R.A.4 - 2 copies
" " - SA/AC Library - 2 copies
Ministry of Defence - Chairman, DRP Staff
" " " - D.S.1
RMCS
RAF Tech College, Arm Div
ASWE - 2 copies
ARDE - 2 copies
SRDE
Bristol A/C Ltd., G.W. Div - 2 copies
Armstrong Whitworth Aircraft
Sperry Gyro Co.
EMI Electronics - 4 copies
English Electric Co.
Ferranti, Wythenshaw - 2 copies
Elliott Bros. Research Lab

Special Distribution

ARC (for information)

Overseas

U.K.(DRS)(A)
W.R.E. - 10 copies

APPENDIX 1

EQUATIONS OF MOTION

Let G,XYZ (Fig.2) be a set of principal axes of inertia fixed in the missile, the origin of the system being at G, the centre of gravity. Then, if, in these axes,

u,v,w are components of linear velocity of the missile

p,q,r are components of angular velocity of the missile

X,Y,Z are components of force on the missile

L,M,N are components of moment on the missile

A,B,C are the moments of inertia,

and m is the mass of the missile, assumed constant, at any rate over a short interval of time, the equations of motion are

$$\dot{u} + qw - rv = X/m \tag{1}$$

$$\dot{v} + ru - pw = Y/m \tag{2}$$

$$\dot{w} + pv - qu = Z/m \tag{3}$$

$$A\dot{p} - (B-C)qr = L \tag{4}$$

$$B\dot{q} - (C-A)rp = M \tag{5}$$

$$C\dot{r} - (A-B)pq = N\,. \tag{6}$$

If V is the total velocity of the missile, so that

$$V^2 = u^2 + v^2 + w^2\,, \tag{7}$$

it follows, on multiplying equations (1), (2) and (3) by u, v, and w, respectively, and adding, that

$$V\dot{V} = \frac{1}{m}(Xu+Yv+Zw) \tag{8}$$

whence, if V is constant,

$$Xu + Yv + Zw = 0\,. \tag{9}$$

Either equation (8), or its particular case (9), may replace equation (1) and be used to define the X force, including the motor thrust, aerodynamic drag and gravity component, necessary to maintain any given variation of V with time, including, as a special case, V = constant. This was done in the simulation. In the case of a symmetrical cruciform missile, it may be assumed that B = C. If, then,

$$k = 1 - \frac{A}{B}\,, \tag{10}$$

the equations (4), (5) and (6) reduce to

$$\dot{p} = L/A \qquad (11)$$

$$\dot{q} - krp = M/B \qquad (12)$$

$$\dot{r} + kqp = N/C \qquad (13)$$

These, with equations (2) and (3), and V = f(t), where the function f(t) is defined, were the equations used to specify the motion. The forces and moments were assumed to be wholly aerodynamic, gravity components being neglected. For the most part, they were assumed to be completely defined by the static aerodynamic characteristics, as measured in the wind tunnel.

The inertia terms arising from the motions of the controls and components of the control system were neglected, i.e., the body was assumed to be rigid, although the dependence of the forces and moments on the control positions was included.

The angular positions of the controls were related to the angular velocities of the missile and the demanded rates through the transfer functions of the control system.

Axis transformations

The transformation of the target motion from earth to missile axes was accomplished by setting up a three gimbal system in which the orders of rotation were pitch, yaw, roll, and the corresponding angles of rotation were Y_G, Z_G and X_G. The relationships between the co-ordinates in the two systems are given in Ref.14 (Appendix III, Section 2.1, Configuration 1), and those between the missile and gimbal angular velocities are also quoted (Section 3, Configuration 1).

The transformation of the components of relative velocity, and of the missile spins, from missile to dish axes was accomplished by setting up a two gimbal system in which the order of rotation was yaw followed by pitch, and the corresponding angles of rotation were ψ_D, θ_D. The resulting relationships between the components in the two systems are the same as those between co-ordinates quoted in Ref.14 (Section 6.4, Homing Equations, or Appendix VI, equations (VI.2)).

The spins, $\dot{\psi}_D$ and $\dot{\theta}_D$, of the dish about its gimbals are equivalent to spins $-\dot{\psi}_D \sin\theta_D$, $\dot{\theta}_D$, $\dot{\psi}_D \cos\theta_D$ about its principal axes. Hence, the total spins of the dish about its axes are:

$$p_s = (p\cos\psi_D + q\sin\psi_D)\cos\theta_D - (r+\dot{\psi}_D)\sin\theta_D$$

$$q_s = -p\sin\psi_D + q\cos\psi_D + \dot{\theta}_D$$

$$r_s = (p\cos\psi_D + q\sin\psi_D)\sin\theta_D + (r+\dot{\psi}_D)\cos\theta_D .$$

These spins were employed in the integration of the relative velocities of target and missile in dish axes into relative positions, in accordance with the standard equations:

$$u_R = \dot{x}_R + q_s z_R - r_s y_R$$

$$v_R = \dot{y}_R + r_s x_R - p_s z_R$$

$$w_R = \dot{z}_R + p_s y_R - q_s x_R$$

where the subscript R denotes "relative".

APPENDIX 2

THE ϕ SERVO

As shown in Fig.2, the angle ϕ is defined by the relation tan ϕ = v/w, and the requirement was for a servo to generate the angle ϕ continuously when supplied with the variables v and w. The resolvers on the shaft would then generate the sines and cosines of ϕ and 4ϕ. The problem is the well-known one of Cartesian to polar co-ordinate transformation, and the method is a standard technique although it had not previously been used on TRIDAC.

By using one sine and one cosine channel on the ϕ shaft (to which the 4ϕ shaft was ganged mechanically), a servo error signal ε is generated from the relation

$$\varepsilon = v \cos \phi - w \sin \phi. \qquad (14)$$

In the steady state, when $\varepsilon = 0$, this gives the required condition tan ϕ = v/w. The error is brought to zero by arranging that the shaft velocity is proportional to ε and in a direction to reduce it.

To do this, the servo used, and represented by K.G(p), in Fig.32(a), was a standard TRIDAC hydraulic closed-loop velocity servo[13]. The overall loop is of the type often termed "implied position", and the arrangement differs from the normal position servo in being highly non-linear in operation.

Using further sine and cosine channels on the ϕ shaft, the servo provided the quantity $V\bar{\theta}$ from the relation:

$$V\bar{\theta} = v \sin \phi + w \cos \phi. \qquad (15)$$

When V was variable, $\bar{\theta}$ was obtained from $V\bar{\theta}$ by division, using a further servo; but, in most of the work, V was constant and $\bar{\theta}$ was obtained merely by scaling $V\bar{\theta}$ suitably.

From (14), it can be seen that, when v and w are both small, the error signal will be small even when ϕ is substantially in error, and may, in fact,be insufficient to drive the servo. It is also apparent that (14) is satisfied in equilibrium by a value of ϕ differing by 180° from the required value. This would, from (15), produce negative values of $\bar{\theta}$. As a servo problem, these difficulties can be illustrated by a rearrangement of the servo loop.

Define a servo input angle ϕ_i such that

$$\sin \phi_i = v/(v^2+w^2)^{\frac{1}{2}}$$
$$\cos \phi_i = w/(v^2+w^2)^{\frac{1}{2}} \qquad (16)$$

where the square root has the positive sign.

The servo output angle being ϕ_o, it is required to make ϕ_o follow ϕ_i. Substituting (16) in (14), it follows that:

$$\varepsilon = (v^2 + w^2)^{\frac{1}{2}} \sin(\phi_i - \phi_o)$$

$$= (v^2 + w^2)^{\frac{1}{2}} \sin \phi_\varepsilon \qquad (17)$$

where

$$\phi_\varepsilon = \phi_i - \phi_o \ .$$

If, now, the error drives a closed-loop velocity servo of transfer function K/p (at low frequencies), i.e.,

$$\frac{\phi_o}{\varepsilon} = \frac{K}{p} \ ,$$

we have

$$\phi_o = \frac{K}{p} (v^2 + w^2)^{\frac{1}{2}} \sin \phi_\varepsilon \ . \qquad (18)$$

Hence, the re-arranged loop is as in Fig.32(b).

Fig.32(c) is a plot of the error function of equation (17) and the normal linear position-servo error-function, shown by the dotted line AOA. For stability equal to that of a linear position servo formed by feedback at fixed gain around the velocity servo, the slope at the origin of the sinusoid corresponding to the maximum possible value of $(v^2 + w^2)^{\frac{1}{2}}$ must be that of the linear servo characteristic. Thus, when $(v^2 + w^2)^{\frac{1}{2}}$ is less than its maximum, and/or ϕ_ε is not small, the effective slope is reduced and performance suffers. The point B is obviously one of unstable equilibrium, since the slope of the characteristic is negative there. Any disturbance from B will produce a velocity towards O, either clockwise or anticlockwise, according to the direction of the disturbance. Failure to do this would result in a negative $\bar{\theta}$ as well as an error of 180° in ϕ_ε, and hence, ϕ_o.

In the above equations, the quantities v and w are voltages representing the velocities of sideslip, which combine to replace the normal single feedback voltage (derived from a fixed reference voltage) of a linear position servo. If the full scale values of v and w are represented by the same voltage as the above reference voltage, the maximum value of $(v^2 + w^2)^{\frac{1}{2}}$ is $\sqrt{2}$ times that voltage. Thus, under conditions of maximum input and small servo error, the loop gain would be $\sqrt{2}$ times that of the linear servo, and gain adjustment at some other point in the loop is required if the same degree of stability is to be maintained.

To combat the falling loop gain for small inputs, a form of automatic gain control was fitted to the servo, whereby the gain of one amplifier in the loop was raised as the value of $(v^2 + w^2)^{\frac{1}{2}}$ fell. When the shaft is in the correct position, the servo forms the quantity $V\bar{\theta}$ which equals $(v^2 + w^2)^{\frac{1}{2}}$. A small auxiliary electric servo, therefore, was driven by this voltage and arranted to control the main loop gain, as indicated in Fig.32(d). Since rapid changes of v and w were not encountered in the problem, the relatively poor dynamic performance of this small servo was immaterial. Full compensation for values of $(v^2 + w^2)^{\frac{1}{2}}$ right down to zero was not, of course, possible, nor was it necessary. A range of gain of 20:1 was found to be about the limit in practice. Nevertheless, ϕ was placed in the right quadrant provided that the value of $(v^2 + w^2)^{\frac{1}{2}}$ equalled, or exceeded, 0·3 per cent of full scale. At the minimum value, the angle ϕ was correct within

half a degree. The effect of this error on the computed value of $\bar{\theta}_1$ is extremely small and could not be measured. For values of $(v^2 + w^2)^{\frac{1}{2}}$ below 0·3 per cent full scale, the angle ϕ could not be held at or near its correct value, the servo tending to drift at random. Under these conditions, however, $\bar{\theta}$ is sensibly zero and the servo had no function to perform.

The above compensation does not alter the theoretical possibility of unstable point operation. Thus, for example, in single plane working where v may change sign, if the angle ϕ is correctly defined for one particular sign, the duty of the servo is to switch as rapidly as possible through 180° as v passes through zero, thus maintaining $\bar{\theta}$ positive. In theory, there is no signal to do this, since ε is always zero but, in practice, there are small drift voltages within the loops which, with the A.G.C. system, receive sufficient gain to switch the servo over.

A simple and yet accurate statement of the servo's dynamic performance cannot be given, realistic inputs being very difficult to specify and reproduce. A test was made in which v and w were sine and cosine signals of the same frequency and amplitude. Under these conditions, the servo shaft rotates at constant speed equal to the circular frequency of the inputs, and lags behind the input vector by a fixed angle which is a measure of performance. Unfortunately, although interesting as a demonstration, this provides no information which is not already known from the constants of the closed-loop velocity servo part of the system.

To approach more nearly an operating condition found in the roll stability investigations, the v and w channels were fed with equal large D.C. pedestal voltages to which small sine-wave signals of equal amplitude, but in exact anti-phase, were added. Such combined inputs produce approximate simple harmonic motion of the ϕ shaft about the $\phi = 45°$ position, and the frequency response method was employed to determine the lag. For inputs consisting of 1 c.p.s. waveforms of r.m.s. amplitude 0·5 per cent full scale on pedestal voltages of 50 per cent full scale, the measurements indicated a rough correspondence to a simple lag of about 40 m.s. At half this frequency and at an r.m.s. amplitude of 1·2 per cent full scale, the equivalent lag was roughly halved.

It was demonstrated by various means, such as the incorporation of phase advance external to the servo, increasing loop gain by a factor of 2 and decreasing loop gain by a factor of 10, that such lags as were present in the ϕ servo did not affect the overall accuracy of the simulation significantly. The servo was, therefore, considered satisfactory.

APPENDIX 3

SIMULATOR FAULTS AND ACCURACY

The fully extended model required some 400 amplifiers to simulate the missile homing in three dimensions, and a further 100 on additional requirements such as the computation of miss distance and total lateral acceleration, and for noise generation. Most of the available capacity and special features of TRIDAC were required, and the problem of keeping the computer "on the rails" became formidable. Much time, therefore, had to be spent in tracing and eradicating faults in the equipment.

Two main types of fault were encountered. The more difficult to cure was the intermittent fault, which would be indicated by a lack of repeatability in homing runs without noise. Such faults were often due to poorly mating uniters in the amplifier brick units. The other main type of fault was that due to the total or partial failure of a component. In this case, the output could be seen to be incorrect when a standard check run was made and the results compared with those of a digital solution. If the fault was not indicated by the automatic monitoring system, as frequently happened, the simulation had to be broken down and tested in sections until the faulty unit was isolated. The tracing of these faults was made more difficult by the many closed loops in the system. Here, the digital solutions were of great assistance.

When the simulator was producing repeatable results, which compared reasonably well with the digital solutions, the main concern was the lack of equality of the miss distance values in homing against targets performing symmetrical manoeuvres. For example, a turn of the target to right or left in the horizontal plane, following a head-on approach, would result in different miss distances, the values depending on the direction of turn.

Prolonged efforts were made to reduce this asymmetry, but the final scatter in miss distance values for noise-free targets making 2g turns in either horizontal or vertical planes was of the same order of magnitude as the miss distance itself. However, within the limits of a 2g target manoeuvre, it was not possible to obtain miss distances greater than 16 ft from a 20,000 ft range, unless noise was introduced.

Fig.30 compares the TRIDAC results with those obtained digitally in the case of single plane homing. The initial range was varied from 20,000 ft downwards. It will be seen that, in spite of the scatter of the simulator results, the general trend of the digital results is confirmed. Four configurations were investigated, namely, target turning upwards, or downwards, in the vertical plane, or to port or starboard horizontally. Hence, four values of miss distance were obtained for each initial range. At values of the latter exceeding 10,000 ft, all four results were valid but, at shorter ranges, some amplifiers in the system were overloaded.. Re-scaling to overcome this was not considered worthwhile as the overloading occurred only when the amplifier output voltage was negative. Consequently, at ranges less than 10,000 ft, there are only two values of miss distance.

The digital and analogue results in three dimensions are compared in Fig.31. In this case, the initial range was kept constant, but the initial roll angle was varied. At each value of the latter, four values of miss distance were obtained, namely, two by simulating the manoeuvre and its mirror image in the yaw plane, and two by repeating the process in the pitch plane. The scatter of the results is attributable to small inaccuracies in the axis transformations which could not be removed. It will be noted, however, that, over much of the range, the mean of the four values at each angle is close to the digital result.

The miss distances shown in Figs.30 and 31 were measured in dish axes, so the digital results shown are not the same as those in Figs.23 and 25, which represent true minimum ranges.

The criterion used to measure the asymmetries of the simulation was the maximum change in the total incidence $\bar{\theta}$ (expressed as a percentage of its full scale value of 0·6 radians) due to changing the sign of the input to the system. In the homing simulation this meant comparing a symmetrical pair of target manoeuvres. In the case of the missile alone, it meant changing the sign of the demands. When biases were deliberately introduced, both signs of bias were used in turn, and the change in $\bar{\theta}$ was divided by twice the modulus of the bias, giving the change in $\bar{\theta}$ per unit bias.

The asymmetries are shown in Table 3. It will be seen that the representation of the missile control system and its aerodynamics was extremely symmetrical. When the homing system was added, and a stationary target was used, so that the earth to missile transformation was not required, the asymmetry in $\bar{\theta}$, in single plane, approached 0·5 per cent, f.s., and that between single planes at 90° averaged 1·0 per cent, f.s.

In single plane homing on to a 2g turning target, the asymmetry was greater, and had a value between 0·4 per cent and 1·7 per cent, f.s., depending on the plane and the sense of the turn. Also, the difference between the two single planes at 90° increased, and asymmetries up to 3 per cent, f.s. occurred. With homing in three dimensions, the asymmetry in one plane was between 1·0 and 2·5 per cent f.s., and, between planes at 90° asymmetries of up to 8 per cent, f.s. occurred. The repeatability of individual results in all runs was better than 1·5 per cent f.s.

It was suspected that much of the asymmetry was due to the resolution of the sine and cosine potentiometers on the hydraulic servo-resolvers, which is limited to one part in 900. To investigate this, two series of tests were conducted after all the sine and cosine potentiometers had been carefully set up and trimmed, and the gains and time constants of the system checked. The first tests were concerned with the intrinsic symmetry of the resolvers and the effects of the limited potentiometer resolution, while the second set investigated the effects of small biases deliberately introduced into the simulation.

The symmetry of the servo-resolvers was ascertained by reversing the sign of the drive to each resolver in turn and, after correcting the signs of the outputs from the sine potentiometers, running the single plane homing with the particular servo-resolver in the reversed condition. As shown in Table 4, in three out of the four cases, the asymmetry was affected by up to 1 per cent full scale.

The terms of the axis transformations which were thought to be inaccurate were $u_{TEE} \sin Y_G$ and $u_{TEE} \cos Y_G \sin Z_G$, in the earth to missile transformation, and $u_{TMM} \sin \psi_D$ and $u_{TMM} \cos \psi_D \sin \theta_D$ in the missile to dish axis transformation. These terms were suspect because appreciable voltages were normally applied to the ends of the sine potentiometers, and the wire to wire movement of the wiper at small shaft angles produced noticeable steps in the output voltage. Also, setting up the potentiometer on the resolver unit could only be done to within ± one half turn, owing to the position of the centre tap.

In order to assess the effect of these wire to wire steps, the sine terms were approximated to by setting $\sin Y_G = Y_G$, etc, and the multiplications were accomplished on the improved electric servo-multipliers[11] referred to elsewhere in this Note. The approximation made it possible to

improve the accuracy by increasing the range of angular displacement of the servo shaft, thus effectually reducing the size of the wire to wire steps by increasing their number. (The resolution of the servo is 0·1 per cent.) An improvement in symmetry of some 0·75 per cent (full scale) resulted but, since large gimbal angles occurred during homing, the approximation could not be retained for general use.

An attempt was then made to improve matters by using two sine potentiometers in parallel. This effected a noticeable improvement in symmetry in the case of $u_{TMM} \sin \psi_D$, and the additional potentiometer was installed permanently. A further improvement was made by replacing the wire-wound feedback potentiometers on two of the servo-resolvers by carbon film potentiometers of the same basic linearity but of much higher resolution. This was done in the case of both servo-resolvers used in the pitch plane in single plane simulation and an improvement in symmetry of 0·5 per cent f.s. was observed. Unfortunately, no more of these potentiometers were available at the time.

A static check of the complete earth to missile axis transformation was made by setting the gimbal angles at preselected values and applying a suitable input voltage in one co-ordinate at a time. The output voltages in all cases were accurate to within 0·5 per cent of the full scale value (i.e. the input voltage). This compares with a static accuracy of 0·3 per cent f.s. for individual resolver units tested by Inspection Department, R.A.E.

Biases were introduced into the simulation of single plane homing in both single planes, and also when simulating homing in three dimensions. The biases were intended to represent possible errors in setting up the sine and cosine potentiometers, and errors in the alignment of the feedback potentiometers of the servo-resolvers. Each of these errors could amount to one half turn of the wire on the potentiometer. The effects of these biases are presented in terms of the maximum change in the value of $\bar{\theta}$ per turn error in the setting of the potentiometer, expressed as a percentage of the full scale value of $\bar{\theta}$, when homing on a target making a 2g turn from a head-on approach. A further type of error simulated by the biases was drift in the voltage representing the angular velocity drive to the servo-resolvers. The effects of this are presented as the maximum change in $\bar{\theta}$ per millivolt of drift, expressed as a percentage of the full scale value of $\bar{\theta}$.

The significant results are listed in Table 5. These show that, for two dimensional homing, the alignment of the dish servo shaft, and of its sine potentiometer operating on u_{TMM}, had an important effect on the results - accuracy being important since u_{TMM} was large - while misalignment of the axis transformation servo shaft and its sine potentiometer operating on u_{TEE} had a lesser effect. Drift in the drive to the dish servo had no effect, while a small change was caused by drift in the servo of the earth to missile transformation.

In three dimensional homing, the most important effect was due to misalignment of the sine potentiometers forming $u_{TEE} \sin Y_G$ and $u_{TEE} \cos Y_G \sin Z_G$ in the earth to missile axis transformation of the target velocity. This affected the results to the extent of causing over 2 per cent maximum change in $\bar{\theta}$, expressed as a percentage of full scale per turn of misalignment.

The next most important effect was that due to biasing of the sine potentiometers involved in generating the components of dish spin rates depending on the missile roll rate, but it was an order of magnitude smaller than the previous one. All the other biases which were applied to the

the servo-resolver drives and shaft initial positions, the sine potentiometers of the missile to dish axis transformation, the earth to missile axis transformation of v_{TEE} and w_{TEE}, and the generation of components of p_s - the dish axial spin - from the missile pitch and yaw rates, had a minor effect.

These tests indicated that the lack of symmetry in the simulation was mostly due to inaccuracies in certain terms of the axis transformations containing sines of the gimbal angles. A secondary cause of error was probably small drifts in parts of the model not in a feedback loop. The drive to the earth to missile axis transformation is a case in point.

It is probable that the accuracy of the axis transformations could be improved by the use of carbon film pencil potentiometers in critical positions. A prototype is under development. A further improvement is to be expected from fitting carbon film feedback potentiometers to all the hydraulic servo-resolvers and multipliers.

More recently, it has come light that drifts have been occurring in some integrators, which have not been indicated by the monitoring system. These may have explained some day to day variations in the results which caused much trouble and loss of time. The short term stability of the simulator was generally very good.

TABLE 1

Basic data on D.4 and W.2 (V.R.725) as simulated

	Units	D.4	W.2 (V.R.725)
Missile Dimensions Length	Feet	18·8	20·8
Body Max. Diameter	Feet	1·71	1·75
Wing Span	Feet	5·33	5·33
Distance from datum(wing tip leading edge)to tail hinge	Feet	5·16	5·96
Reference Area S	$Feet^2$	1·767	1·767
Reference Length c	Feet	1·5	1·5
Mass			
At end of boost	Slugs	60·7	73·5
At end of sustainer	Slugs	39·8	53·1
Used in simulation	Slugs	59·8	59·9
Moment of Inertia A			
Used in simulation	Slug ft^2	36·6	31·2
Moments of Inertia B and C			
Used in simulation	Slug ft^2	887·1	1177
Distance of C.G. ahead of datum (wing tip leading edge)			
Used in simulation	Inches	6·3	8·5
Shift during burning of sustainer motor	Inches	1·9	5·0
Maximum incidence of wind tunnel tests			
(Nominal) M = 1·6		22°	35°
M = 2·0		25°	40°

TABLE 2

Control surface deflection coefficients

$D_z = D_m / \bar{x}_h$

$D_y = -D_n / \bar{x}_h$

$D_\ell\ (\theta\ \phi\ -\sigma_1) = -D_\ell\ (\theta\ 180 - \phi\ \sigma_1)$

$D_m\ (\theta\ \phi\ -\sigma_1) = -D_m\ (\theta\ 180 - \phi\ \sigma_1)$

$D_n\ (\theta\ \phi\ -\sigma_1) = +D_n\ (\theta\ 180 - \phi\ \sigma_1)$

$D_\ell\ (\theta\ \phi\ \sigma_2) = +D_\ell\ (\theta\ \phi + 90\ \sigma_1)$ $\quad$ $D_\ell\ (\theta\ \phi\ -\sigma_2) = -D_\ell\ (\theta\ 90 - \phi\ \sigma_1)$

$D_m\ (\theta\ \phi\ \sigma_2) = -D_m\ (\theta\ \phi + 90\ \sigma_1)$ $\quad$ $D_m\ (\theta\ \phi\ -\sigma_2) = -D_m\ (\theta\ 90 - \phi\ \sigma_1)$

$D_n\ (\theta\ \phi\ \sigma_2) = +D_n\ (\theta\ \phi + 90\ \sigma_1)$ $\quad$ $D_n\ (\theta\ \phi\ -\sigma_2) = -D_n\ (\theta\ 90 - \phi\ \sigma_1)$

$D_\ell\ (\theta\ \phi\ \sigma_3) = +D_\ell\ (\theta\ \phi + 180\ \sigma_1)$ $\quad$ $D_\ell\ (\theta\ \phi\ -\sigma_3) = -D_\ell\ (\theta\ 360 - \phi\ \sigma_1)$

$D_m\ (\theta\ \phi\ \sigma_3) = -D_m\ (\theta\ \phi + 180\ \sigma_1)$ $\quad$ $D_m\ (\theta\ \phi\ -\sigma_3) = +D_m\ (\theta\ 360 - \phi\ \sigma_1)$

$D_n\ (\theta\ \phi\ \sigma_3) = -D_n\ (\theta\ \phi + 180\ \sigma_1)$ $\quad$ $D_n\ (\theta\ \phi\ -\sigma_3) = -D_n\ (\theta\ 360 - \phi\ \sigma_1)$

$D_\ell\ (\theta\ \phi\ \sigma_4) = +D_\ell\ (\theta\ \phi + 270\ \sigma_1)$ $\quad$ $D_\ell\ (\theta\ \phi\ -\sigma_4) = -D_\ell\ (\theta\ 270 - \phi\ \sigma_1)$

$D_m\ (\theta\ \phi\ \sigma_4) = +D_m\ (\theta\ \phi + 270\ \sigma_1)$ $\quad$ $D_m\ (e\ \phi\ -\sigma_4) = +D_m\ (\theta\ 270 - \phi\ \sigma_1)$

$D_n\ (\theta\ \phi\ \sigma_4) = -D_n\ (\theta\ \phi + 270\ \sigma_1)$ $\quad$ $D_n\ (\theta\ \phi\ -\sigma_4) = +D_n\ (\theta\ 270 - \phi\ \sigma_1)$

$\xi = \frac{1}{2}(\sigma_1 + \sigma_3) = \frac{1}{2}(\sigma_2 + \sigma_4)$ $\quad$ $\sigma_1 = \eta + \xi$

$\eta = \frac{1}{2}(\sigma_1 - \sigma_3)$ $\quad$ $\sigma_2 = \zeta + \xi$

$\zeta = \frac{1}{2}(\sigma_2 - \sigma_4)$ $\quad$ $\sigma_3 = -\eta + \xi$

$\sigma_4 = -\zeta + \xi$

D_ℓ, D_m, D_n represent the changes in the respective moment coefficients resulting from the deflection from zero of one control panel. Couplings between panels are neglected.

TABLE 3

Observed asymmetries in $\bar{\theta}$, maximum change in $\bar{\theta}$: % full scale

(3% F.S. ≙ 1° change in $\bar{\theta}$)

Target Manoeuvre	Dimensional complexity of problem	Asymmetries	
		In-Plane	Between Planes at 90°
Missile alone	3	0-0·1	0·1-0·3
Offset stationary target (range = 20 K ft)	2	0·3-0·5	0·5-1·5
2g target (" ")	2	0·4-1·7	2·0-3·0
2g target (" ")	3	1·0-2·5	3·0-8·0
Repeatability with 2g target	3	0-1·5	0-1·5

TABLE 4

Effect of modifications on asymmetry, maximum change in $\bar{\theta}$: % full scale

Modification	Dimensional Complexity of Problem	Maximum Change	Notes
Reversal of dish servo in			
(a) Yaw,	2	0·5	
(b) Pitch	2	1·0	
Reversal of gimbal servo in			
(a) Yaw,	2	0	
(b) Pitch	2	0·5	
Replacement of sine potentiometers by high performance electric servo multipliers in			Approximation, only valid for small shaft angles
(a) Yaw,	2	0·75	
(b) Pitch	2	0·75	
Paralleling sine potentiometers on dish servo resolver in			Permanently installed
(a) Yaw,	2	2·0	
(b) Pitch	2	0	
Paralleling sine potentiometers on gimbal servo resolver in			
(a) Yaw,	2	0	
(b) Pitch	2	0·5	
Carbon film feedback potentiometers fitted to the servo resolvers in Pitch plane	2	0·5	Outputs considerably smoother

TABLE 5

Asymmetries due to applied biases

Maximum change in $\bar{\theta}$: % full scale

Quantity Biased	Dimensional Complexity of Problem	In-Plane Asymmetry Resulting
u_{TEE} sin (gimbal angle)	2	0·2 per turn
Gimbal position (initial)	2	0·2 per turn
Gimbal drive	2	0·2 per mV
u_{TMM} sin (dish angle)	2	0·6 per turn
Dish initial position	2	0·6 per turn
Dish drive	2	0 per mV
u_{TEE} sin (gimbal angle)	3	1·4-2·2 per turn
p sin (dish angle)	3	0·1 per turn

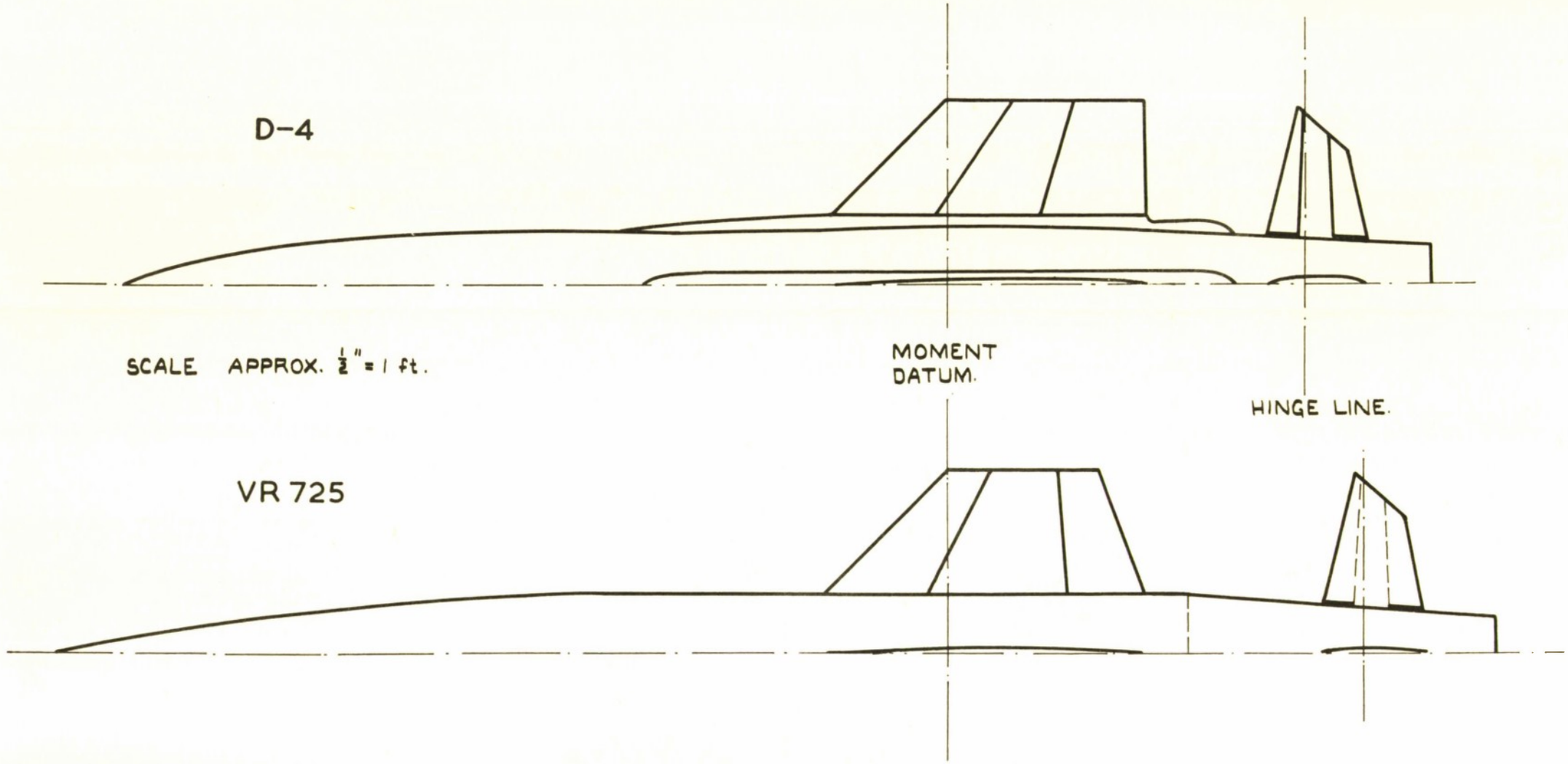

FIG. 1. APPROXIMATE HALF SECTIONS OF D4 & VR725.

FIG. 2

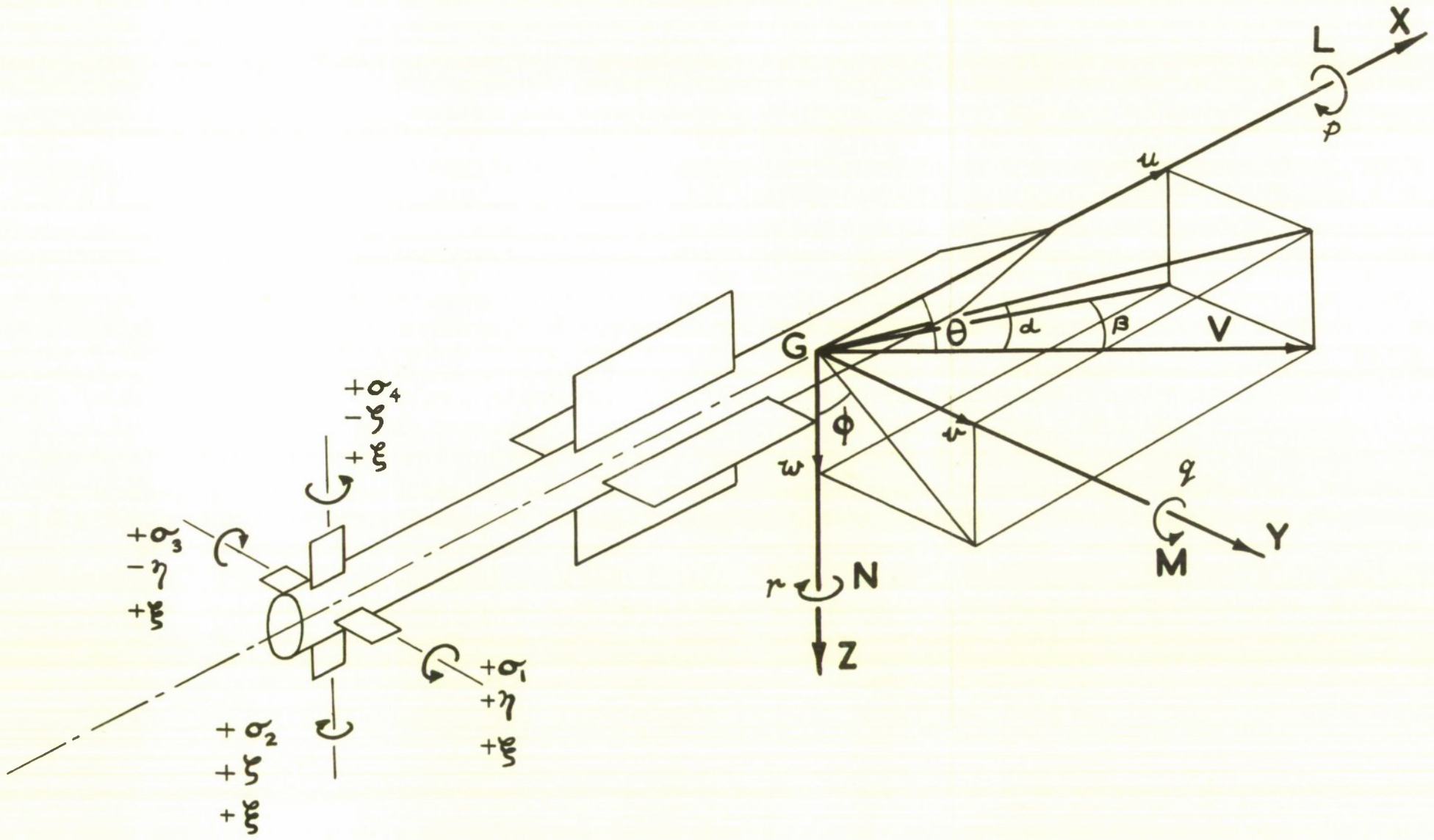

FIG. 2. DIAGRAMMATIC REPRESENTATION OF MISSILE

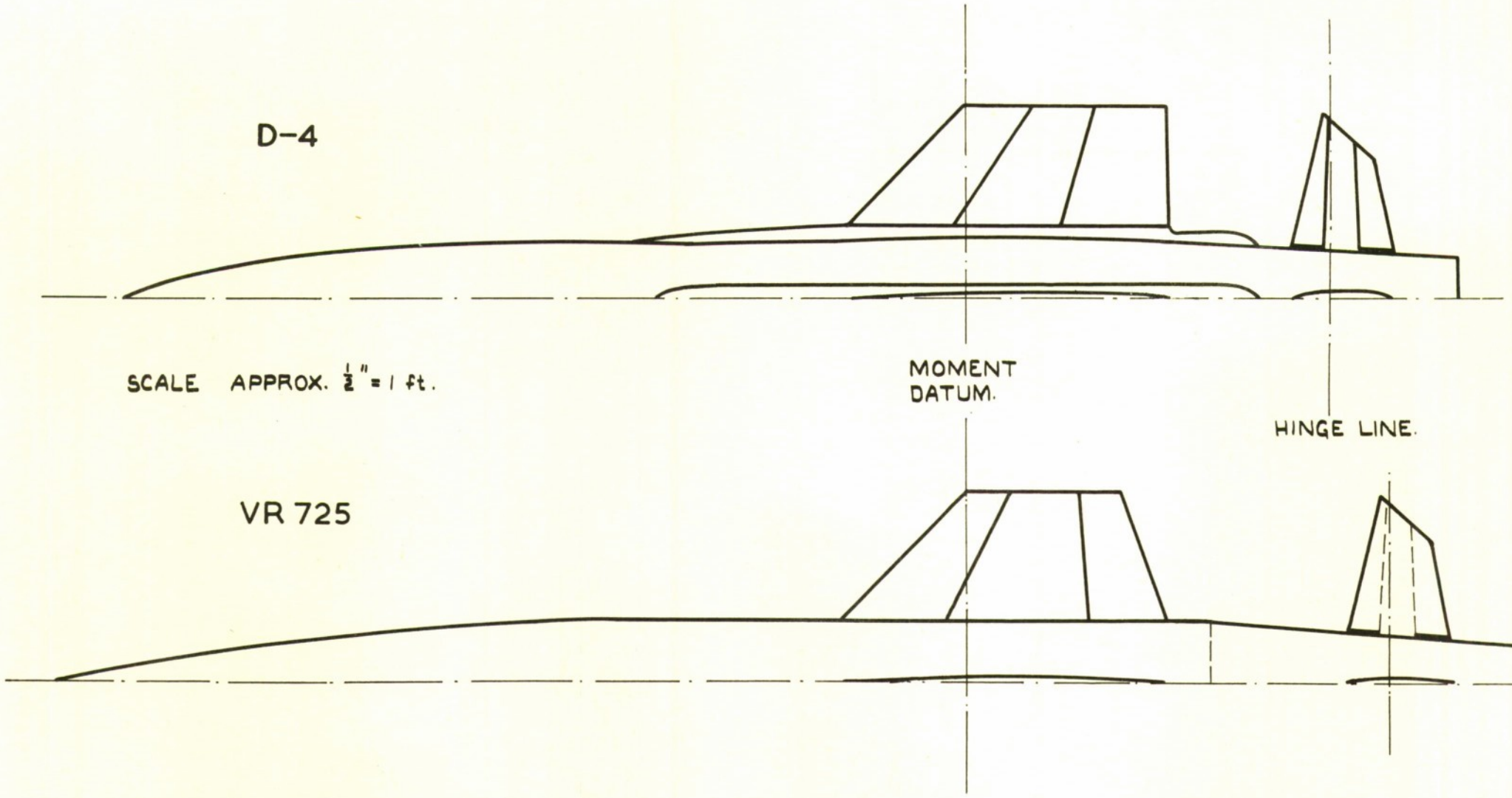

FIG. 1. APPROXIMATE HALF SECTIONS OF D4 & VR725.

T.N.WES FIG. 1.

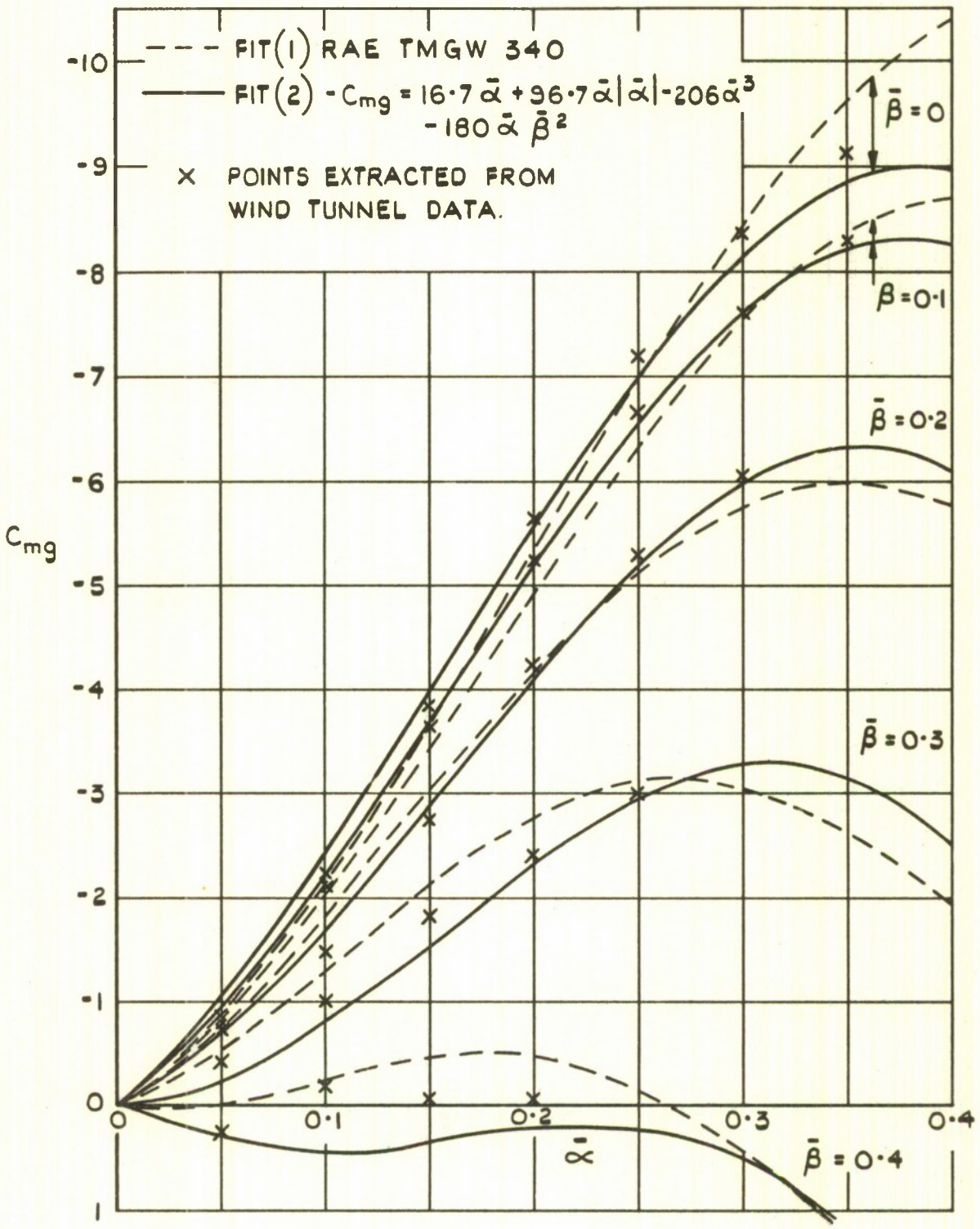

FIG. 3. POLYNOMIAL FITS TO D-4 PITCHING MOMENT DATA.

MACH No. 1·58

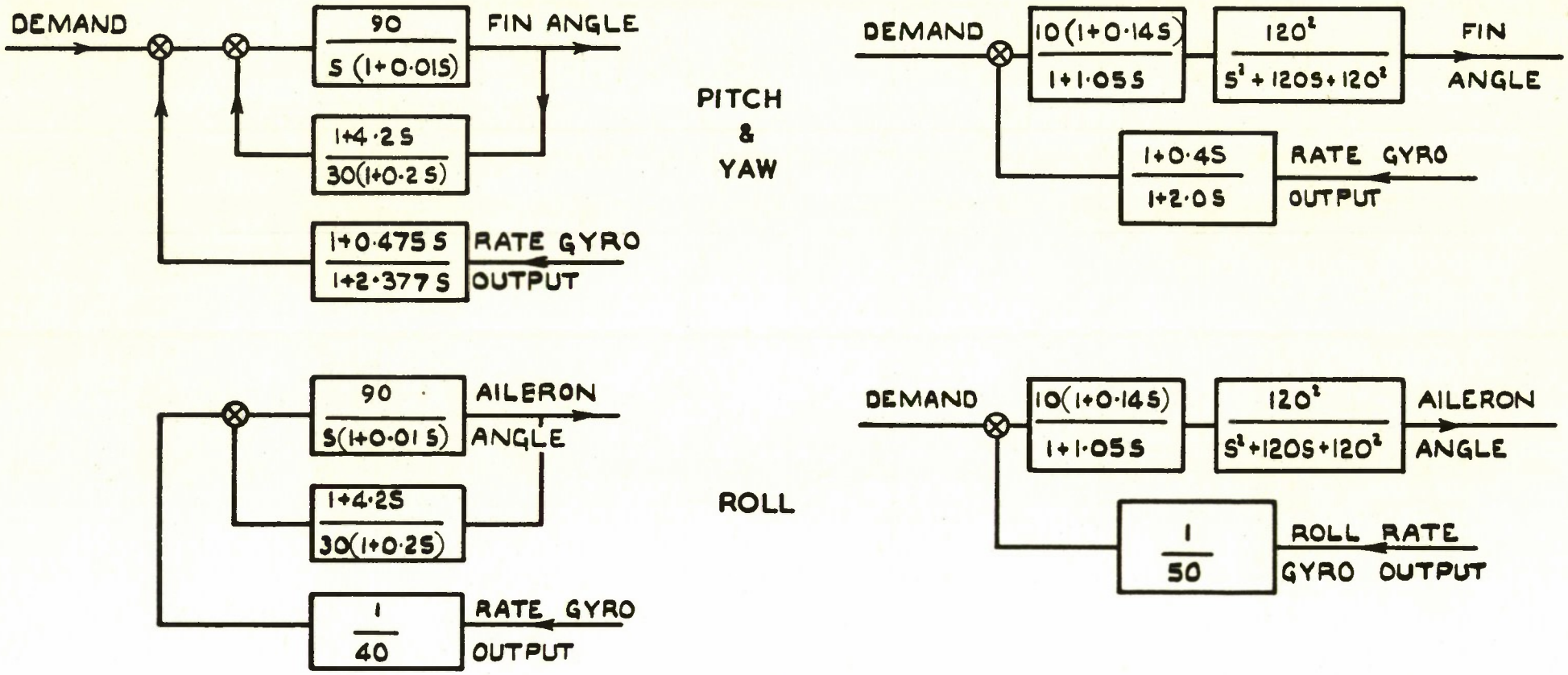

(a) WITH D-4 AERODYNAMICS

(b) WITH VR 725 AERODYNAMICS

FIG. 4. (a. & b.) AUTOPILOTS USED IN THE SIMULATION.

T.N. WE. 5
FIG. 4. (a. & b.)

FIG. 5.

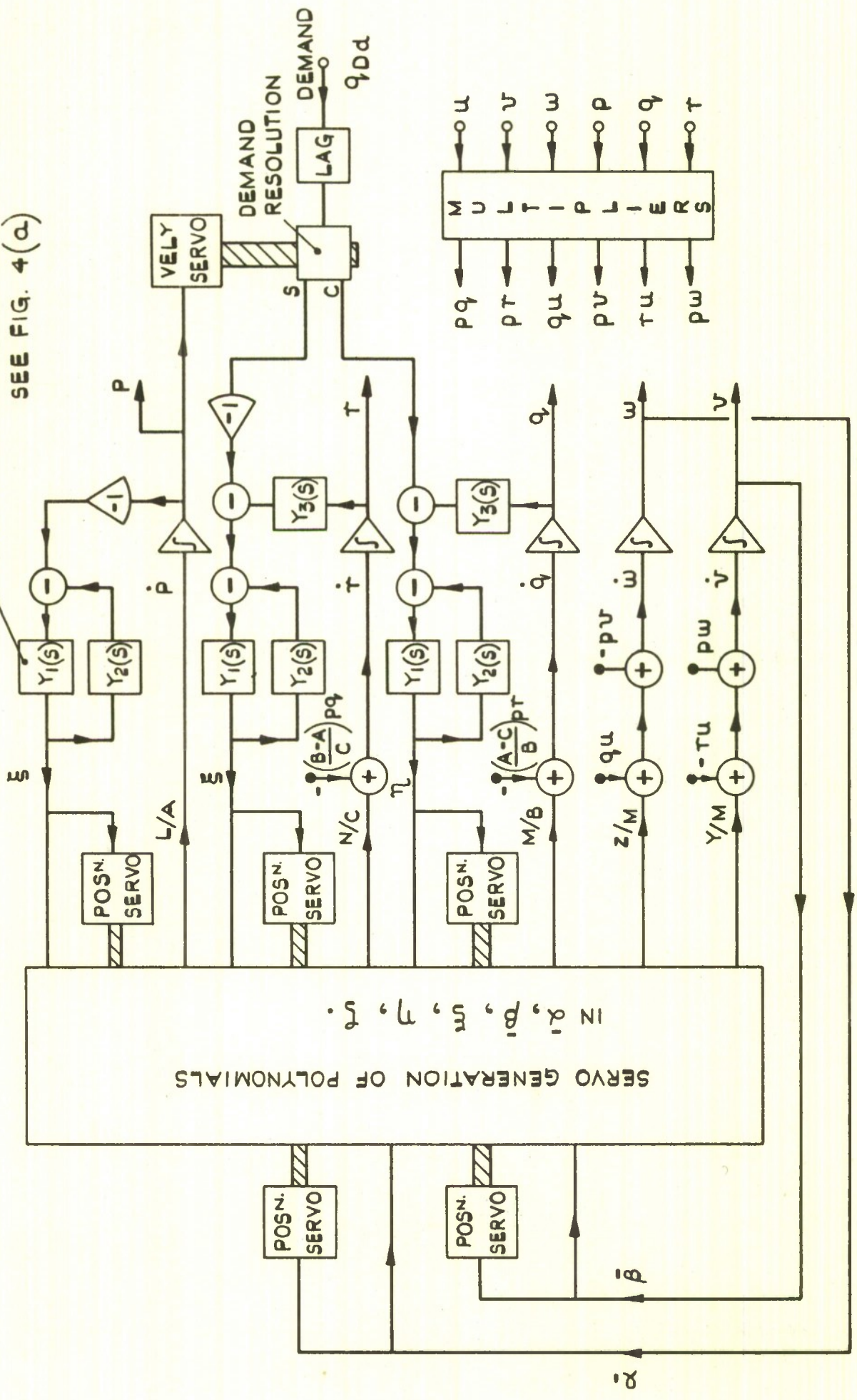

FIG. 5. BLOCK DIAGRAM OF D4 SIMULATION.

FIG. 6.

$C'_m = F_1(\theta, M) + F_2(\theta, M)\cos 4\phi.$

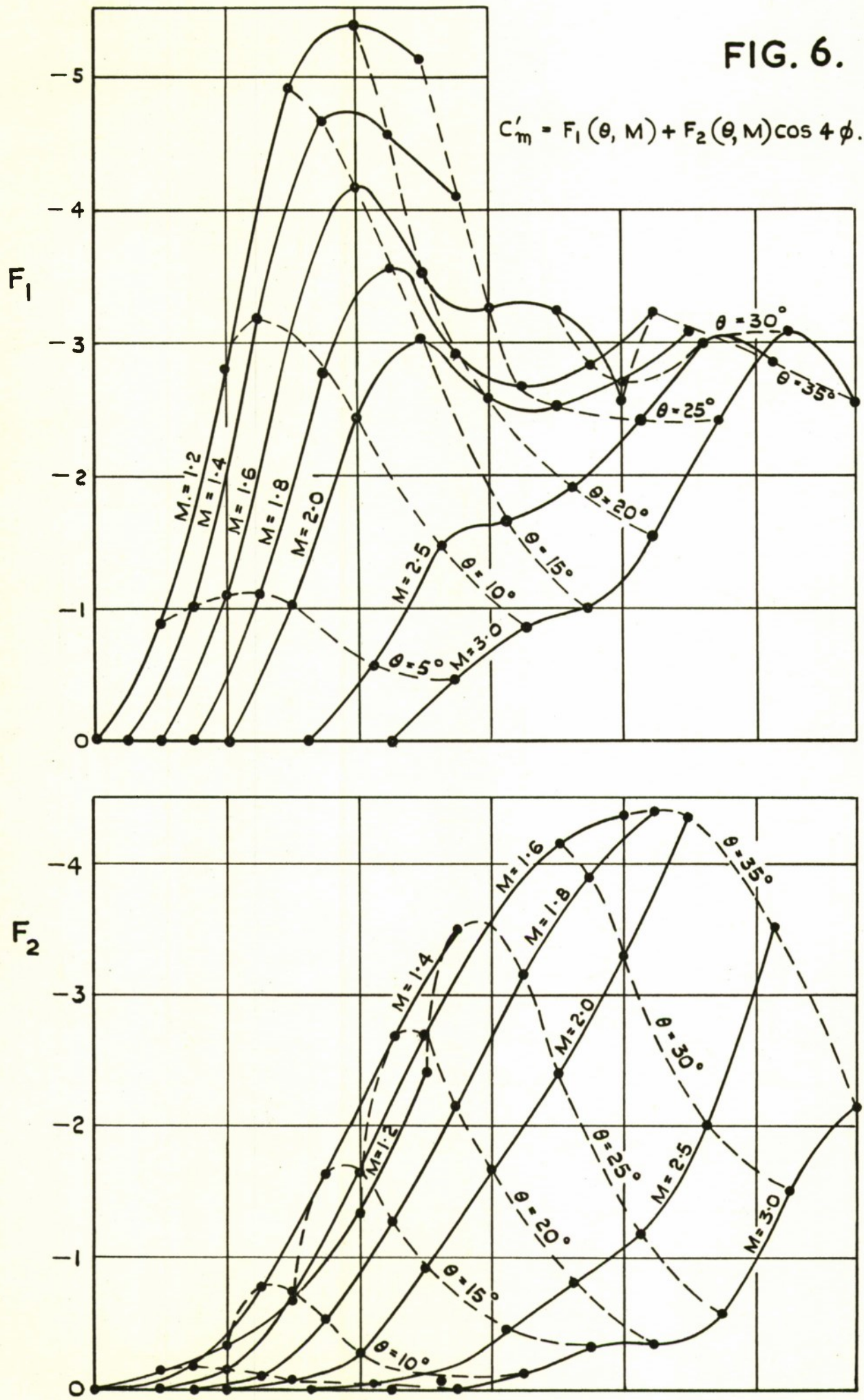

TAIL-FIXED AERODYNAMICS OF V.R. 725 MODEL.

FIG. 6. F-FUNCTIONS CONTRIBUTING C'_m.

FIG. 7.

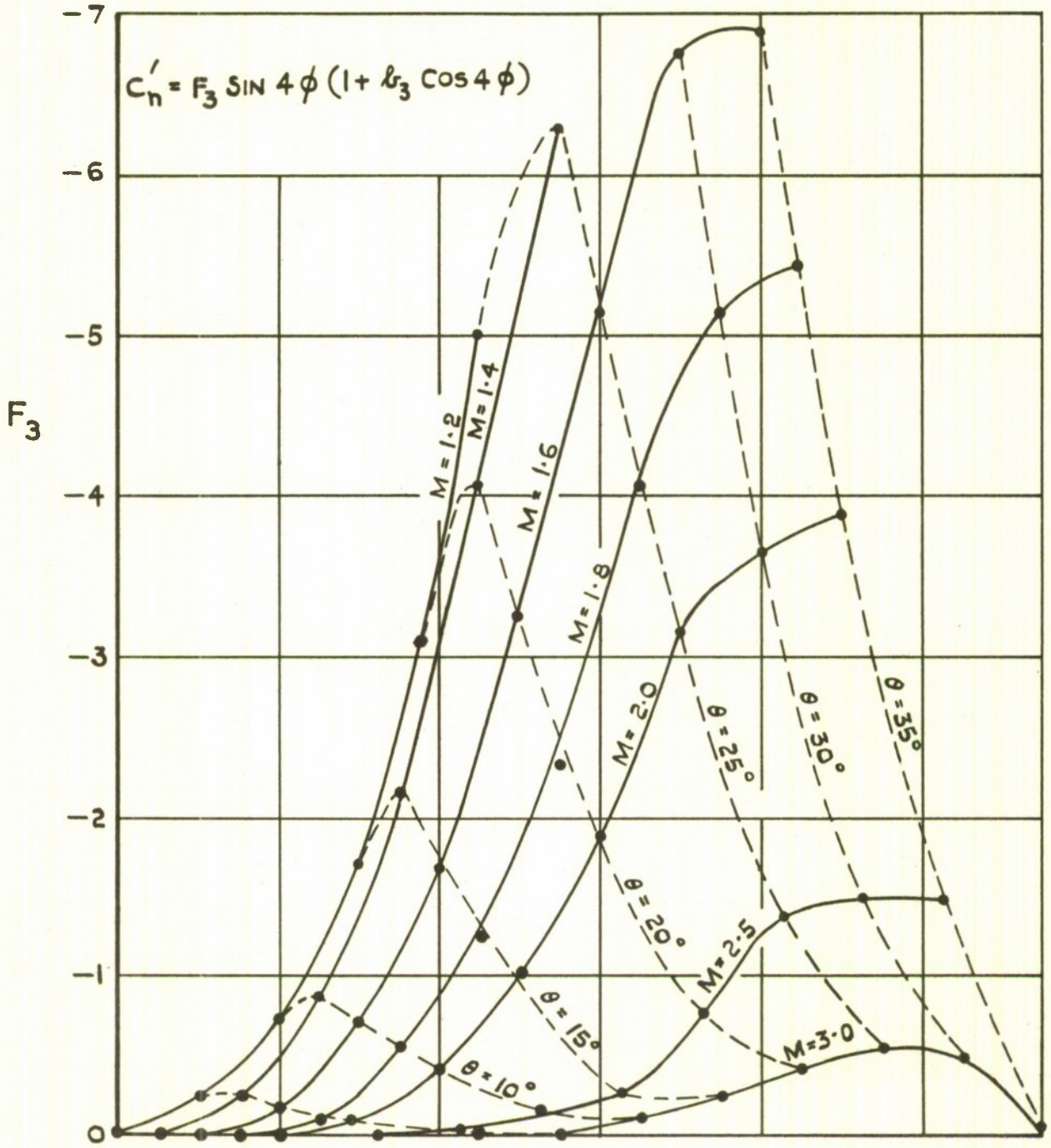

FIG.7. F-FUNCTION CONTRIBUTING TO C_n'.

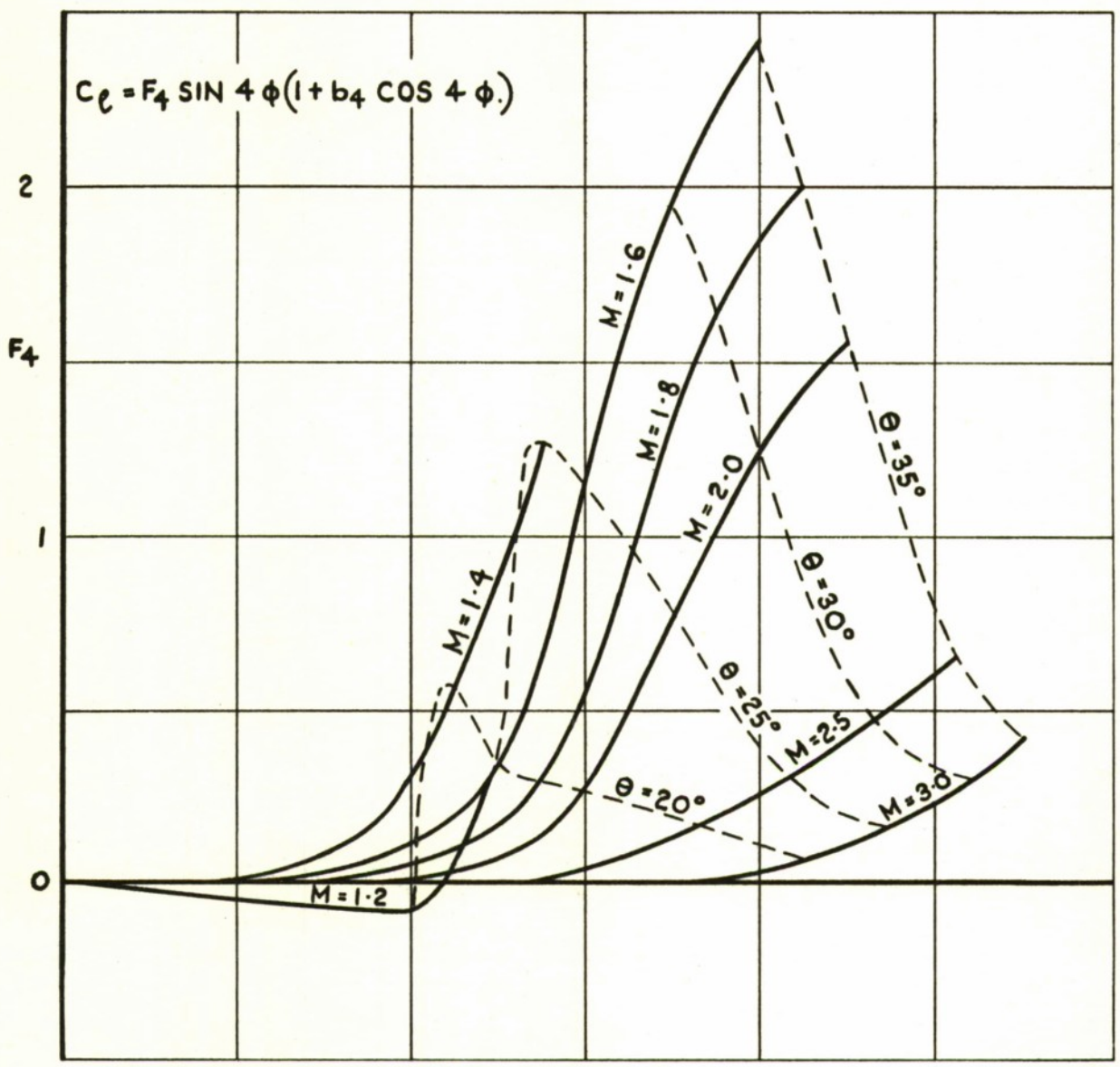

FIG. 8. F-FUNCTION DEFINING INDUCED ROLLING MOMENT.

FIG. 9.

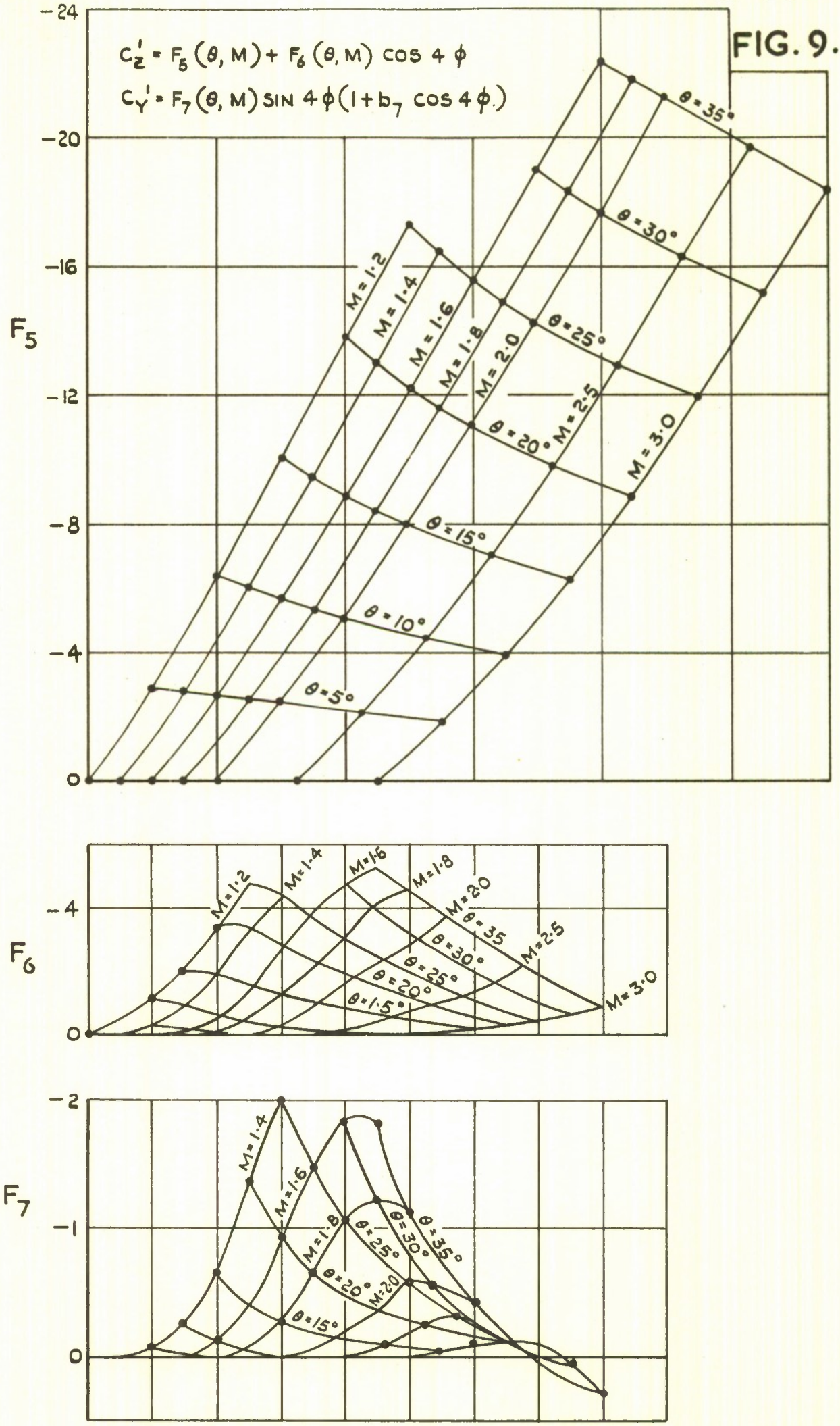

FIG. 9. F-FUNCTIONS CONTRIBUTING TO NORMAL FORCES

FIG. 10.

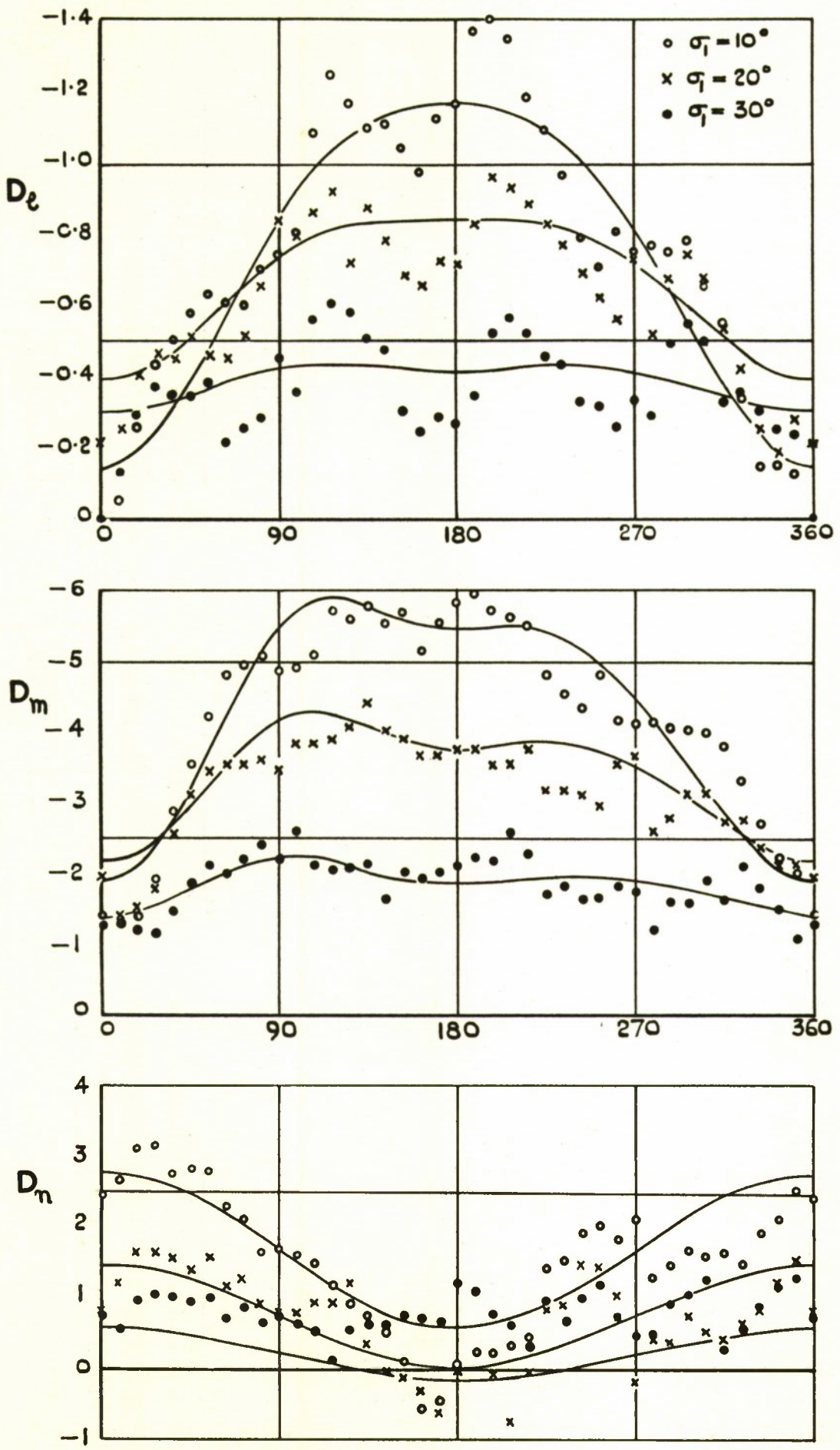

FIG. 10. VARIATION OF D-FUNCTIONS WITH ROLL ANGLE ϕ.
$\theta = 20°$, $M = 1{\cdot}6$, $\sigma = 10°, 20°, 30°$.
(SEE TABLE 2)

FIG. II.

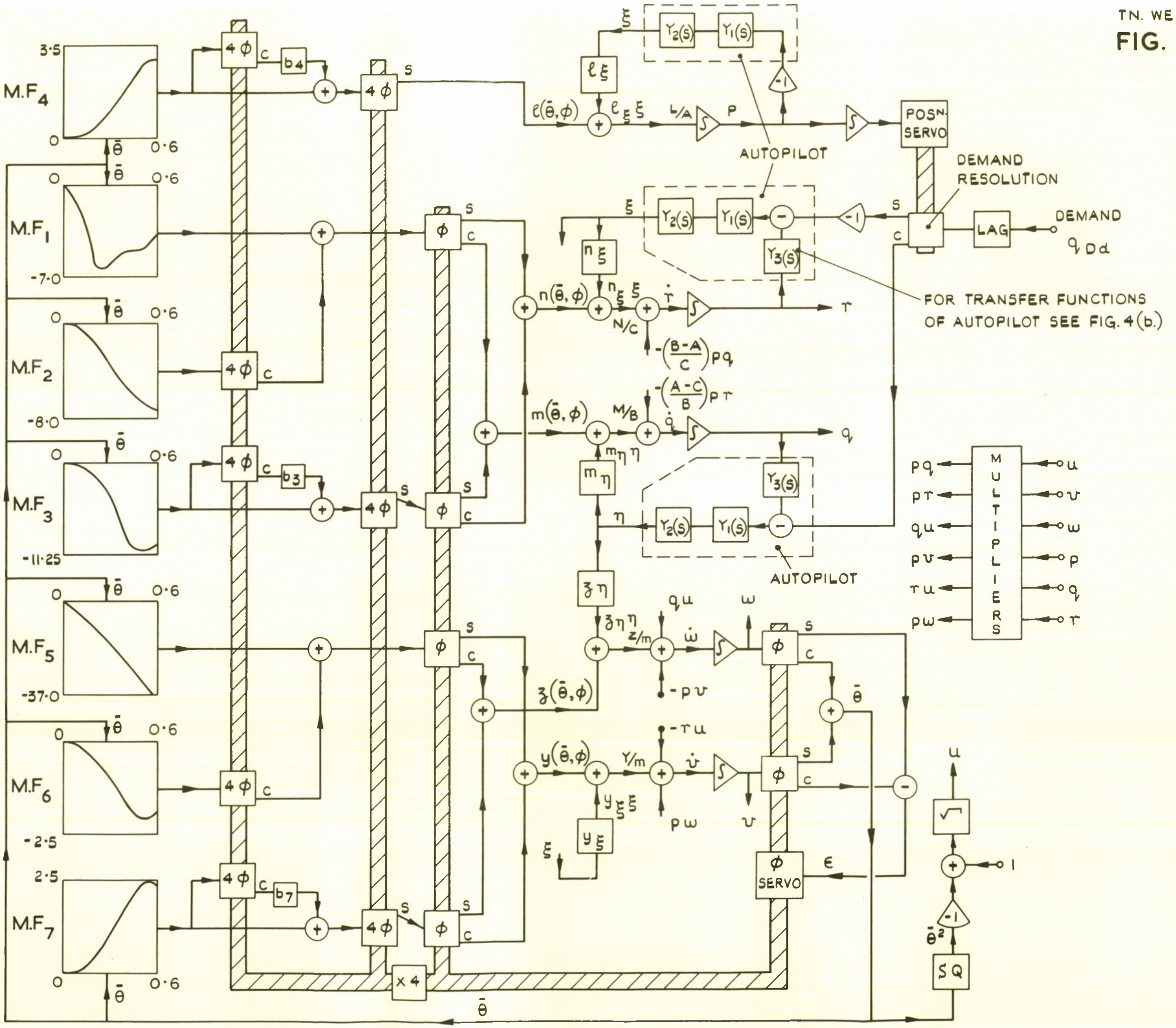

FIG. II. BLOCK DIAGRAM OF VR 725 SIMULATION AT CONSTANT MACH No.,

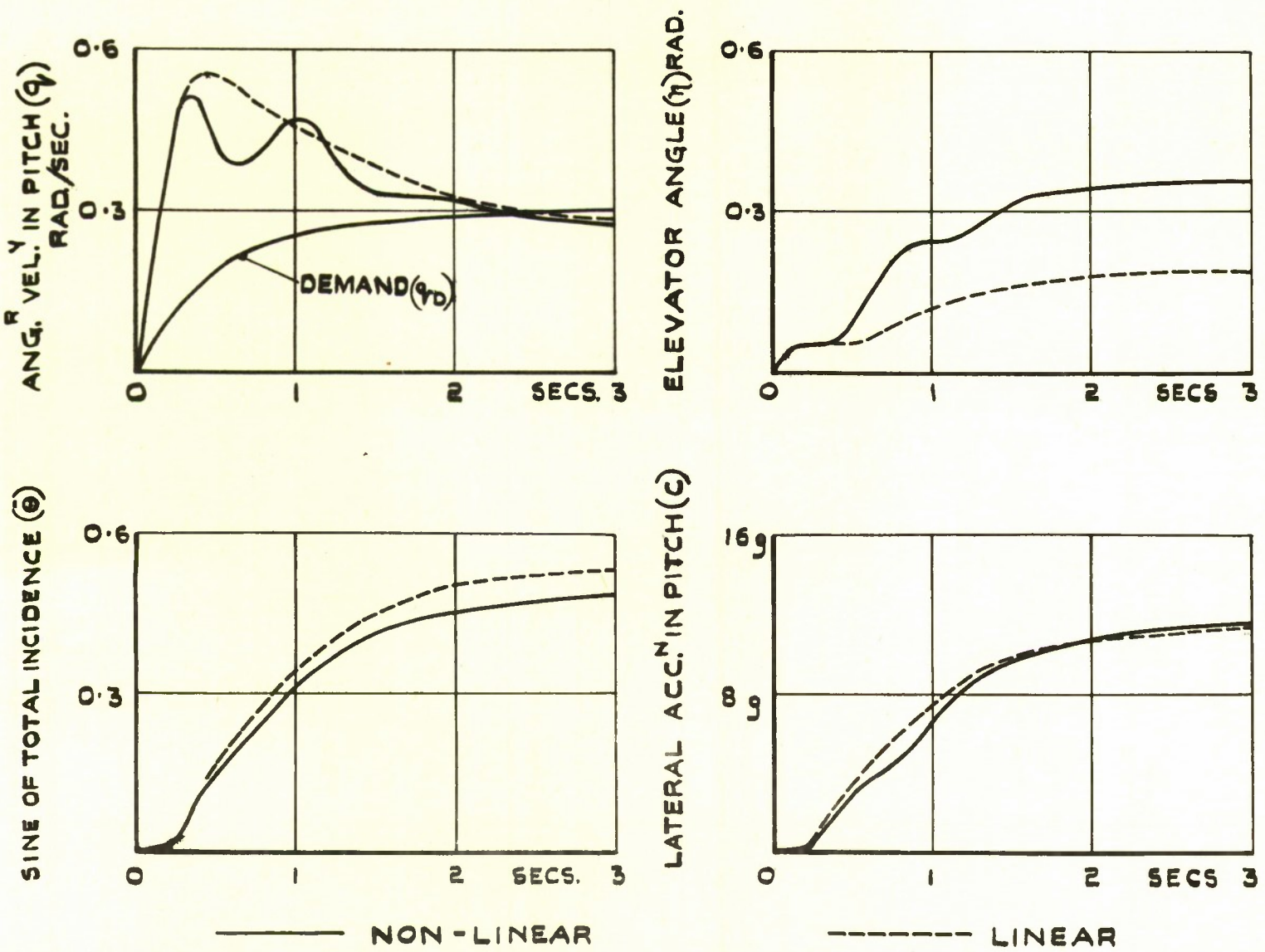

FIG. 12 RESPONSE OF MODEL IN SINGLE PLANE TO RATE OF PITCH DEMAND WITH LINEAR AND NON-LINEAR AERODYNAMICS.

T. N. WE 5
FIG. 13

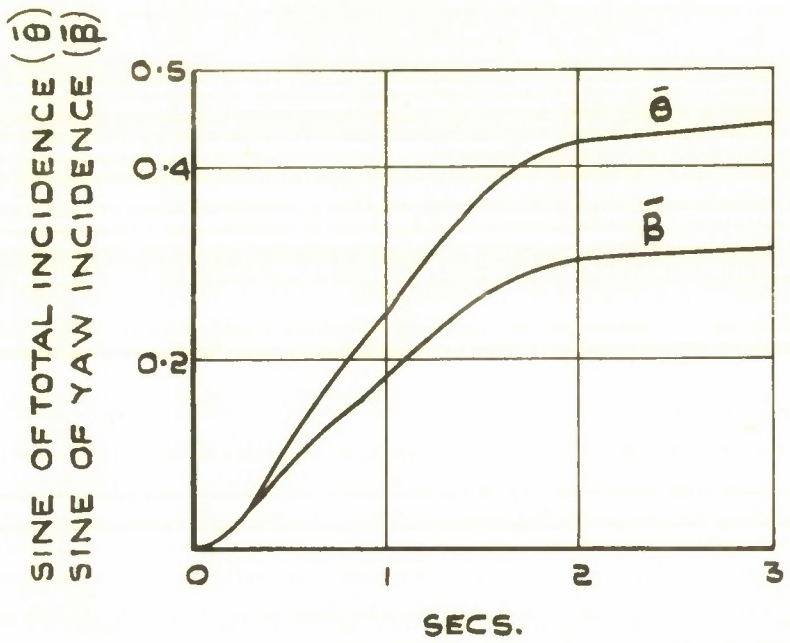

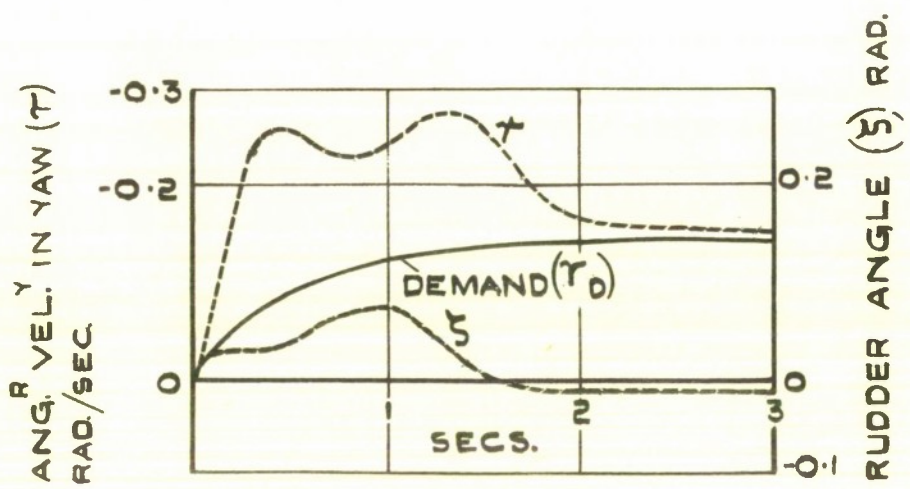

FIG. 13 YAW PLANE RESPONSE OF MODEL TO EQUAL YAW & PITCH RATE DEMANDS.

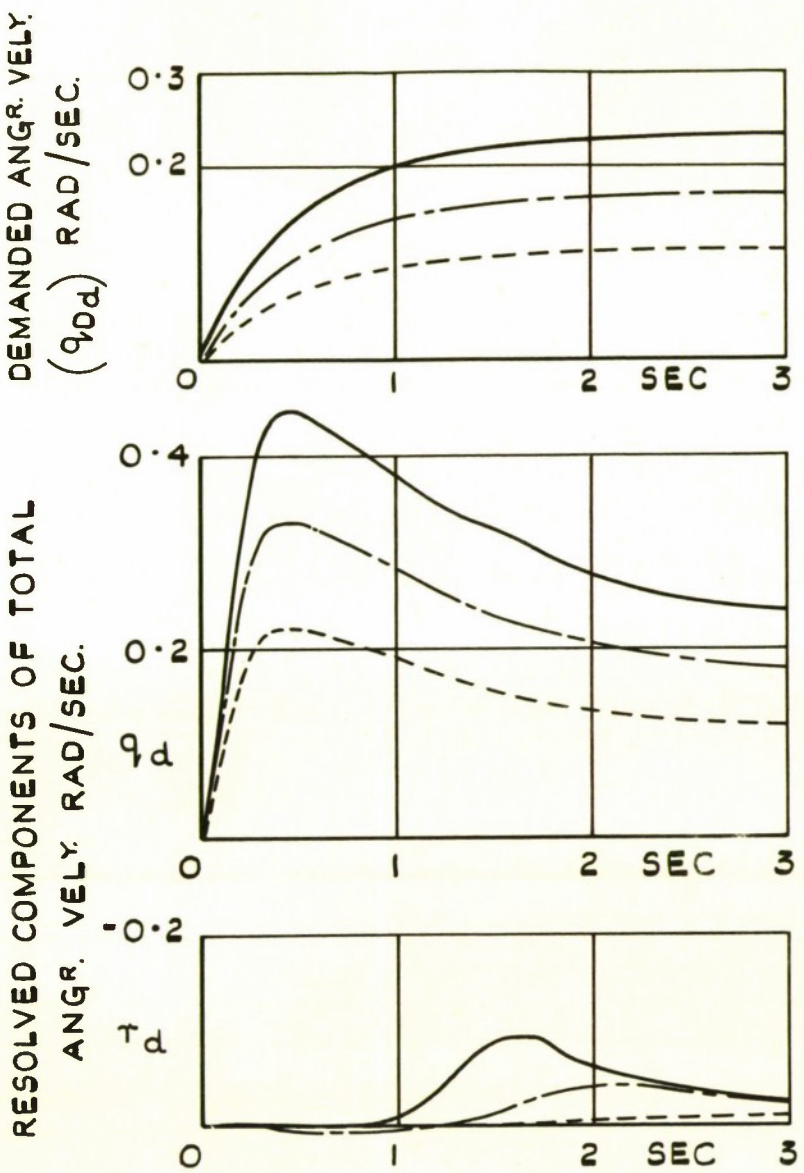

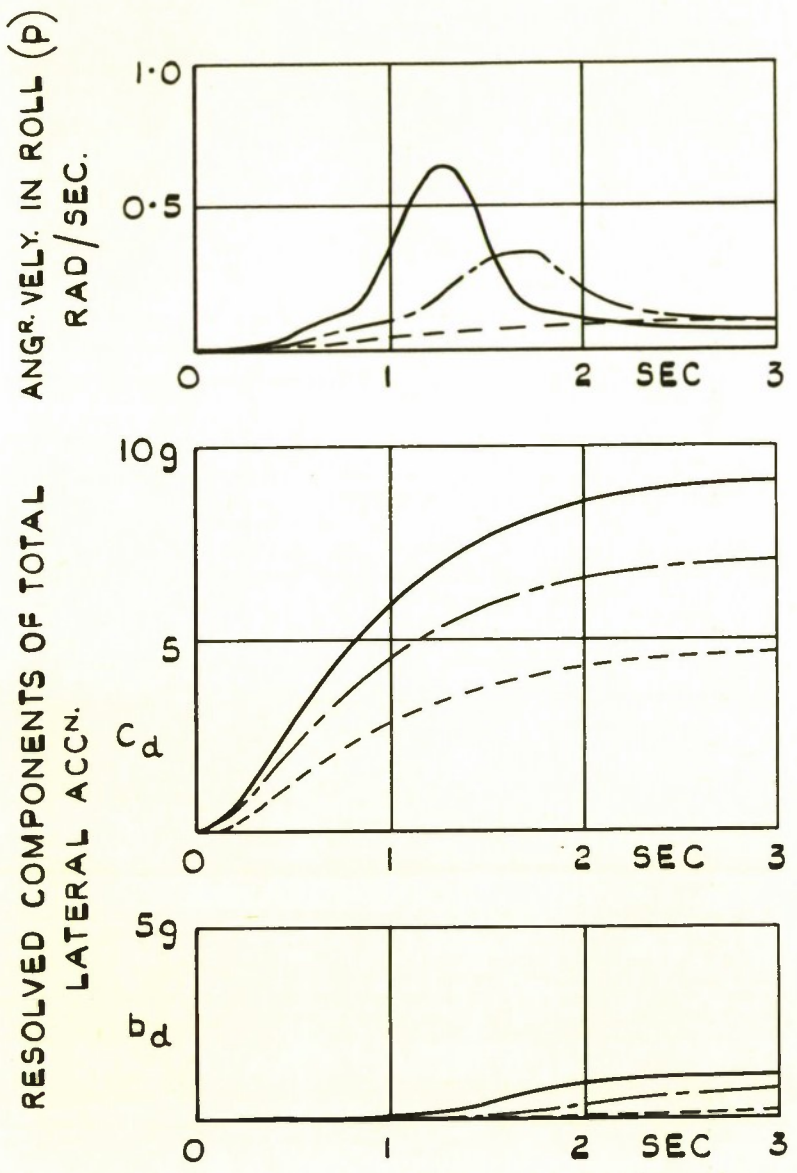

NOTE :- SUFFIX d DENOTES MEASUREMENT IN ROLL-STABILISED AXES.
THE ROLL AXIS COINCIDING WITH THAT OF THE MISSILE
WHICH HAS AN INITIAL ROLL ANGLE $X_{GO} = 5°$

FIG. 14. RESPONSE OF MODEL IN 3 DIMENSIONS TO 3 DEMANDS FOR ANGULAR VELOCITY IN ROLL STABILISED AXES.
LINEAR BODY-WING AND CONTROL SURFACE AERODYNAMICS.

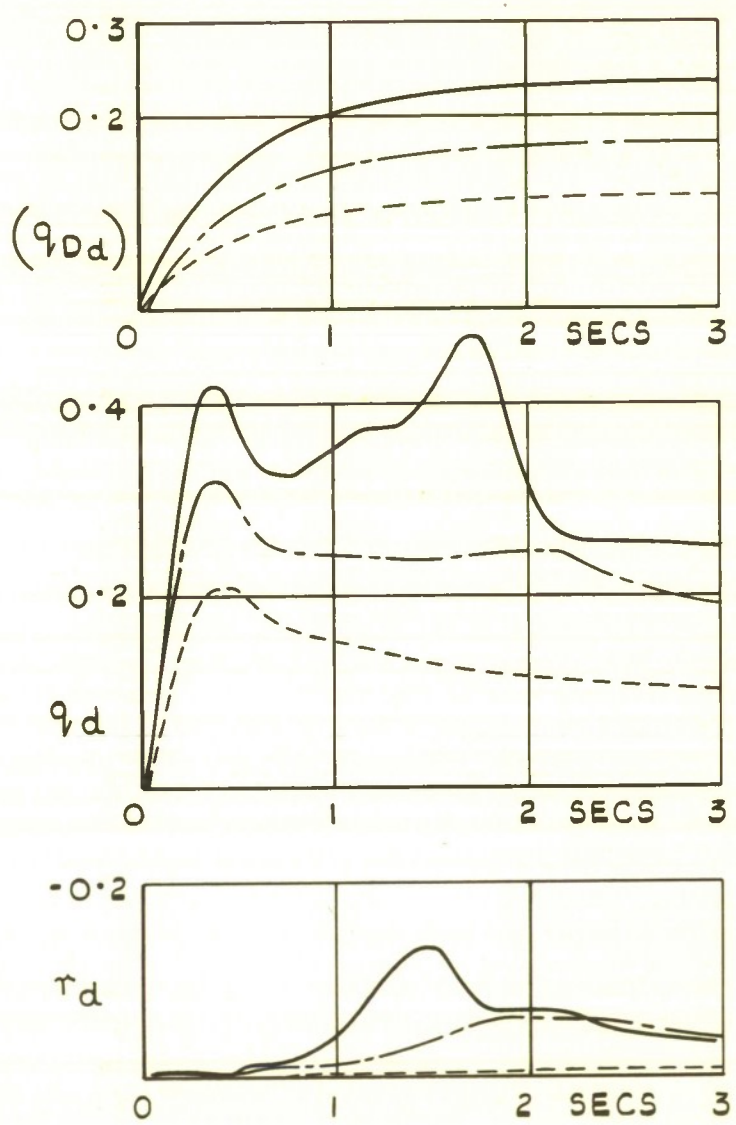

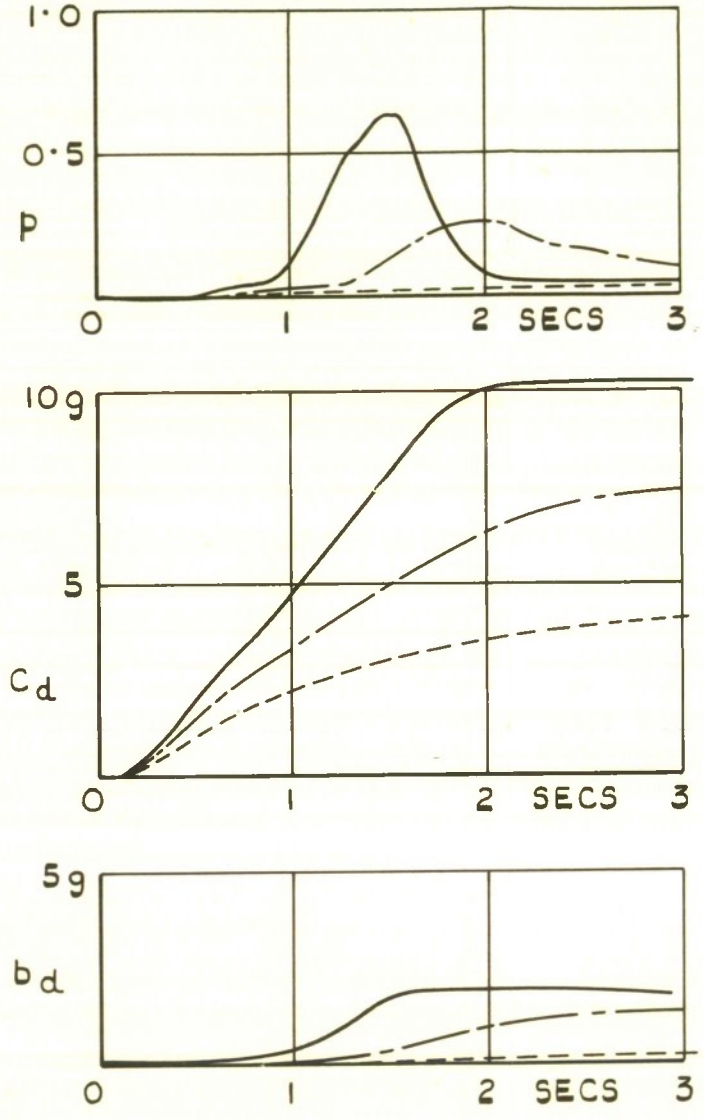

NOTE :- SUFFIX d DENOTES MEASUREMENT IN ROLL-STABILISED AXES. THE ROLL AXIS COINCIDING WITH THAT OF THE MISSILE WHICH HAS AN INITIAL ROLL ANGLE $X_{GO} = 5°$

FIG. 15. RESPONSE OF MODEL IN 3 DIMENSIONS TO 3 DEMANDS FOR ANGULAR VELOCITY IN ROLL STABILISED AXES.
NON-LINEAR BODY-WING AND LINEAR CONTROL SURFACE AERODYNAMICS.

TN. WE 5
FIG. 16

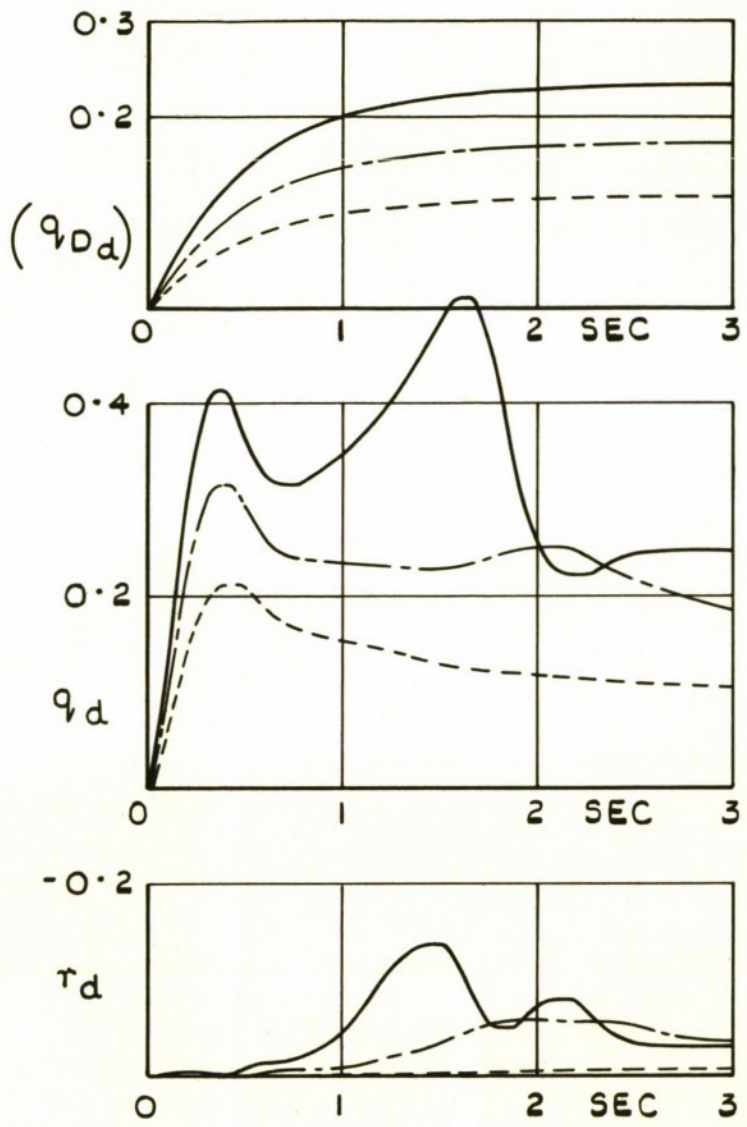

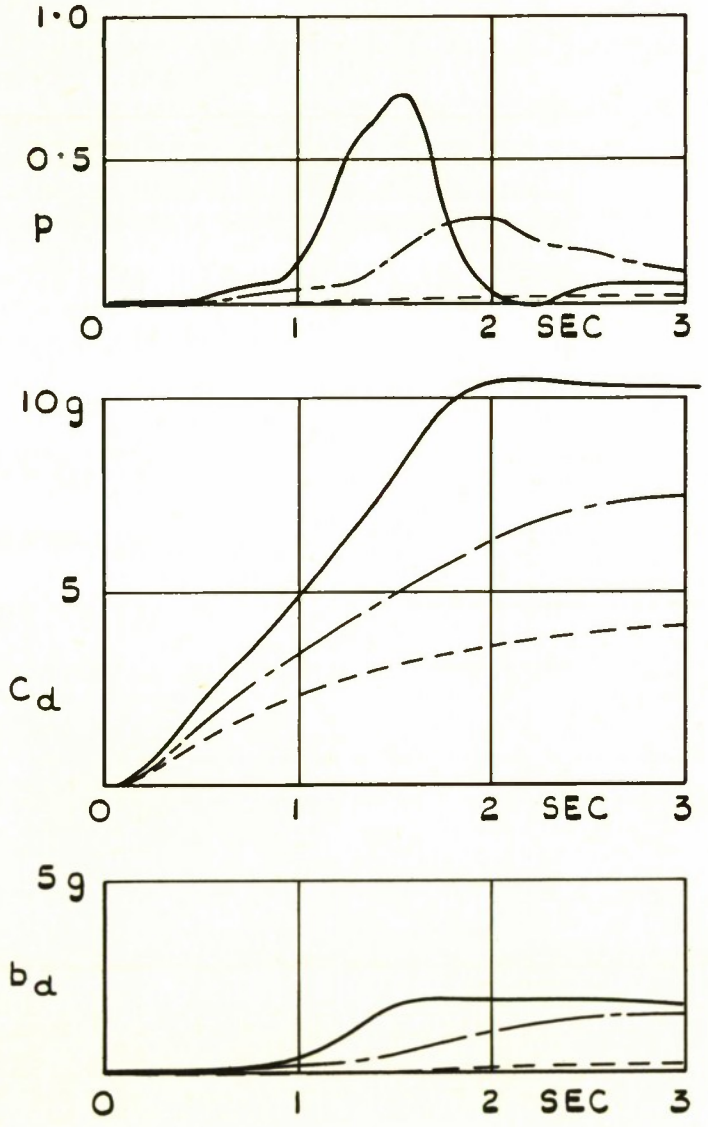

NOTE:- SUFFIX d DENOTES MEASUREMENT IN ROLL STABILISED AXES.
THE ROLL AXIS COINCIDING WITH THAT OF THE MISSILE
WHICH HAS AN INITIAL ROLL ANGLE $X_{GO} = 5°$

FIG. 16. RESPONSE OF MODEL IN 3 DIMENSIONS TO 3 DEMANDS FOR ANGULAR VELOCITY IN ROLL STABILISED AXES.
NON-LINEAR BODY-WING AND CONTROL SURFACE AERODYNAMICS.

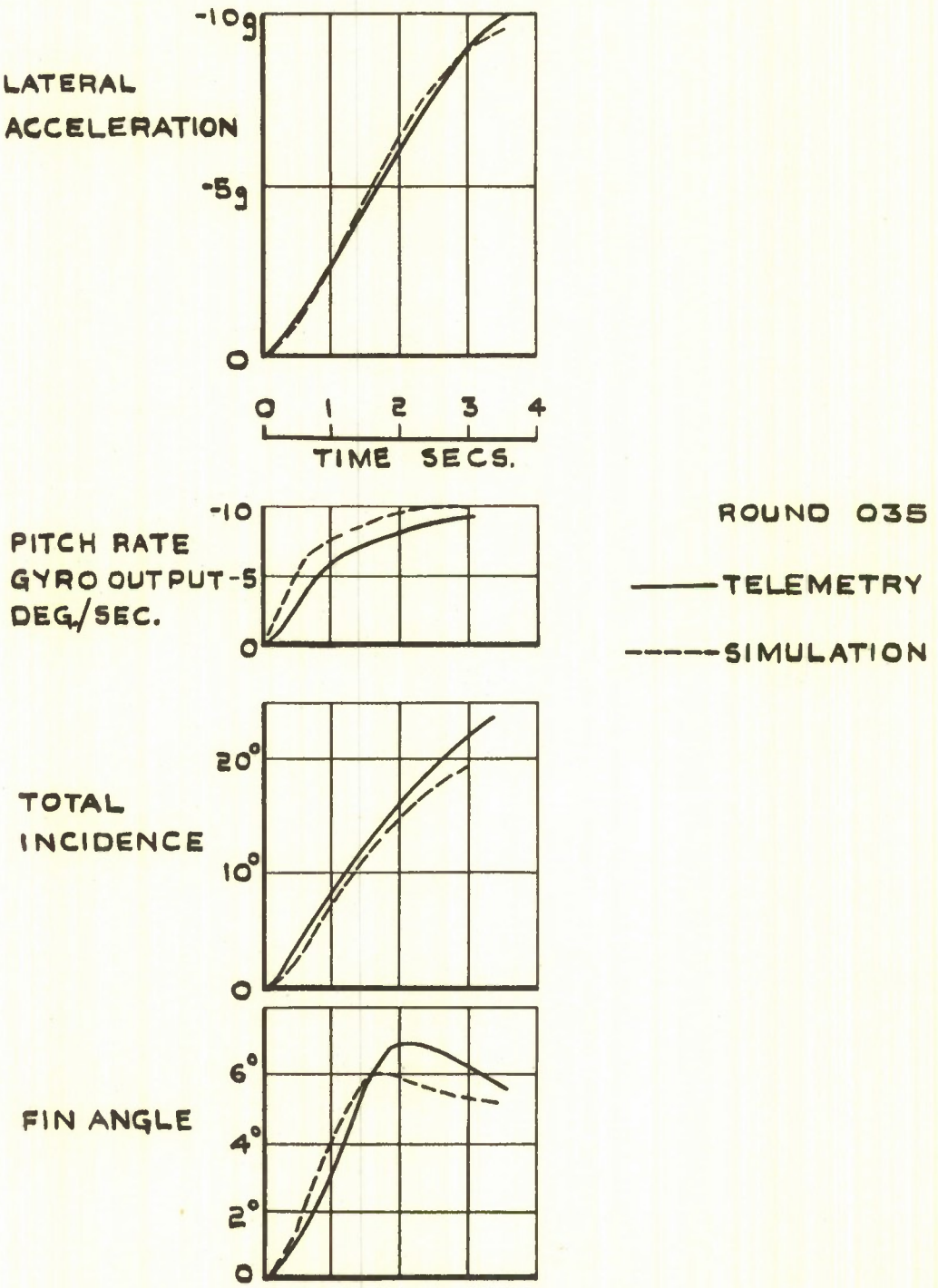

FIG. 17 COMPARISON OF SIMULATION WITH TELEMETRY RECORDS FOR ROUND 035.

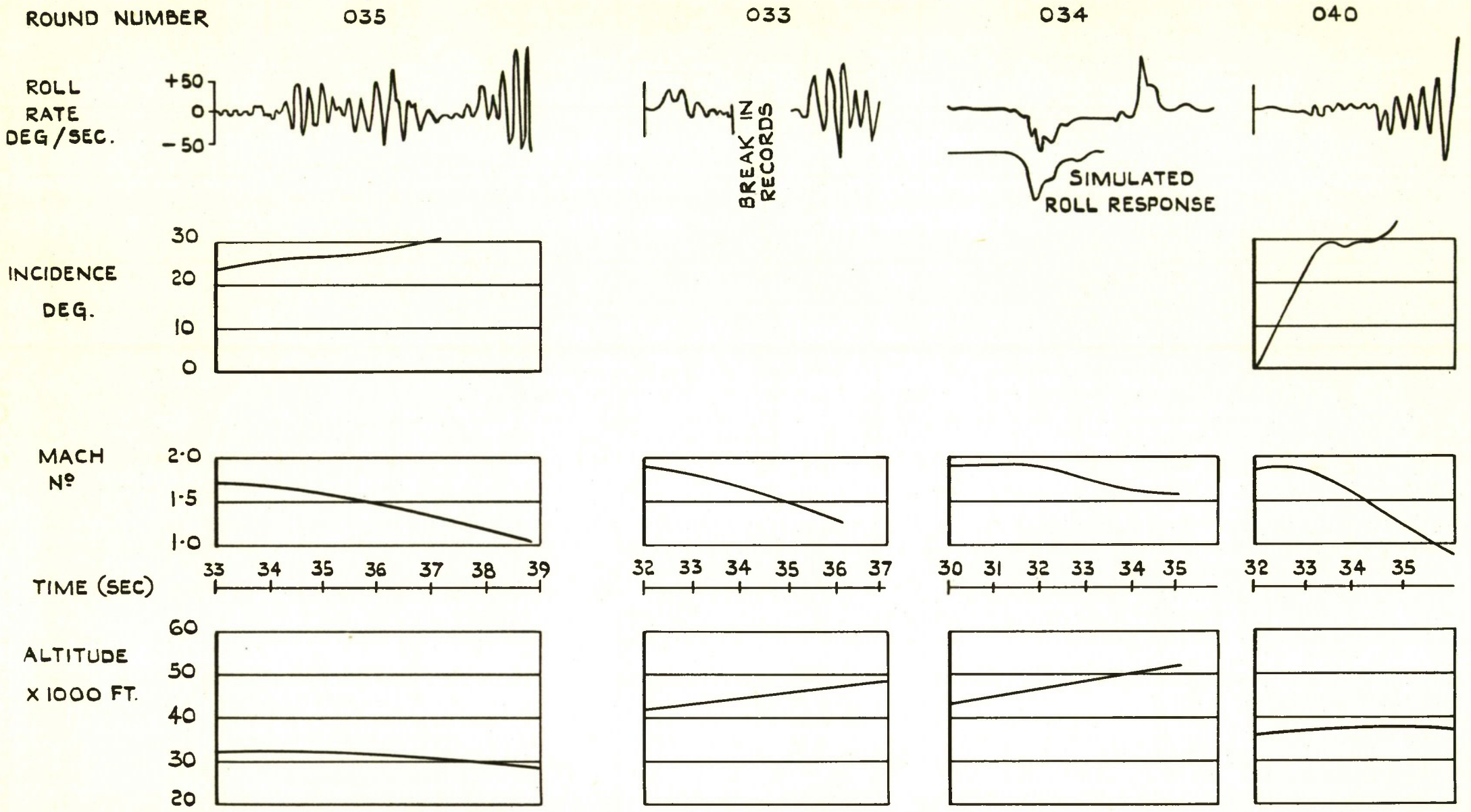

FIG.18.

TN. WE 5.

FIG.18. DETAILS OF CONTROL ROUNDS INCLUDING TELEMETERED ROLL RESPONSE.

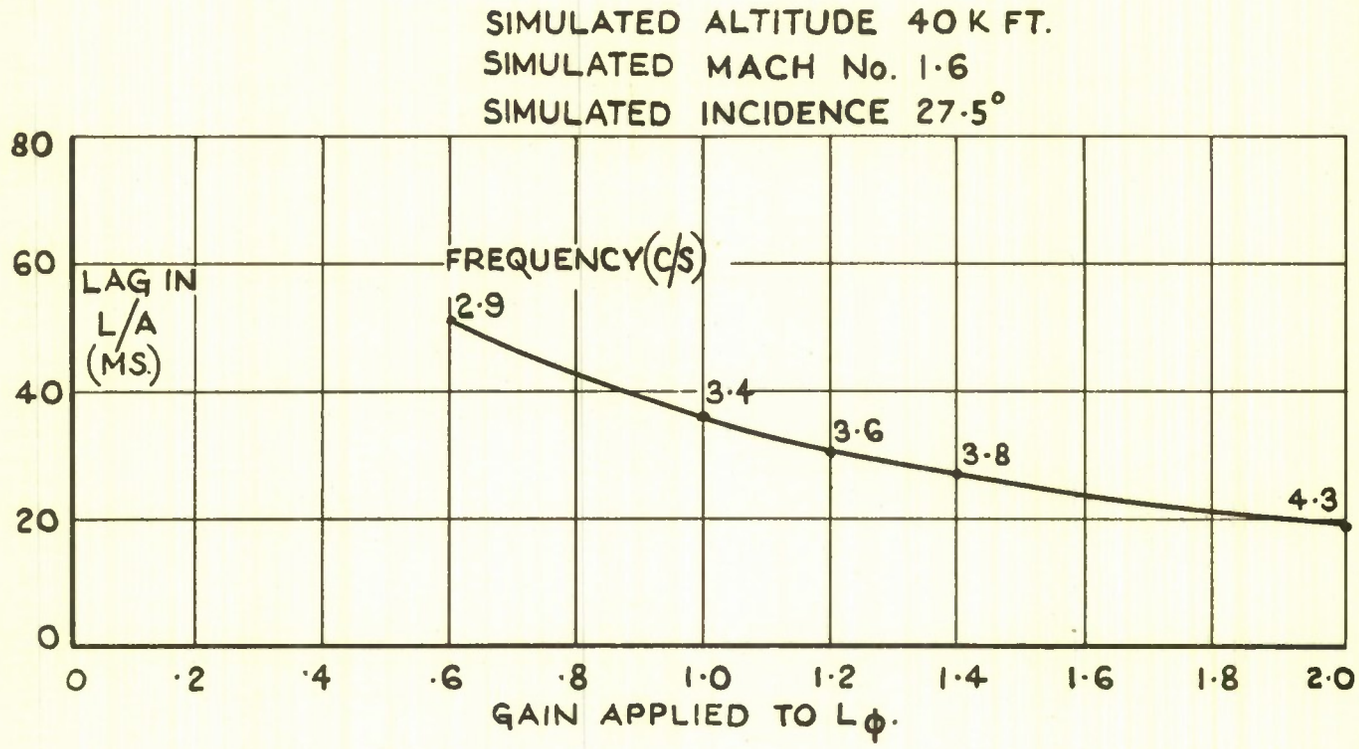

FIG. 19. DEPENDENCE OF LAG AND ROLL OSCILLATION FREQUENCY ON L_ϕ.

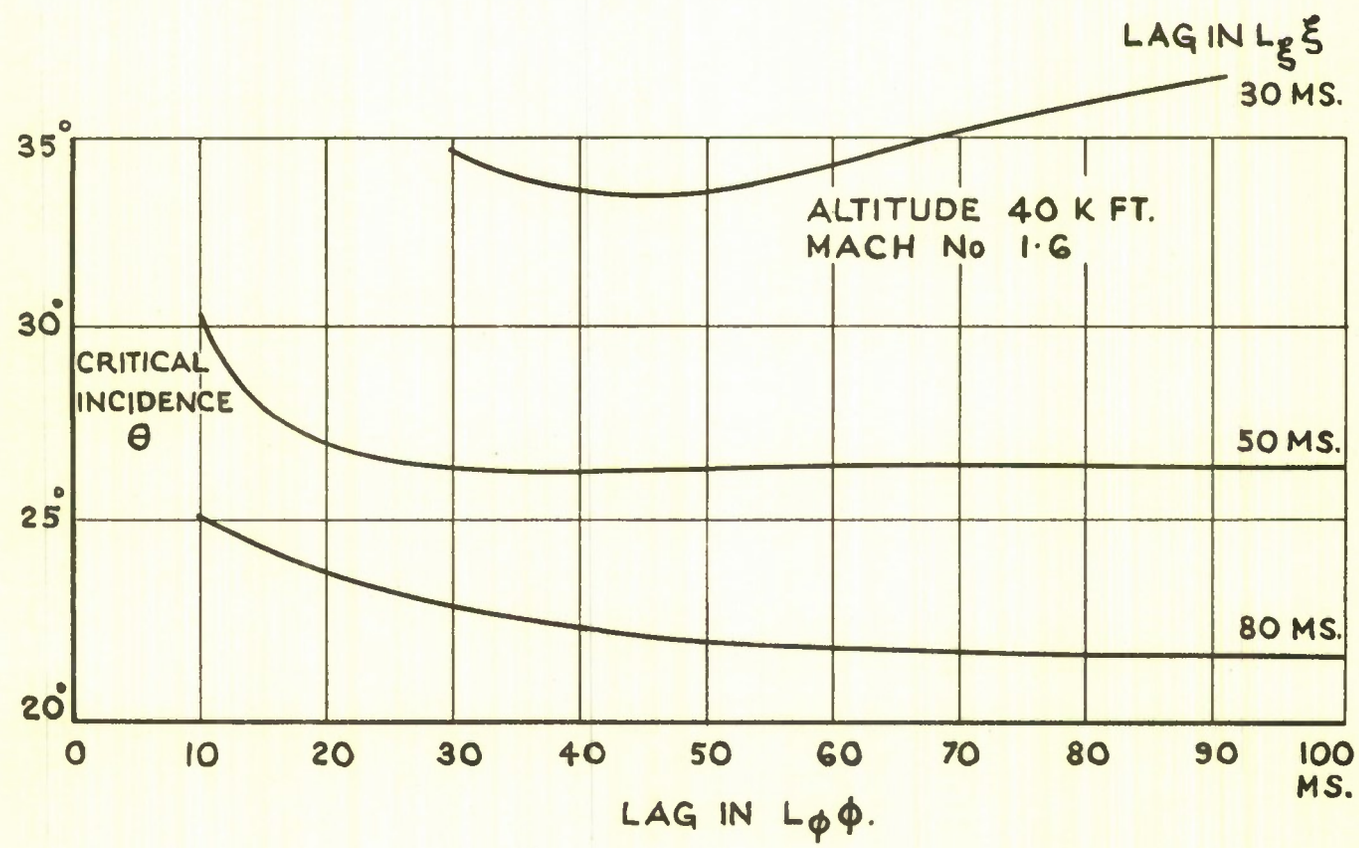

FIG. 20. EFFECT OF LAGS ON CRITICAL INCIDENCE.

FIG. 21

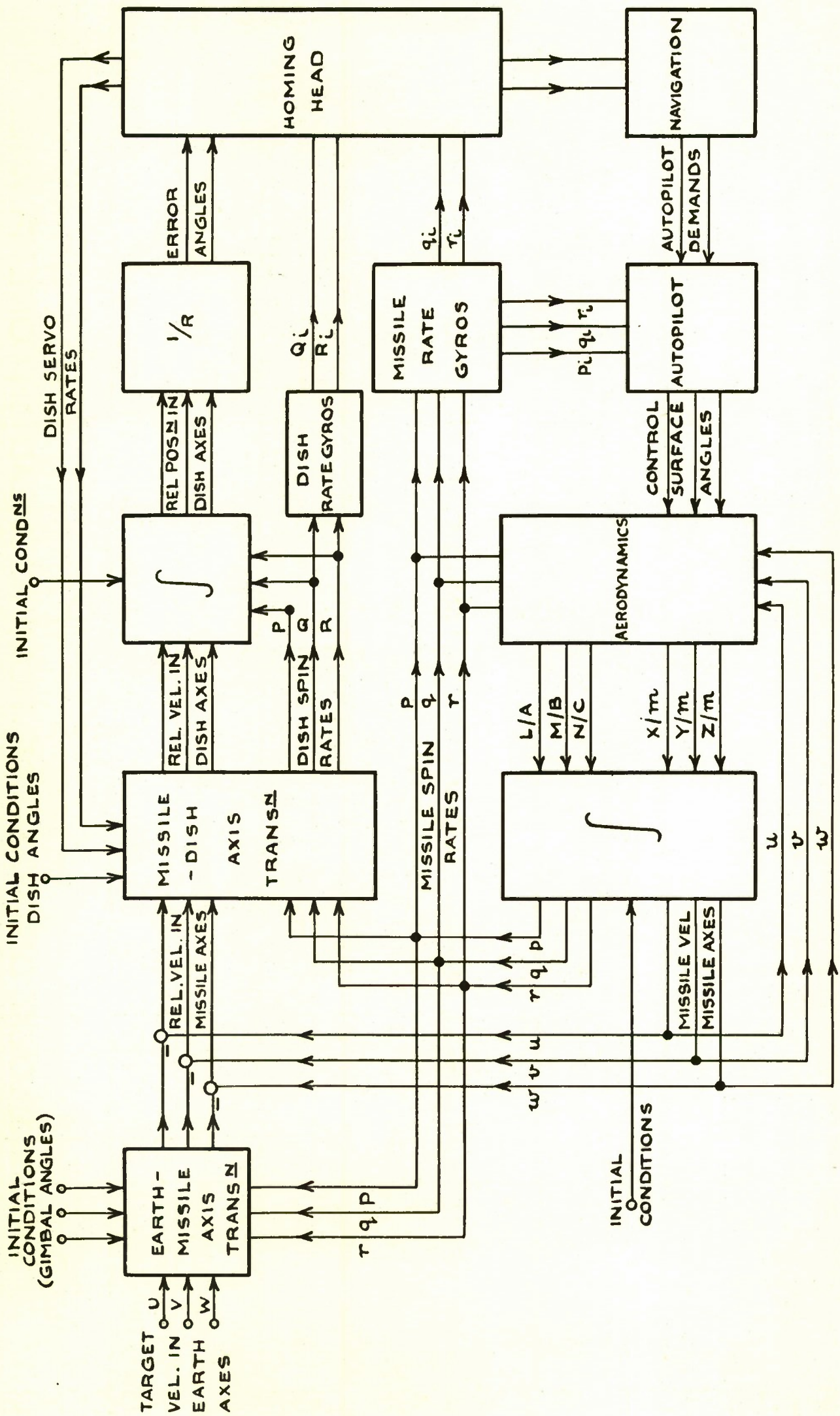

FIG 21. BLOCK DIAGRAM OF HOMING MISSILE SIMULATION.

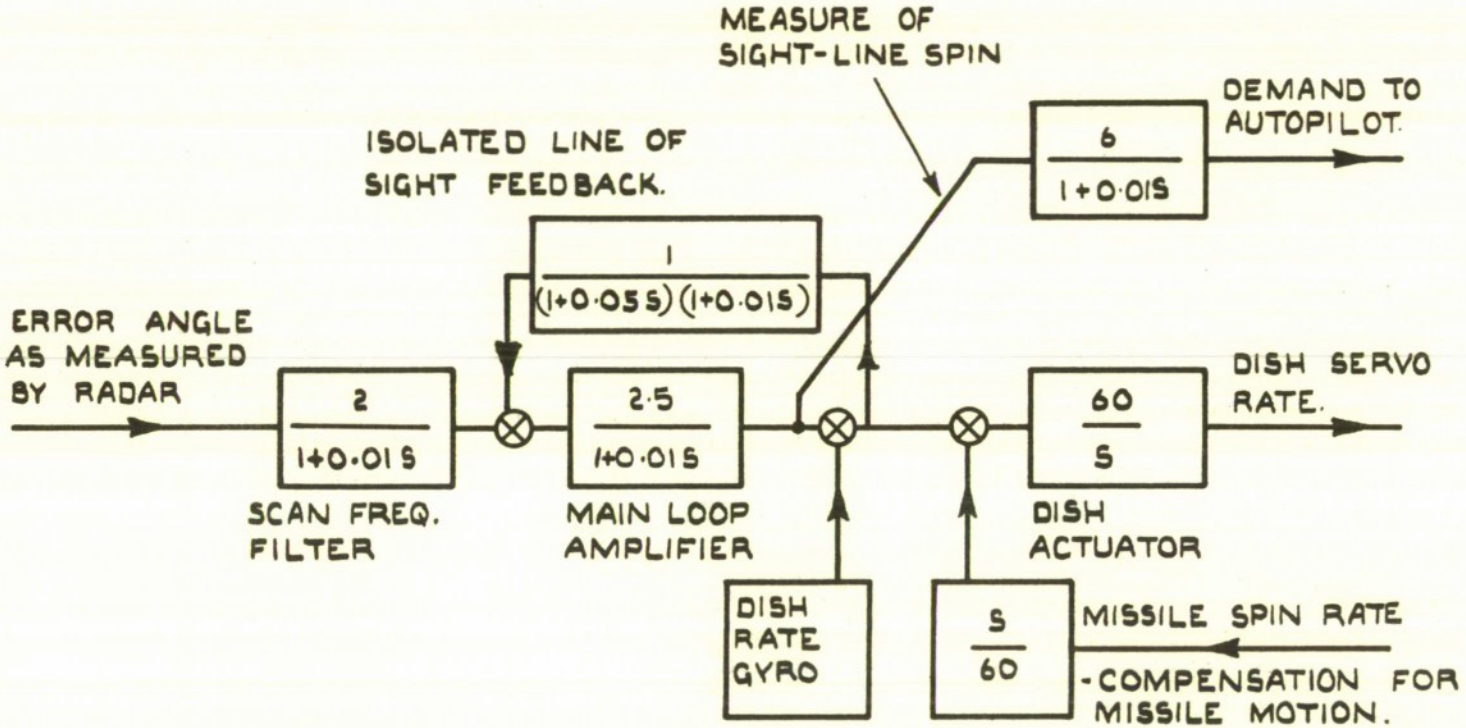

FIG. 22. BLOCK DIAGRAM OF HOMING HEAD IN ONE PLANE.

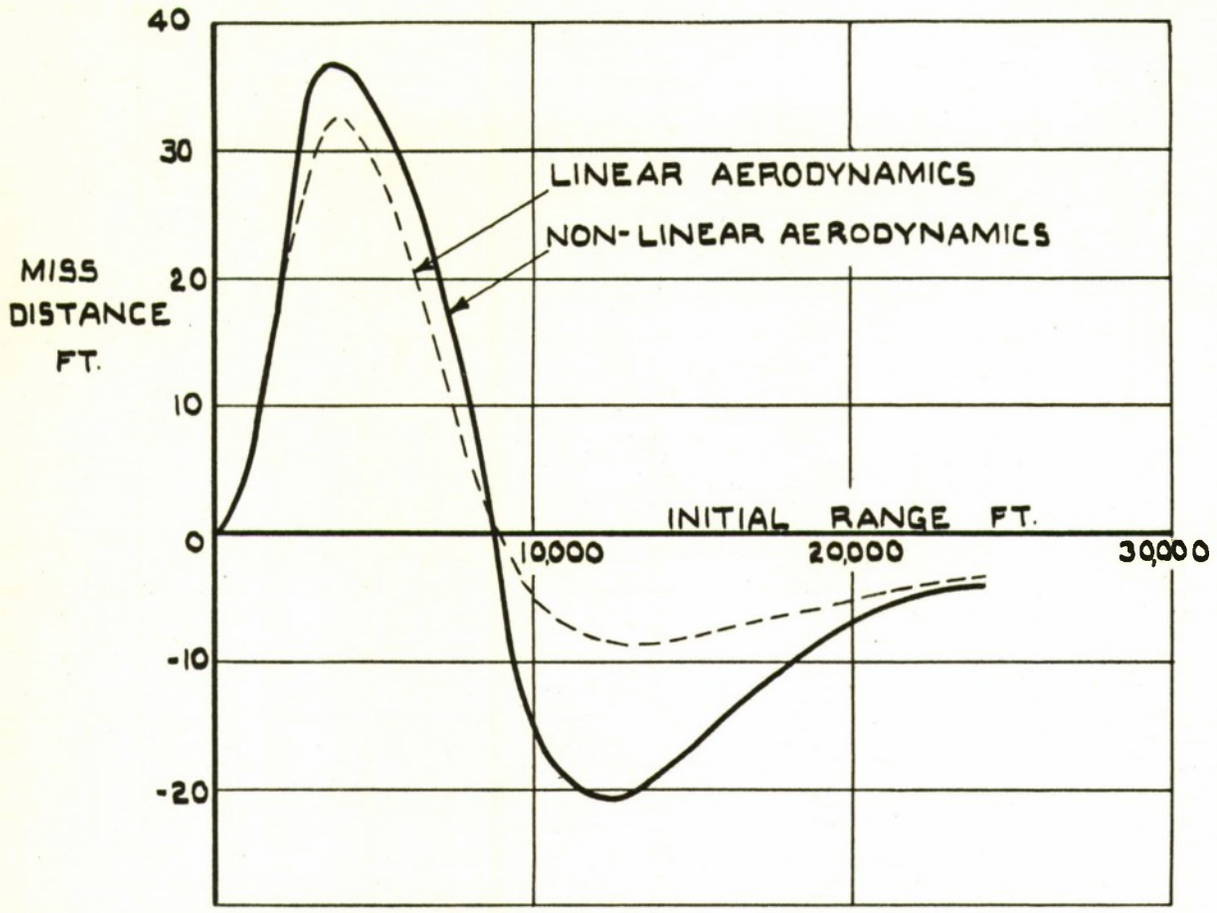

FIG. 23. MISS DISTANCE v. INITIAL RANGE IN SINGLE PLANE HOMING.

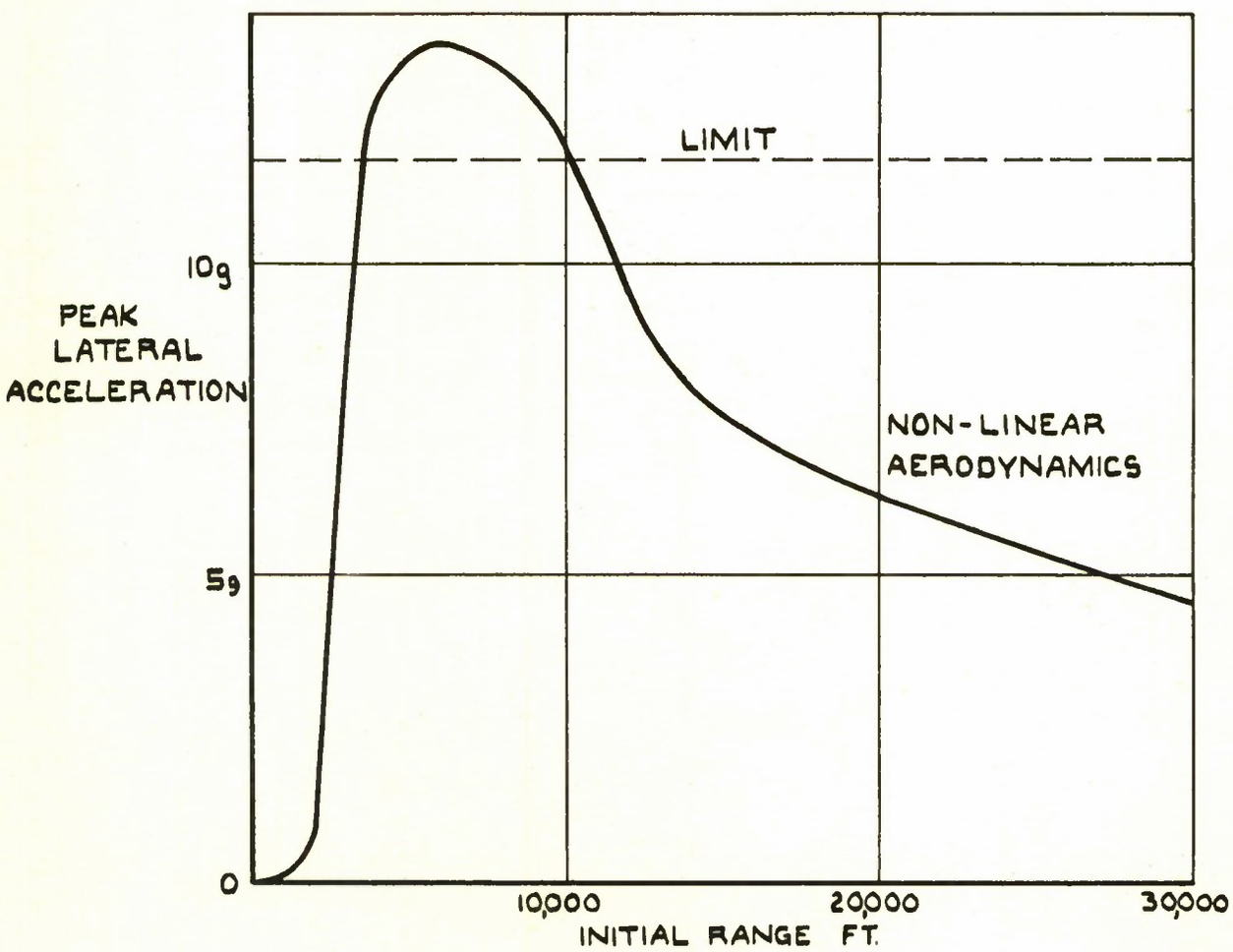

FIG.24. PEAK LATERAL ACCELERATION v. INITIAL RANGE IN SINGLE PLANE HOMING.

FIG. 25. (a & b)

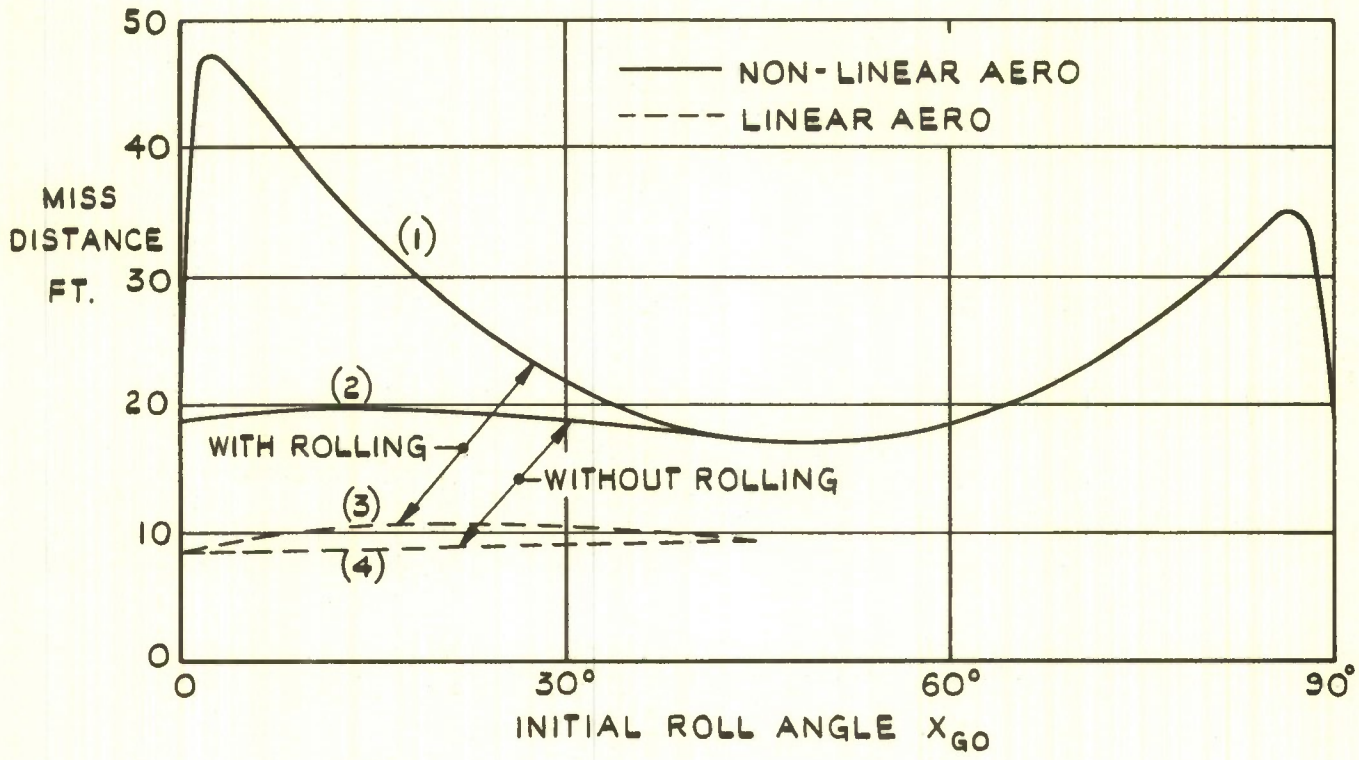

(a) INITIAL RANGE 14,000 FT.

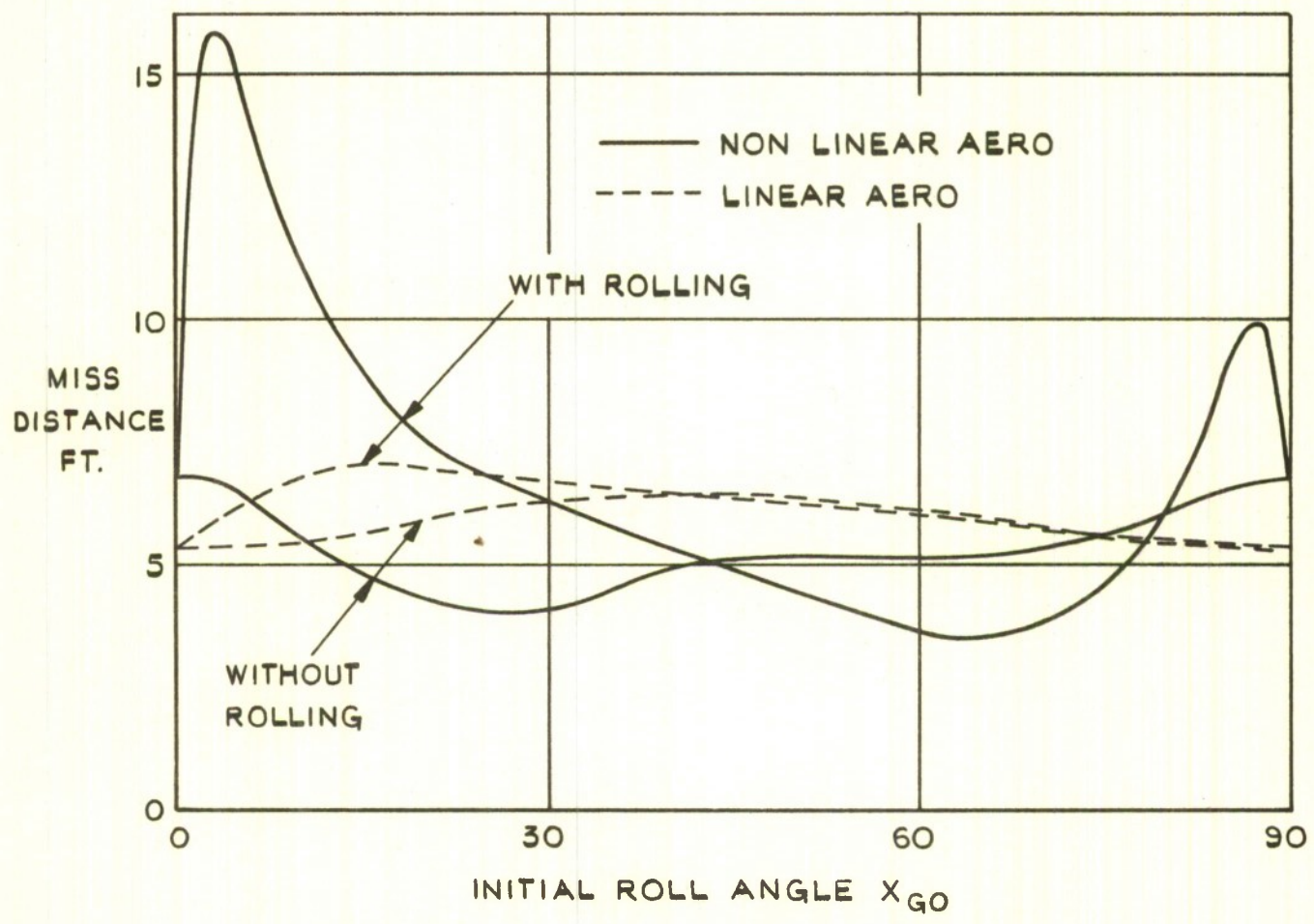

(b) INITIAL RANGE 20,000 FT.

FIG. 25. (a & b) MISS DISTANCE v. INITIAL ROLL ANGLE IN 3-DIMENSIONAL HOMING FROM TWO INITIAL RANGES.

FIGS. 26 & 27.

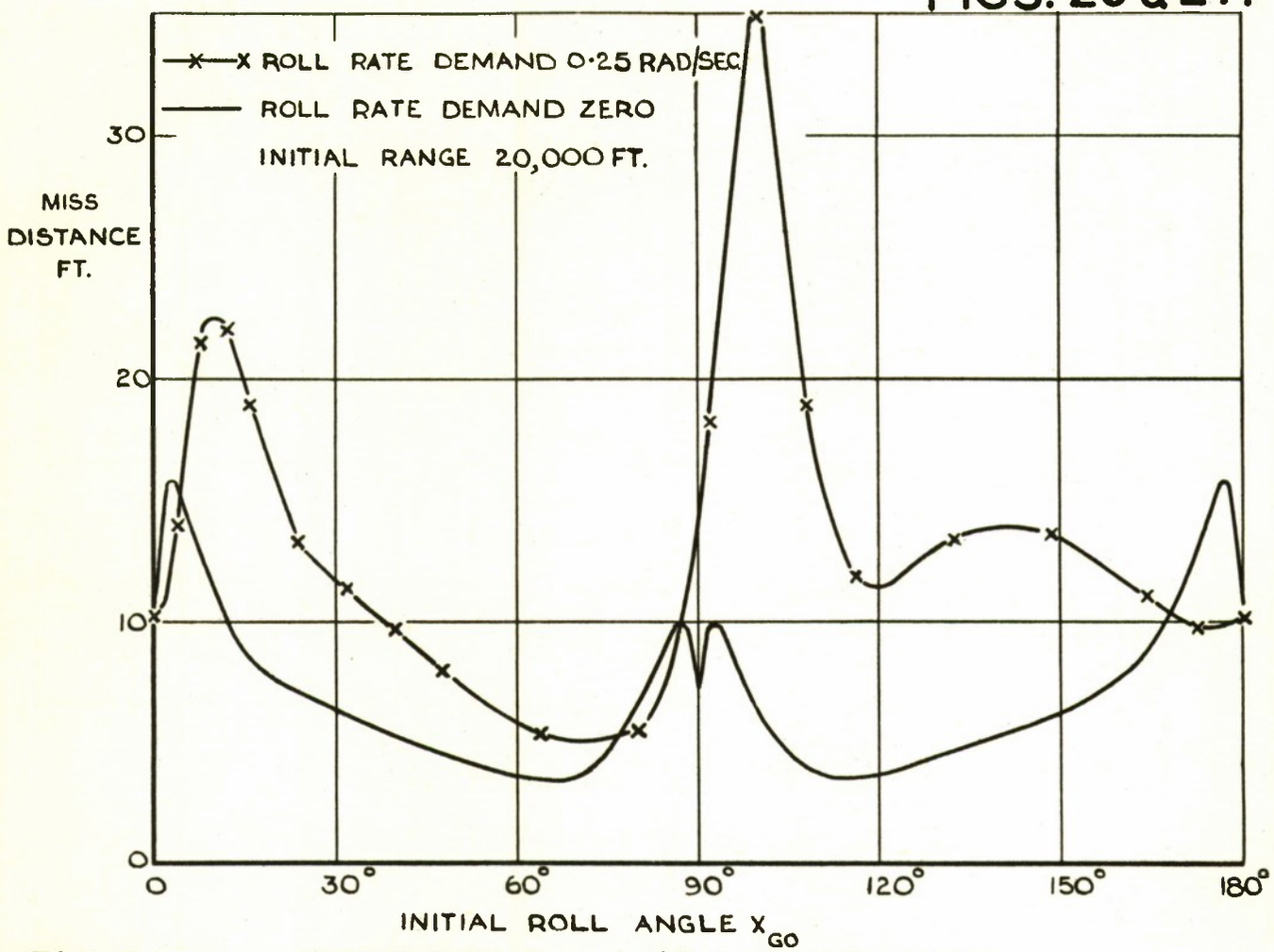

FIG.26. EFFECT ON MISS DISTANCE OF A STEADY ROLL RATE

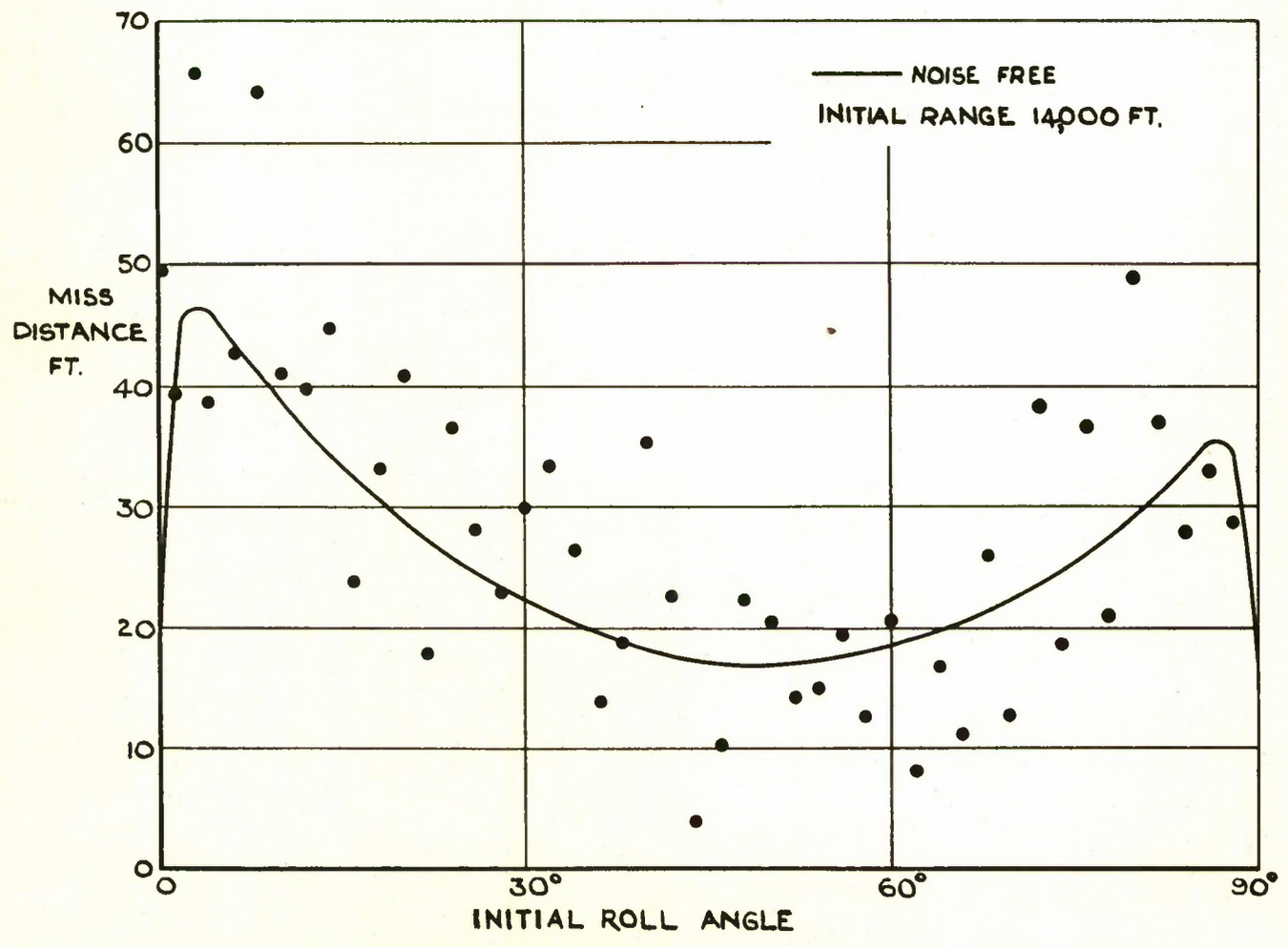

FIG. 27. EFFECT ON MISS DISTANCE OF ANGULAR NOISE

G.W./P. 9978

T.N. W.E. 5
FIG. 28

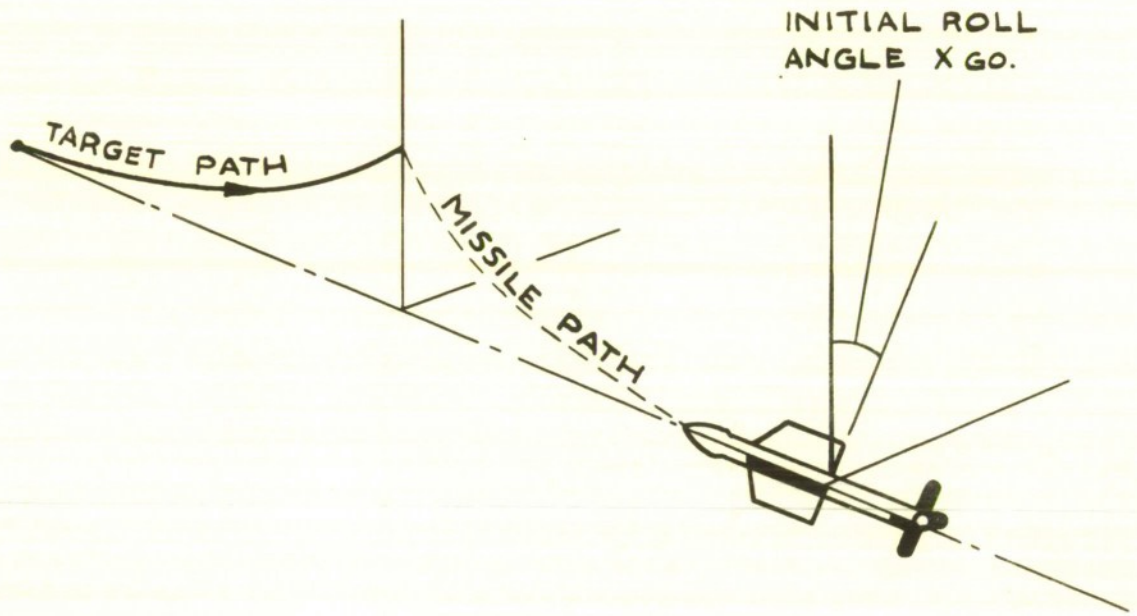

FIG 28. DIAGRAMMATIC REPRESENTATION
OF HOMING IN THREE DIMENSIONS.

V.R. 725 MODEL

MACH. NO. 1·6

HEIGHT 40,000 FT.

INITIAL ROLL ANGLE $X_{GO} = 5°$ (SEE FIG 28)

DEMAND IN ROLL FIXED AXES $q_{Dd} = 0{\cdot}24$ RAD./SEC.

⊙ DIGITAL VALUES

T.N. W.E. 5.
FIG. 29.

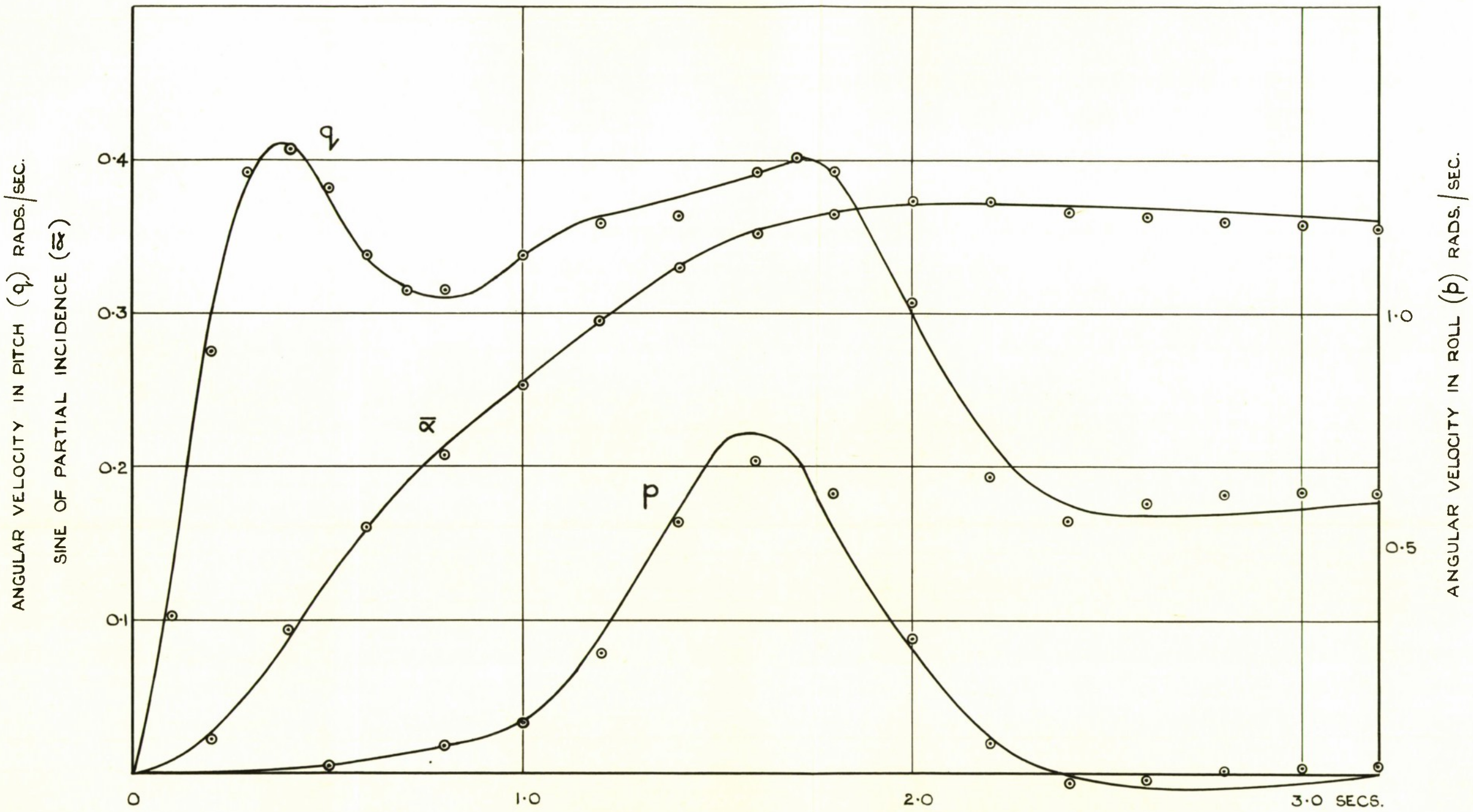

FIG. 29. RESPONSE IN 3 DIMENSIONS:
COMPARISON OF DIGITAL AND ANALOGUE RESULTS

FIG. 30.

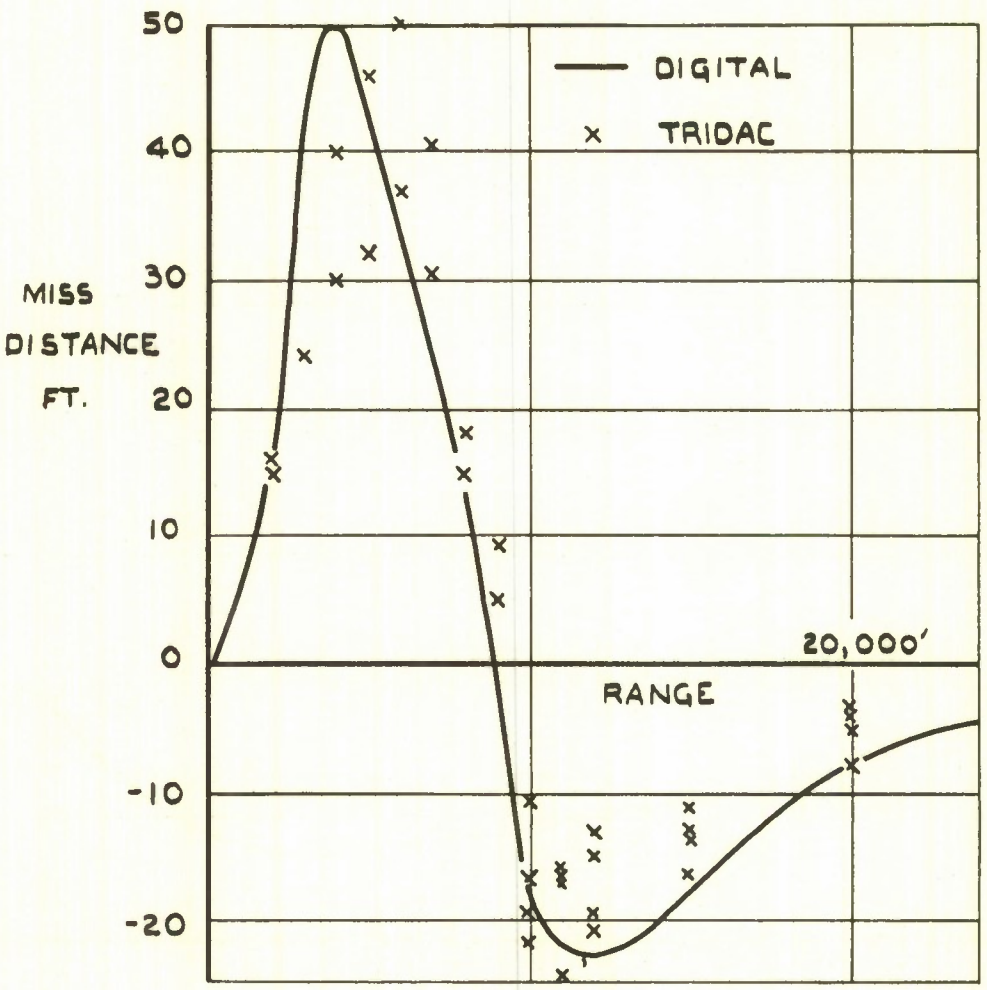

FIG.30. COMPARISON OF ANALOGUE AND DIGITAL RESULTS IN SINGLE PLANE HOMING.

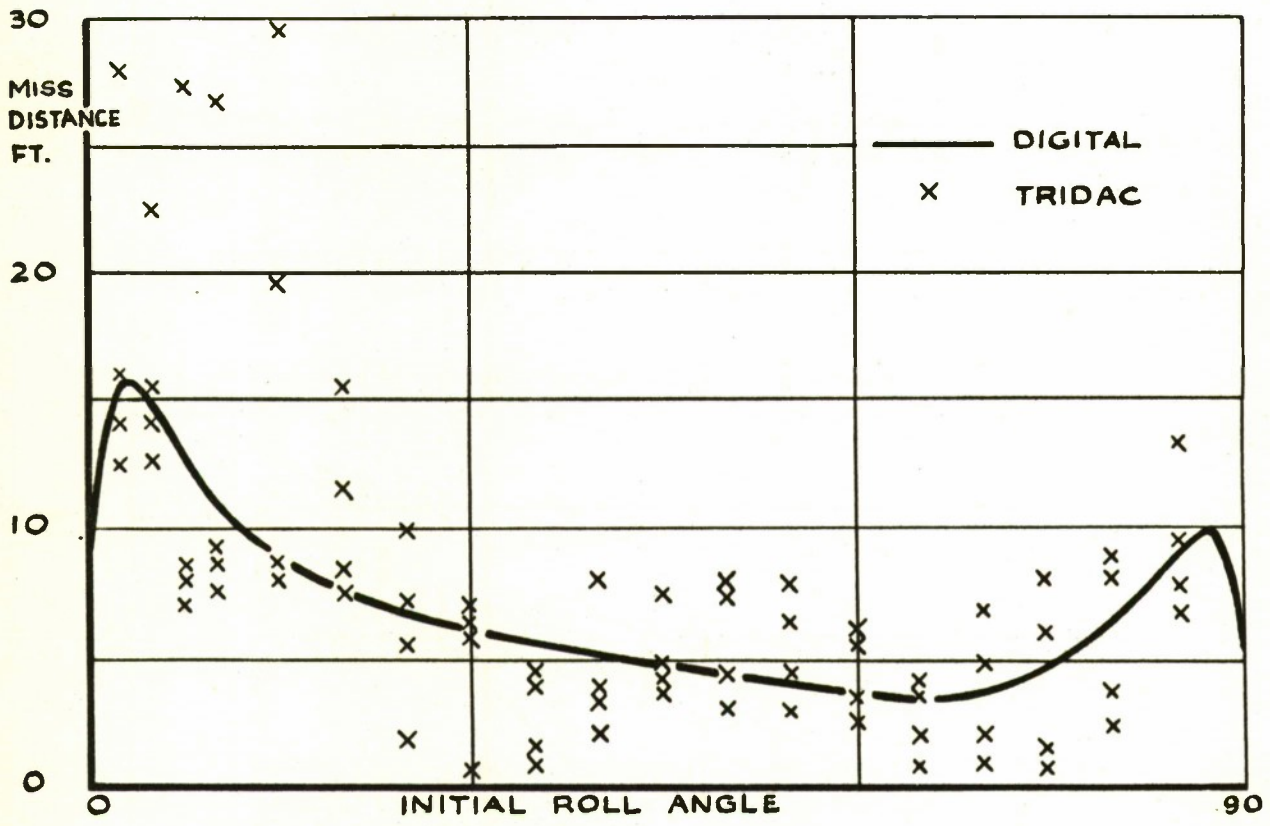

FIG 31. COMPARISON OF ANALOGUE AND DIGITAL RESULTS IN THREE DIMENSIONS.

FIG. 32 (a - d)

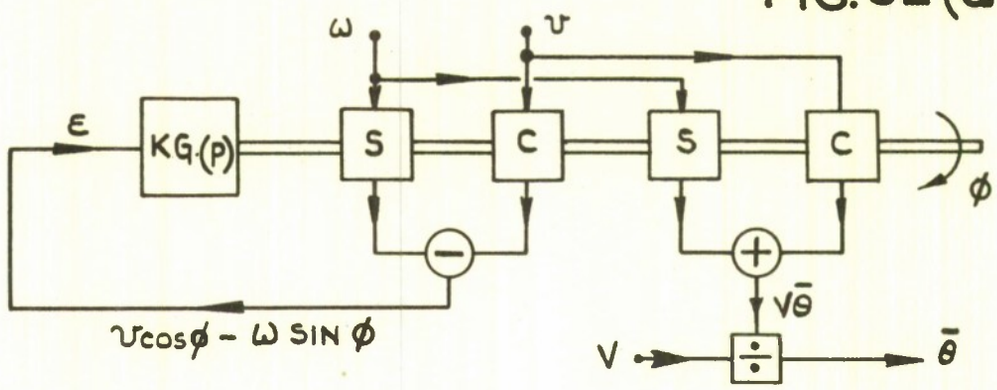

(a) GENERATION OF ϕ AND $\bar{\theta}$

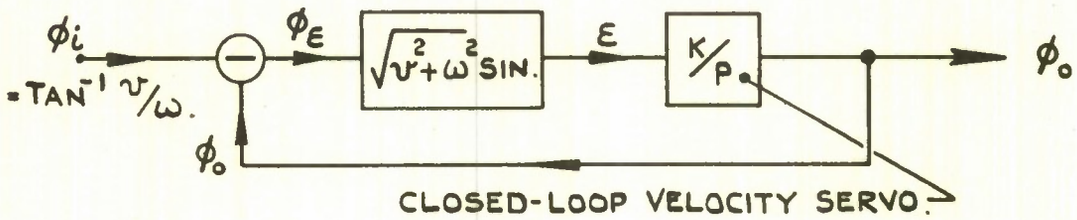

(b) RE-ARRANGED SERVO LOOP.

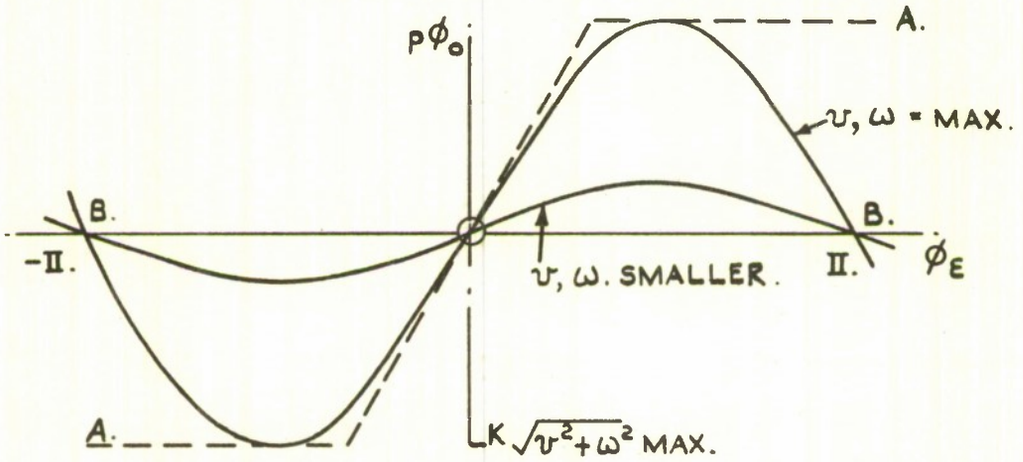

(c) ERROR CHARACTERISTIC

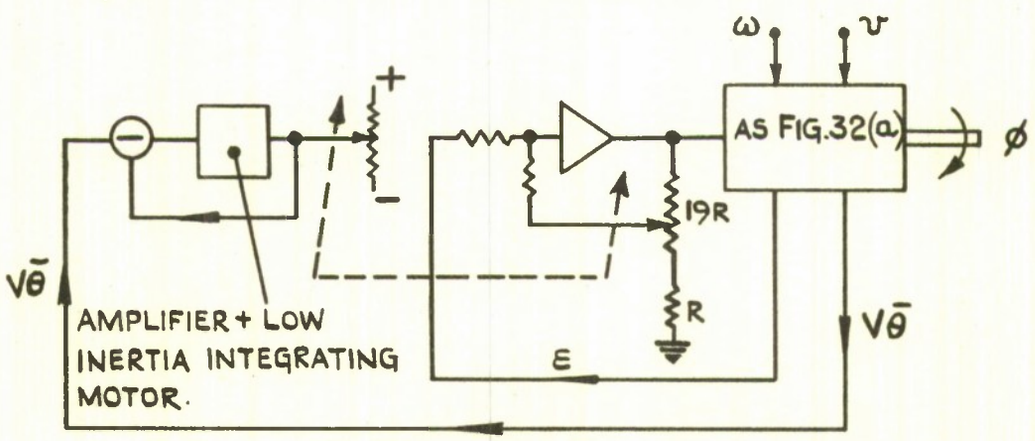

(d) ADDITION OF A.G.C.

FIG. 32 (a-d) SERVO ARRANGEMENT FOR GENERATION OF ϕ AND $\bar{\theta}$

94-2
Rept.-1198-TN-2 Conf. to Uncl.
Cutler-Hammer, Inc., Deer Park, N. Y. Airborne Instruments Lab.
FLOW PATTERN STUDY AND MIXING FLOW ANALYSIS OF AN AEROSPIKE IN HYPERSONIC FLOW
J. A. F. Hill and L. D. Lorah Jan. 1962 63 p refs Prepared in cooperation with Mithras, Inc.
(Contract AF 04(694)-29)
(AD-360563; X65-83258) Declassified 9/28/66

94-3
RTD-TDR-63-4268 Conf. to Uncl.
Boeing Co., Seattle, Wash. Aero-space Div.
EXPERIMENTAL STUDIES OF THE UNSTEADY AERODYNAMICS OF PANELS AT OR NEAR FLUTTER WITH A FINITE BOUNDARY LAYER MACH NUMBER 1 TO 10 Final Report, Jul. 1962 - Nov. 1963
G. W. Asher and A. W. Brown Wright-Patterson AFB, Ohio, AF Flight Dyn. Lab. Dec. 1964 114 p refs
(Contract AF 33(657)-8704)
(AD-356821; X65-13854) Declassified 9/13/66

SECTION I DECLASSIFIED

95-1
AFML-TR-65-148 Conf. to Uncl.
Whittaker Corp., San Diego, Calif. Narmco Research and Development Div.
BORON FIBERIZATION FROM THE MELT Technical Report, 1 Sep. 1964 - 30 Apr. 1965
R. A. Jones Wright-Patterson AFB, Ohio, AF Mater. Lab., May 1965 41 p refs
(Contract AF 33(615)-2113)
(AD-362554; X66-15828) Declassified 11/21/66

95-2
FDL-TDR-64-6 Conf. to Uncl.
Boeing Co., Seattle, Wash.
PANAL FLUTTER ANALYSES AND EXPERIMENTS IN THE MACH NUMBER RANGE OF 5.0 TO 10.0
D. J. Ketter and H. M. Voss Wright-Patterson AFB, Ohio, AF Flight Dyn. Lab., Mar. 1964 158 p refs
(Contract AF 33(657)-7912)
(AD-351273; X66-11987) Declassified 9/13/66

SECTION II DOWNGRADED

95-3
RAE-TN-WE-5 Secret to Conf.
Royal Aircraft Establishment, Farnborough (England).
(TITLE CONFIDENTIAL)
W. S. Brown, W. E. Dean, P. Hampton, H. Lewis, and D. I. Paddison
London, Min. of Aviation, May 1962 72 p refs
(X63-50100) GP. 1 Downgraded 8/16/66

CONFIDENTIAL

[redacted]

[redacted]

CONFIDENTIAL

[dstl]

Information Centre
Knowledge Services
[dstl] Porton Down
Salisbury
Wilts
SP4 0JQ
22060-6218
Tel: 01980-613753
Fax 01980-613970

Defense Technical Information Center (DTIC)
8725 John J. Kingman Road, Suit 0944
Fort Belvoir, VA 22060-6218
U.S.A.

AD#: AD331749

Date of Search: 11 December 2008

Record Summary: DSIR 23/30207
Title: Effect of aerodynamic non-linearities and cross-couplings on performance of a cruciform missile (RAE TN WE 5)
Availability Open Document, Open Description, Normal Closure before FOI Act: 30 years
Former reference (Department) ARC 24370
Held by The National Archives, Kew

This document is now available at the National Archives, Kew, Surrey, United Kingdom.

DTIC has checked the National Archives Catalogue website (http://www.nationalarchives.gov.uk) and found the document is available and releasable to the public.

Access to UK public records is governed by statute, namely the Public Records Act, 1958, and the Public Records Act, 1967.
The document has been released under the 30 year rule.
(The vast majority of records selected for permanent preservation are made available to the public when they are 30 years old. This is commonly referred to as the 30 year rule and was established by the Public Records Act of 1967).

This document may be treated as UNLIMITED.